1-1-1974

The equivalent width of blended molecular absorption lines.

Harold Irving Heaton
University of Massachusetts Amherst

THE EQUIVALENT WIDTH OF BLENDED MOLECULAR ABSORPTION LINES

A Dissertation Presented

By

Harold Irving Heaton

Submitted to the Graduate School of the
University of Massachusetts in partial
Fulfillment of the requirements for the degree of

DOCTOR OF PHILOSOPHY

September 1974

Physics and Astronomy

This research was supported by the Office of Naval Research under Contract #N00014-67-A-0230-0002.

THE EQUIVALENT WIDTH OF BLENDED

MOLECULAR ABSORPTION LINES

A Dissertation

by

Harold Irving Heaton

Approved as to style and content by:

John D Strong

Dr. John D. Strong, Chairman of Committee
Professor of Physics and Astronomy
University of Massachusetts

Waltraut C Seitter

Dr. Waltraut C. Seitter
Professor of Astronomy
Smith College and Observatorium Hoher List

Marcel Vanpée

Dr. Marcel Vanpee
Professor of Chemical Engineering
University of Massachusetts

Gerald A. Peterson

Dr. Gerald A. Peterson
Professor of Physics and Astronomy
University of Massachusetts

Dr. Leroy F. Cook, Department Head
Professor of Physics and Astronomy
University of Massachusetts

August 1974

ACKNOWLEDGMENTS

I particularly thank Professor John Strong who enthusiastically allowed me independence in my research. His guidance and encouragement never ceased. I also thank the staff of the Astronomy Research Facility.

Recognition is extended to the Finch Paint and Chemical Company and to the Ace Glass Company for materials.

This research was supported by the Office of Naval Research under Contract #N00014-67-A-0230-0002.

A grant from the University of Massachusetts Computing Center made completion of the computations possible.

The Equivalent Width of Blended Molecular Absorption Lines (September 1974)

Harold I. Heaton, B.A., University of Massachusetts
M.S., University of Massachusetts
Directed by: Dr. John D. Strong

A theory specifying whether two neighboring infrared absorption lines are nearly free of overlapping, or so blended as to nearly coincide, is formulated. The procedure only applies to lines which absorb in the square root region of the curve of growth but encompasses a broad range of environmental conditions. In intermediate cases, it has been possible to specify the deficiency, Δ, of the blended equivalent width from its value at either of these extreme cases.

Experimental confirmation at room temperature of that formulation is then presented. HCl gas in a 3.34m path is used at pressures from 2 to 750 torr. The experiment consists of sequentially pressure blending fundamental band isotopic doublets of that molecule, comparing predictions from the aforementioned technique to measured doublet equivalent widths. The comparison is made as a function of pressure, using previously published S and γ values.

Published line strength values for the HCl fundamental agree well only in the upper R branch (J = 7,8). These lines were used to test the theory. Predictions based upon divergent S values in the remainder of the band

were then compared to the experimental results. These confirm the accuracy of the $S\gamma$ products of Ref. 12 in most cases.

A polynomial representation of the logarithm of the Ladenburg-Reiche function is given. This will be useful in extending the procedure to the linear region of the curve of growth.

Because of discrepencies between measured and calculated baselines in this experiment, an evaluation of a published technique to locate 100% transmission levels is presented. An alternate, less empirical approach to that baseline technique is also given.

The theory verified here should greatly extend the number of isolated infrared vibration-rotation band members that may be measured and tested for the validity of assigned line parameters, and tested for the assumed Lorentz shape.

A new experiment is described based upon the confirmed theory. It allows the validity of the Lorentz shape to be assessed as a function of pressure for various foreign broadeners and interaction potentials.

Finally, an application of the theory to determinations of cometary abundances or sizes is discussed.

TABLE OF CONTENTS

LIST OF TABLES

LIST OF ILLUSTRATIONS

Frontispiece 1:

The earliest astronomy in the Five Colleges was carried out at Amherst College. Pictured here is the original Observatory erected on College Hill in 1847 which installed the 7 1/4 inch Clark telescope in 1853. That telescope was probably the first complete equatorial telescope built and sold by the Clark's. It was one of the foremost observatories in the nation at that time.

(From E. Loomis, Recent Progress in Astronomy, Harper & Bros., New York, 1856.)

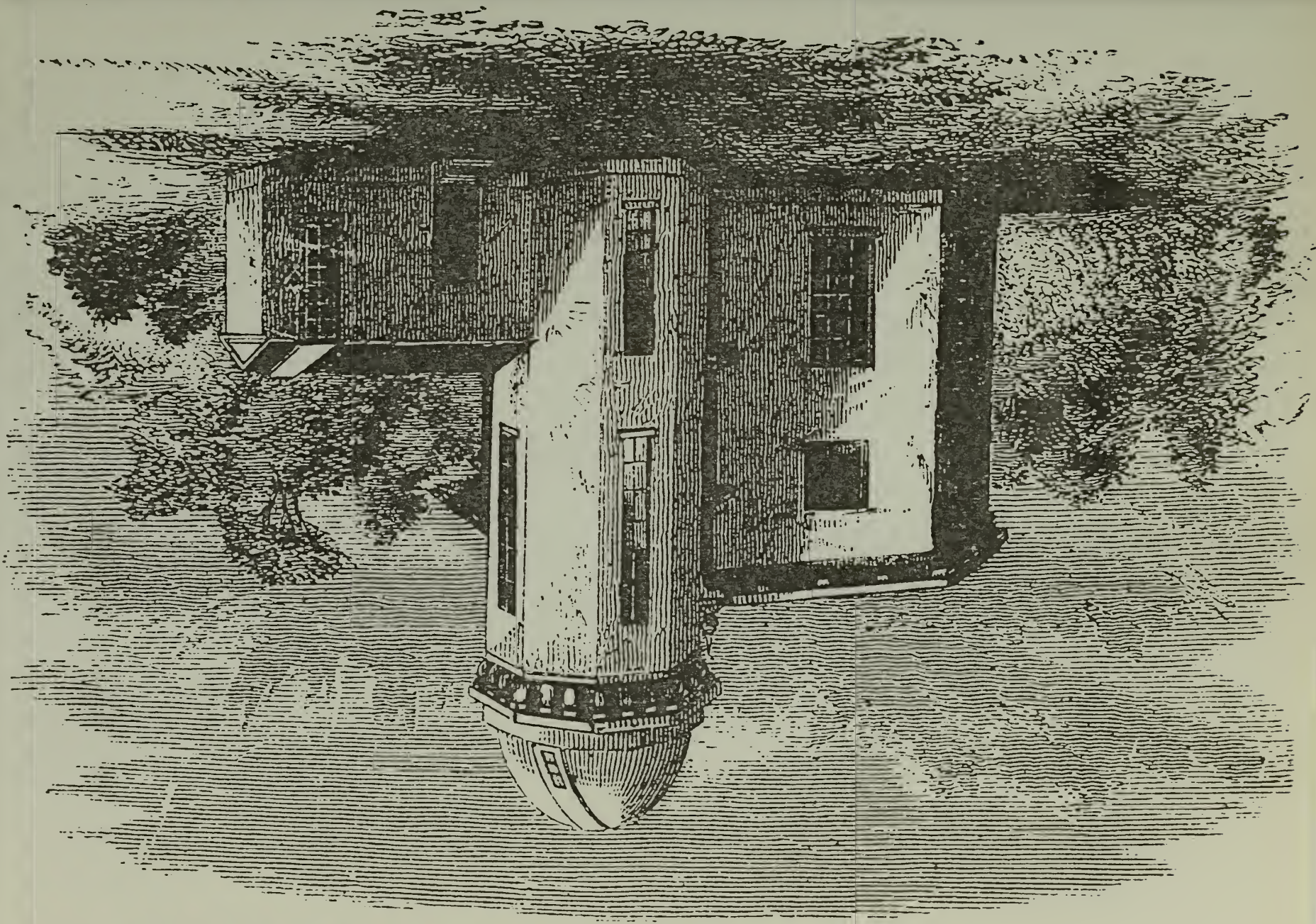

Frontispiece 2:

Ancient science was weakened by the lack of experimentation. Superstition and fear guided the interpretation of natural events.

> Alphonsus VI, king of Portugal, hearing of the appearance of the Comet of 1664, rushed to his terrace, showered it with abuse and threatened it with his pistol. The comet pursued its course with dignity. (Ref. 1)

Such breaches of rationality have continually pervaded our reflections on an often hostile world which seemed to sponsor threats for no reason. The perfectly ordered, Earth-centered universe of the first sixteen centuries after Christ spoke not only to our ego, but to our need for security as well. As experimentation accrued, new securities were needed. Here, a curious fellow looks behind the celestial sphere in an attempt to discover its mechanisms.

(From J. C. Brandt and S. P. Maran, New Horizons in Astronomy, W. H. Freeman, San Francisco, 1972.)

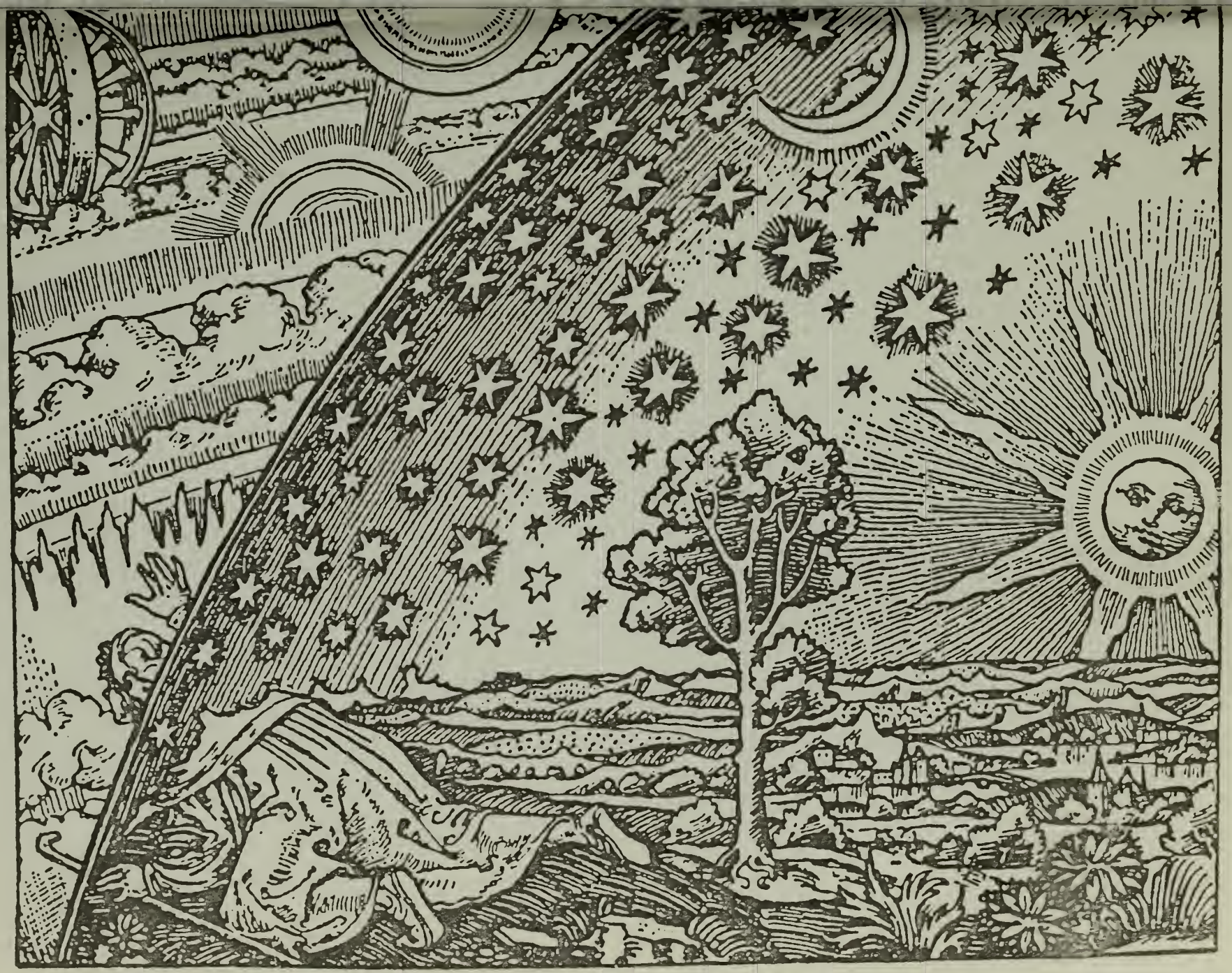

C H A P T E R 1

We search mere light beams. In our modern sophistication, we often take for granted how little we actually have to work with; how readily available the starlight dispersed in the greatest observatories is to us all. Seneca (4 B.C. to 65 A.D.) of Rome (and much later, Newton) realized that realms of color were unlocked by passing white light through a glass prism. The experimental science of spectroscopy had only to lie dormant through the European dark ages until Wollaston and Fraunhofer finally applied it to the sun.

Interpretation of molecular and atomic spectra has continually progressed as better techniques have been developed to squeeze more information from these colored ribbons. Understanding the formation of line spectra awaited Rutherford's experiments on atomic structure and the development of the ideas of quantization by Planck, Einstein, Bohr and Heisenberg.

Early planetary models of the atom had failed. They predicted unstable, continuously radiating atoms which decayed, contrary to observation, in less than 10^{-8} seconds. By applying the correspondence principle to the hydrogen atom, Bohr arrived at the quantization of the orbital angular momentum. He assumed,

> . . . (1) that the radiation is sent out in quanta $h\nu$ and (2) that the frequency of the radiation emitted

> during the passing of the system between successive stationary states will coincide with the frequency of revolution of the electron in the region of slow vibrations.[2]

Bohr showed that quantization of the orbital angular momentum was a necessary consequence of applying these two postulates.[3] His model of the atom radiated in the ultraviolet, but was stable. It was, however, a concocted semiclassical wonder of nature!

Common experience shows that light propogates through air, glass and many other materials. These materials appear macroscopically homogeneous in spite of their atomic structure, even though the electric charges in each atom or molecule must interact with the engulfing electromagnetic disturbances.

The materials appear homogeneous because the phenomena under study depend not upon the individual response of isolated atoms or molecules, but on the collective reaction of a large number of systems. The electric and magnetic fields of light remain nearly uniform over distances[4] $\sim \lambda/2\pi \sim 10^{-5}$ cm for visible light. A volume $(\lambda/2\pi)^3$ contains $\sim 10^8$ atoms of a dense material and $\sim 3 \times 10^4$ molecules of any gas at normal pressure.

The large mass difference between electrons and nuclei compel them to respond to light in widely differing frequency ranges. The electric fields within atoms are so strong, ~ 1

volt/Å or 10^8 volts/cm, that the electromagnetic fields of the engulfing light are a minor perturbation except for high intensity laser sources.[4] The internal fields are $\sim 10^8$ times as strong as the average fair weather potential gradient in Earth's atmosphere.[5] The speed of orbiting electrons is normally much lower than c. Hence magnetic effects of the radiation, proportional to v/c, are negligible.

Thus, we deal with the linear response of electrons to high frequency electric fields in the case of electronic excitation and lower frequency electric fields in the instance of vibrating nuclei.

Molecules, like atoms, exhibit discrete frequency spectra. They possess discrete energy states and produce or absorb a photon whose frequency depends upon this set energy difference, when changing states. Electronic transitions are only one instance of quantization in molecules, though. Molecular internal energy is partly shared, as well, by rotations and vibrations of the entire molecule. The advantages of examining spectral lines caused by these motions are many.

Pure rotation state changes involve the smallest energies. Typical energy differences in a rotational transition involve a few hundredths of an electron volt. Lines from these transitions fall in the far infrared and microwave

spectral regions. It is these lines which reveal the swirling interstellar gases to radio astronomers.

If vibrational modes are excited, by energies of the order of a few tenths of an electron volt, the vibration-rotation spectrum appears in the near infrared. Symmetric molecules such as Methane show rotation lines only in conjunction with such vibrational excitation. Vibration-rotation levels are schematically shown in Fig. 1. Each vibrational level has superimposed upon it a ladder of rotational levels. Bands arise from transitions between rotational levels (quantum number J) in successive vibrational states (quantum number V). The P, Q and R branches appear typically according to whether ΔJ is +1,0, -1 respectively. It is these bands in H_2O, CO_2 and the pollutant molecules that are responsible for atmospheric opacity in the infrared, even though these gases are only minor constituents of the atmosphere.

Electronic transitions, which effect structural changes in the molecule, involve a few electron volts. These lines appear in the visible and ultraviolet wavelengths.

It is these spectral threads from atoms and molecules which reveal to us most of our information regarding the composition, abundance, temperature and even spatial extents of the variety of gases and environments in our atmosphere, the atmospheres of the other planets and stars, and in the

remote cosmic cold. Under contrasting situations, when these conditions are known, spectral contours often provide detailed information about intermolecular forces operative during molecular collisions; the level populations and transition probabilities in the radiating species are also derivable. Experimental results are often clouded by practical difficulties, some of which are discussed in Chapter 4, but spectroscopy has provided a wealth of exact detail. Theoretical solutions for the frequencies and parameters of spectral lines are only approximate and then possible only for the simplest molecules.

§ 1.1 - Theoretical Framework for Understanding Spectra

Theory seeks approximations to make complex problems tractable. To deal with molecular systems, the nuclear motions of vibration or rotation and electronic motions are often taken to be independent. This results because electronic motions occur much more rapidly than any nuclear motions due to the small mass of the electron. Of course, strictly, they are not. The variation of electronic energy with the configuration of the nuclei is then treated as a contribution to the potential energy of the interatomic forces. A separate Schroedinger equation results for electronic motion. This is the Born-Oppenheimer approximation.

Stationary states of molecules are classified to a large extent according to constants of the motion of the

entire system, such as angular momenta, parities and other symmetries. Selection rules limit the symmetry of the final state of a transition according to the symmetry character of the initial state and of some external agent such as radiation.

When a chemical reaction occurs, the reacting groups differ from the initial constituents; a change in the electronic state often arises. This, in itself, implies a partial breakdown of the Born-Oppenheimer approximation as does electronic energy degradation into nuclear motions which often occurs in a single molecule. In fact, it is this type of neglected coupling, which is the crux of the Born-Oppenheimer approximation, that gives rise to the Λ doubling transitions of OH in interstellar space.

When a pure rotation photon is absorbed or emitted, the kinetic energy of free rotation about the molecule's center of mass is changed. Examination of the resulting spectrum allows these energy changes to be sorted out from other energy changes. The determination of these rotational energies, in turn, provides accurate data on the moments of inertia or diatomic molecules and thereby their internuclear distances. For more complicated tetrahedral molecules, moments of inertia cannot be determined from the fine structure of one band alone.[6]

Transitions which occur without any change of electronic state emit or absorb radiation intensely only when the molecule has a net average dipole moment, that is, only when the average positions of the electronic and nuclear charges do not coincide. Hence, intense infrared and microwave spectra are not observed for simple homonuclear molecules such as O_2, H_2 and N_2. For these molecules, rotational transitions result only from a change in the electronic state which gives rise to a dipole moment; they appear, as well, in Raman spectra.

For diatomic molecules, the rotational quantum number N is related to the rotational energy E_r, using the Born-Oppenheimer approximation, by

$$E_r = B(R)\, N(N+1) \qquad (1)$$

where the rotational spacing is given by

$$B(R) = \hbar^2/2\bar{M}R^2 \qquad (2)$$

and

R is the internuclear distance,

$\bar{M}$ is the reduced mass of the nucleus and

$\hbar$ is Planck's constant divided by 2π.

For the HCl molecule studied in Chapter 4, R = 1.27460 $\pm$ 0.00005Å using this approximation.[6] The dependence of B(R) on R is averaged over the state of vibrational motion. The quantum number N identifies the total angular momentum of

free rotation exclusive of coupling to the electron spin (Hund's cases) or nuclear spin (hyperfine splitting).[4,6]

For infrared and microwave spectra, where the moment of inertia remains nearly constant over the transition, rotational energy changes result from a speeding up or slowing down of the rotational speed. As E_r is a linear function of this change, spectral bands of equally spaced lines would be expected to arise, each line corresponding to a different initial value of N. In actuality, a progressive decrease is often seen in the spacing of lines arising from the higher N levels since the mean value of B(R) is decreased by rotational stretching.[4]

Observation of the intensity distribution of lines within rotation bands then indicates the temperature of the responsible medium. This only occurs when the gas is in thermal equilibrium; an unusual state of the gas is indicated otherwise.

In many cases, molecules naturally consist of two or more isotopes of slightly differing masses. Rotation bands from each molecule appear superimposed but somewhat displaced from one another. The effect is very small for atoms but is rather large for molecular vibrational and rotational spectra. The rotational constant for deuterium, for example, is only one half as large as for H_2. However, these constants differ by only 3% for $^{16}O^{16}O$ and $^{16}O^{17}O$. The relative

strengths of isotope lines is indicative of abundance differences of the various species.

Hyperfine splittings occur in molecular spectra and are quite pronounced. These splittings have provided detailed information about the magnetic and electric fields which prevail at the location of the nuclei and thus on the distribution of currents and charges within these aggregates.

Vibrational motion is often treated by using harmonic oscillator theory, which predicts evenly spaced vibration levels. Quantum jumps $\Delta V > 1$ are not allowed, where V is the vibrational quantum number. Both circumstances are violated in natural spectra, but the harmonic oscillator is still a good provider for the approximate energy change in such transitions.

Harmonic or overtone bands do appear at reduced intensity when $\Delta V = 2,3 \ldots$ And level spacings crowd together in the potential well when energies near the dissociation energy are reached. Of course, this is expected by the correspondence principle.

When energy less than the dissociation energy is absorbed by stable molecules, nuclei may find themselves considerably displaced from their old equilibrium positions as electronic changes take place. They vibrate with large amplitude. The relative probability for excitation of various vibrational modes was found by Franck and Condon and is expressed today by a principle which bears their name.

§ 1.2 - Types of Simple Molecules

Hence, many theoretical expectations guide experimenters who seek either to verify those theories or to engage in research of practical importance. Molecules come in various configurations; each reveals itself under different conditions of excitation. The number of quantum numbers that are necessary to specify the state of a simultaneously vibrating and rotating molecule depends upon this geometry. If we call I_a, I_b and I_c the moments of inertia about the three principal axes, then:

a) linear molecules, such as H_2 and CO_2 have $I_a = I_b$ with I_c equal to zero.

b) symmetrical top molecules, such as O_3, have $I_a = I_b \neq I_c$ where I_c is non zero.

c) asymmetrical top molecules, such as H_2O have $I_a \neq I_b \neq I_c$.

d) spherical top molecules, such as CH_4 have each moment equal, $I_a = I_b = I_c$.

Only when the various spectral transitions from these molecules are suitably calibrated can they be beneficent to mankind.

Remote sensing of atmospheric CO_2 and H_2O lines by orbiting vehicles is meteorologically useful.[7] It provides temperature and moisture profiles as a function of depth for our atmosphere at many more locations than could be measured

by radiosondes. Various pure rotation lines allow the investigation of eddying gases in space and in protostellar systems where huge quantities of energy must be radiated away to preserve the nascent star.[8] Vibration-rotation bands of pollutant molecules such as CO, NO_2, NO, SO_2, N_2O and PAN which may threaten our livelihood as a race, provide effective monitors indicating which areas are most endangered.[9,10] Spectral transitions of chlorophyll and silicates allow satellite identification of plant blights and geological terrain. Ocean currents may be remotely identified, as well. Medically, hemoglobin, Vitamin C and many other organic substances may be spectroscopically identified.

The uses for spectroscopy are many and varied. Aristotle realized that water droplets caused rainbows. It is well worth continuing the search for keys, started by Seneca and Aristotle, to further unlock useful regions of the electromagnetic spectrum for our benefit.

CHAPTER 2

Molecular spectra are often very complex and severely blended. Examples of laboratory spectra[9] for NO mixed with H_2O are shown in Fig. 2. Frequently, in order to reduce blending from adjacent lines, laboratory gases must be maintained at low pressures. While such an environment may approximate the upper atmosphere, these laboratory pressures fall short of the approximate conditions in the troposphere and exceed those found in the interstellar medium.

To fully exploit molecular spectral line contours, it would be desirable to develop a technique whereby useful environmental information could be extracted from overlapped spectra at or near atmospheric pressure.

To be able to carry out such a project, we need to know how the detailed distribution of opacity in the line, called the line absorption profile, depends upon localized conditions in the absorbing gas, such as temperature and density. Any theoretical investigation of overlapping must assume an initial approximation to the true line profile. Accordingly, we will turn to a discussion of the various theories of spectral line broadening. The primary profiles which will be encountered are the Lorentz profile, applicable to naturally and collisionally broadened lines and the Doppler profile. The Voigt profile, a mixture of the two, is also important.

First, however, the relationship between the line absorption profile, $K(\nu)$, and the observed transmission must be set in perspective.

When a beam of radiation with a known intensity distribution, $I^{\circ}(\nu)$, traverses a thin layer of absorbing gas, the observed intensity is given by Lambert's Law:

$$I(\nu) = I^{\circ}(\nu)e^{-k(\nu)\rho\ell} \tag{3}$$

Here, ρ is the mass density of absorbers (g/cm^3) and ℓ is the absorption path length (cm). The observed transmission is defined as the ratio

$$T(\nu) = \frac{I(\nu)}{I^{\circ}(\nu)} = e^{-k(\nu)\rho\ell} \tag{4}$$

The observed absorption, $A(\nu)$, and transmission, $T(\nu)$, are often suitably normalized so that

$$A(\nu) + T(\nu) = 1 \tag{5}$$

A convenient quantity for studying spectral lines is the equivalent width,

$$W = \int A(\nu)d\nu = \int(1 - e^{-k(\nu)\rho\ell})d\nu \tag{6}$$

W is a modified version of the area under the spectral absorption curve observed on the laboratory chart trace, shown in Fig. 3. The line absorption profile is buried within a transcendental function and is not directly observable.

The equivalent width is a convenient quantity for the following reasons. A monochromator, centered upon a particular frequency ν' within the line, always has some response

to light at adjacent frequencies. The frequency distribution of the normalized magnitude of this response is called the slit function, $s(\nu-\nu')$. It arises from the lack of experimental realization of infinite resolving power due to optical aberrations, diffraction effects and finite slit widths.

The shape of this function is generally taken to be triangular, $(\sigma - |\nu-\nu_o|)/\sigma$ or gaussian, $\exp\{-4 \ln(2) (\frac{\nu-\nu_o}{\sigma})^2\}$, where σ is the spectral resolution and ν_o is the line center frequency, but it is never well known. One approach to the investigation of line absorption profiles would be to convolute the assumed line absorption profile with an assumed intrumental slit function,

$$\bar{A}(\nu)_{obs} = 1 - \frac{\int T(\nu'-\nu_o)\, s(\nu-\nu')d\nu'}{\int s(\nu-\nu')d\nu'} \qquad (7)$$

comparing the resultant absorption with the experimental chart trace. Because the resultant convoluted transmission (or absorption, see Eqn. 5) is so sensitive to the poorly known slit function shape (see Fig. 4) though, comparison to real spectra to establish the validity or lack thereof of the assumed line profile is rarely made.

Instead, because of the finite resolutions which must be worked with, a curve of growth (shown in Fig. 5) portraying the increase of the equivalent width with pressure, is usually employed. Table 1 shows that W is independent of the resolving power[12] and hence, slit function shape, over a

broad range of resolutions in the square root region of the curve of growth. In fact, W is identical to that which would be measured with an instrument of infinite resolution. This result is true regardless of the actual lineshape.

§ 2.1 - The Line Absorption Profile

Theories of the shapes of spectral lines are often only approximate. This results due to the complexity of and uncertainties involved in the plethora of interactions between molecules of various species which are in a variety of excited states. Classically, there is a line absorption profile caused simply by the finite duration of the emitted wavetrain. This is determined by the decay of the radiation process itself and is referred to as natural or radiation damping. This profile is extremely narrow.

The various forms of line broadening will be of interest to us later in the development of further techniques for extracting environmental information from blended absorption lines.

Natural damping is distinguished from broadening due to perturbations of the wavetrain by other atoms, molecules or charged particles interacting with the radiating particle. These latter processes are referred to as pressure broadening.[14] Pressure broadening by molecules will be of considerable interest here. The resultant frequency distribution of opacity can be calculated using a damped classical

oscillator.

Much of the early theory of this oscillator was developed by H. A. Lorentz within the framework of the electron theory of matter. The theory relates to the atomic model of J. J. Thomson , according to which electrons are held elastically at equilibrium positions within a continuous distribution of positive charge. Even though this model did not prove microscopically correct, most of the deductions from this theory regarding the macroscopic electromagnetic behavior of matter stand today. This means that the basic assumptions of the electron theory of matter are <u>independent</u> of the unwarranted features of the Thomson -Lorentz model.[4]

§ 2.2 - Natural Line Width

If we imagine a molecule to be a classical dipole, bathed in monochromatic light of angular frequency ω_o, its oscillations are described by

$$m\ddot{r} + m\gamma_f\dot{r} + m\omega_o^2 r = eE_o\exp(-i\omega t) \qquad (8)$$

Here, m is the mass of the electron, ω_o is the natural angular frequency (rad/sec) of vibration, r is the one-dimensional displacement of the electron from its equilibrium position, E_o is the amplitude of the incident electric field and e is the electronic charge.

$$\gamma_f = \frac{2}{3}\frac{e^2}{mc^3}\omega_o^2 \text{Sec}^{-1} \quad \text{(cgs)} \qquad (9)$$

is known as the classical damping constant, due to its formal resemblance to a viscous damping term. A trial solution to this equation leads to a result which is simply an exponentially damped oscillation.[14] The Fourier transform of this solution, $F(\omega)$, is revealing.

$$E(\omega) = \frac{1}{2\Pi} F^{*}(\omega) F(\omega) \tag{10}$$

is called the energy spectrum and is a direct measure of the energy in the wavetrain at angular frequency ω, where

$$F(\omega) = \frac{r_o}{i(\omega-\omega_o) + \gamma_f/2} \tag{11}$$

and the asterisk denotes complex conugation. This oscillator continually loses energy but maintains its natural angular frequency.

When we consider an ensemble of such radiators, created at a constant rate but with random phases, the energy delivered per unit time is called the power spectrum of the ensemble and is related to the energy spectrum of an individual oscillator. Properly normalized, the power spectrum is given by

$$P(\omega) = \frac{\gamma_f/2\Pi}{(\omega-\omega_o)^2 + (\gamma_f/2)^2} \tag{12}$$

This is known as the Lorentz profile. γ_f is the full width at half maximum of the distribution.

Classical electromagnetic theory predicts a definite value for γ_f; in wavelength units [14,15]

$$\Delta\lambda_c = \frac{2\pi c}{\omega_o^2}\gamma_f = \frac{4\pi e^2}{3mc^2} = 1.16 \times 10^{-4}\ \text{Å}. \qquad (13)$$

This width is very much smaller than those actually observed in laboratory or stellar spectra.

The quantum mechanical analogue is constructed by assuming the radiation to arise from transitions of a molecule from an excited state to the ground state. Because of the universal relation

$$A_{ji} = \frac{8\pi h\nu^3 n^3}{c^3} B_{ij}$$

between the Einstein coefficient of spontaneous emission, A_{ji} and coefficient of absorption, B_{ij}, where i and j are the lower and upper levels of the transition respectively, the intensity of absorption is proportional to that of emission for a single atom. Here, n is the index of refraction. Hence, we are at liberty to apply either point of view.[15]

The probability of finding that molecule in the excited state j is

$$P_j(t) = \psi_j^* \psi_j\, e^{-\Gamma t} \qquad (14)$$

where $\Gamma = A_{ji}$ is the reciprocal mean lifetime of the originating state. ψ_j is the statefunction.

The upper state is no longer infinitely sharp but has some spread in energies due to its construction as a superposition of various energy states, consistent with the Heisenberg uncertainty principle. The upper state is no longer

strictly stationary and the lifetime of the state is limited by the decay to zero of the probability for its existence. The frequency distribution of the emitted radiation is identical in form to Eqn. 12, but not in interpretation:

$$P(\omega) = \frac{\Gamma/2\pi}{(\omega-\omega_o)^2+(\Gamma/2)^2} \qquad (15)$$

Even though the decay may be long, the time is finite and the Fourier transformed distribution never vanishes. If the initial state decays by radiation only, then Γ is identical to γ_f of the classical treatment. Doppler broadened astrophysical lines are theoretically broadened in this manner in low density media. The Lyman-α line of atomic hydrogen in interstellar space is a good example.

§ 2.3 - Pressure Broadening

Spectral line profiles may also be broadened by changing the absorber concentration in the radiation path. This broadening arises due to the forces which exist between the interacting species. Half-widths of these lines always contain a term due to radiation damping, as well. These forces depend upon the state of excitation of the various species, upon the angle of encounter for polar molecules and upon whether or not the molecules possess permanent dipole moments.

Broadening has been treated in two limiting cases. When the collisional velocities are sufficiently small, the

line profile is predicted by statistical theory. When encounter velocities are large, the impact theory of Lorentz is applied.[17]

§ 2.4 - Statistical Theories of Line Broadening

Here, the molecule is considered to be radiating within the field of an ensemble of perturbers. This ensemble gives rise to some field which will fluctuate about some mean value in a statistical way. At a given value of the field, the energy levels of the radiator will be slightly shifted. Correspondingly, the line frequency will be altered. The intensity of the radiation at some specific frequency shift will be proportional to the statistical frequency with which the perturbation of the appropriate field strength occurs.

§ 2.5 - Impact Theory of Line Broadening

Alternatively, impact theories assume that the molecule undergoes a collision that occurs essentially instantaneously. The collision interrupts the radiating wavetrain by introducing a sudden phase shift, or by inducing a transition. The effect of these collisions is to start and stop the radiator in intervals of finite duration. Fourier analysis leads to a spread in frequency of the radiated wavetrain. When averaged over all atoms within the ensemble,

the result is a broadened spectral line whose shape is given, once again, by the Lorentz profile.

These instances represent limiting cases to more general theories. Many modifications of the impact theory [14,18,19] have been undertaken, particularly by Weisskopf and Lindholm.

The physical mechanism assumed by Lorentz[20] entails the absorption or emission of a sharp frequency, ν_o, during the time between two collisions. Each collision completely stops the radiating process: electronic vibration energy being wholly converted into kinetic energy. The theory is an impact theory in its purest form. This line profile is also applicable to collision broadened lines due to vibrations and rotations of the molecule as a whole. It is expressed below in slightly different form. This form will be directly useable in subsequent developments which predict the equivalent width of blended molecular absorption lines.

§ 2.6 - The Lorentz Profile

The Lorentz profile is usually expressed as[21]

$$k(\nu) = \frac{S\gamma}{\pi} \frac{1}{(\nu-\nu_o)^2 + \gamma^2} \qquad (16)$$

for molecular absorption lines, where

ν_o is the line center frequency,

ν is the frequency of interest,

γ (henceforth) is the half-width at half-intensity of a plot of $k(\nu)$ with frequency (in cm^{-1}) and

S is the line strength or line intensity.

The line strength is directly related to transition probabilities and level populations within the molecule. It is given by

$$S = \int k(\nu)d\nu, \tag{17}$$

which by the Fuchtbauer--Ladenburg relationship[22] becomes

$$S = \frac{c^2 A_{ji}\, g_j}{8\pi\nu_o^{\,2} n^2 g_i} \left(N_i - \frac{g_i}{g_j} N_j\right) \tag{18}$$

where n is the index of refraction,

$g_{i,j}$ are statistical weights for levels i, j and

$N_{i,j}$ are the lower and upper level populations.

Normally, the line strength is expressed as

$$S = S' \ (cm^{-1}/g\ cm^{-2})\ \rho \tilde{=} S^{o}\ (cm^{-1}/atm)\ p \tag{19}$$

In addition to the line shape, the line strength and half-intensity half-width are the most revealing quantities sought in molecular interaction studies.

A method often employed to determine the strengths of individual lines entails broadening the lines at high pressure in order to force γ to greatly exceed σ. This reduces the instrumental modification of the true spectrum.

In this case, the strength of the entire band is measured. Individual line strengths may then be computed from quantum-theoretical formulae which relate those strengths to the band strength.[12] However, at pressures $\sim$ 50 atm., the band strength per unit pressure itself becomes a function of pressure.[23] This accordingly influences derived line strength values (for polar molecules).

To measure individual line parameters, experimenters usually work under two sets of advantageous conditions. When radiation traverses a short path of gas at high pressure, energy is removed from the beam at or near line center. The line then absorbs in the linear region of the curve of growth (see Fig. 5). When Lorentz lines are measured in the linear region, the line strength is directly derivable from the equivalent width: $W = S'\rho\ell$.

In contrast, a long path may be utilized at lower gas pressures. Here, because the total number of absorbers is large, there is considerable absorption at frequencies far from the line center. Energy at frequencies at or near to the line center will be completely removed. In the square root region, which these conditions typify, the equivalent width of Lorentz lines $W = 2(S'\gamma\rho\ell)^{1/2}$. In concert with strength measurements from the linear region, square root measurements yield half-width values.

Here, investigators seek to measure S' or S° for as many lines as possible in a vibration-rotation band. This

allows the relative line strengths within the band to be compared to theory. Secondly, the strengths of various vibrational bands of a particular molecule, $S_v^\circ = \sum_J S_{v,J}^\circ$, may be evaluated. These band strengths may then be related to the electric dipole moment of the molecule. This in turn indicates the character of the bonding within the aggregate of atoms.

For the case of pure rotational transitions such as observed in interstellar space, the line strengths may be related to the oscillator strengths, or f_J values. For a transition from state J_i to state J_j,[24]

$$f_J = (mc^2/\pi e^2 N_{J_i})S \tag{20}$$

where N_{J_i} is the number of molecules cm^{-3} in the medium that initially lie in the lower rotational state.

The half-intensity half-width for a Lorentz line may be written as[16]

$$\gamma = \gamma_o(cm^{-1}/atm)\ p \sim \gamma'(cm^{-1}/amagat)\ \rho \tag{21}$$

or, for gas mixtures

$$\gamma = \sum_i \gamma_i {}^{\circ}p_i \sim \sum_i \gamma_i \rho_i \tag{22}$$

where i denotes the individual species and 1 amagat equals 1 $gram/cm^3$.

Other techniques for determining S and γ are given in Ref. 16.

> Of the variety of techniques listed by Benedict, the equivalent width measurement is to be thought of as most directly yielding the Lorentz γ_o in as much as it most heavily weights the regions of low $(\nu-\nu_o)$ which are most certain to be governed by the impact shape.

§ 2.7 - Temperature Dependence of S and γ

Line strengths and widths depend upon the temperature. For measurements in the vibration-rotation region, when T varies, it is best to reduce all measurements of S to some standard temperature, T'. Hence,[11]

$$\frac{S(T)}{S(T')} = \left(\frac{T'}{T}\right)^{3/2} \left\{\frac{1 - e^{-1.4388\nu_0/T}}{1 - e^{-1.4388\nu_0/T'}}\right\} e^{1.4388\left(\frac{1}{T'} - \frac{1}{T}\right)\nu_i} \tag{23}$$

where ν_i is the lower state energy of the transition in cm^{-1}. Values for the Planck and Boltzmann constants and c have been inserted. It has been suggested that the second factor should be set equal to unity[25] but a small error accrues by following this practice.[11]

The temperature dependence of the half-width is given by[26]

$$\frac{\gamma(T)}{\gamma(T')} = \left(\frac{T'}{T}\right)^n \tag{24}$$

where n, which equals 1/2 in the kinetic theory,[27] must be measured for each gas composition. It appears in the literature for H_2O - N_2 collisions.[26] Because all experimental data reported herein was collected at 300K $\pm$ 2K (within 2K of the temperatures at which the employed S values were measured by other investigators), no temperature correction has been applied to S or γ. However, $u = \rho\ell$ (see Eqn. 30) was corrected for temperature variations.

§ 2.8 - Doppler Broadening

Thermal motions of the molecules in a gas will contribute to the diffuseness of an absorption line. If a gas can be characterized by a temperature, T, then the velocity distribution of its molecules will be Maxwellian. The probability of finding a molecule with a velocity along the line of sight between ξ and $\xi + d\xi$ will be

$$P(\xi)d\xi = \frac{1}{\sqrt{\pi}} \exp(-\xi^2/\xi_o^2)\, d\xi/\xi_o \qquad (25)$$

where

$$\xi_o = (2kT/m)^{1/2} = 12.85 \frac{T^{1/2}}{10^4 M} \text{ km/sec.}$$

If an experimenter observes the gas at frequency ν, the molecule with velocity component ξ actually absorbs at $[\nu - \nu(\xi/c)]$ in its own reference frame. If all of the absorbers were at rest, they would absorb at the sharp frequency ν_o, showing only the natural line width when observations are made with a (hypothetical) instrument of infinite resolving power at low pressure.

The Doppler line absorption coefficient

$$k_D(\nu) = ((\ln 2)/\pi)^{1/2} (S/\gamma_D) \exp\{-(\ln 2)[(\nu-\nu_o)/\gamma_D]^2\} \qquad (26)$$

where

$$\gamma_D = [2 \ln 2/(mc^2/kT)]^{1/2}\nu_o \sim 3.58 \times 10^{-7}(T/M)^{1/2}\nu_o. \qquad (27)$$

Here, T is the absolute temperature in K, M is the molecular weight and γ_D is the Doppler half-width.

Figs. 6 and 7 show plots of γ_D for various temperatures as a function of frequency for the H_2O and HCl molecules respectively. At room temperature, the near infrared Doppler half-widths are $\sim$ 0.002 to 0.008 cm^{-1} for HCl, DCl, CO, CO_2 and H_2O ($\nu \sim$ 1800 to 6000 cm^{-1}).[16]

Thus, while the natural line width is approximately frequency independent on a wavelength scale (see Eqn. 13), Doppler broadening on a wavelength scale diminishes at smaller wavelengths and may be neglected relative to natural broadening in the X-ray region. These two broadening effects become of equal magnitude at $\lambda \sim$ 100Å.

§ 2.9 - The Voigt Profile

The absorption coefficient for each molecule in the gas may be written as $k[\nu-\nu(\xi/c)]$. The total observed absorption coefficient is $k(\nu) = \int_{-\infty}^{\infty} k[\nu-\nu(\xi/c)]\, P(\xi)d\xi$.

This coefficient describes the combined effect of either collisional or natural broadening with the Doppler effect. It finds application in density transition regions where neither profile is applicable by itself. It is usually written as $k(\nu) = k_{DM}(\nu)\, H(a, \nu-\nu_o)$. Here, $k_{DM}(\nu)$ is the maximum value of the absorption coefficient for a line with pure Doppler broadening and $H(a, \nu-\nu_o)$ is the dimensionless Voigt function. The parameter $a = a(p) = (\ln 2)^{1/2} (\gamma_L/\gamma_D)$. Extensive tables of the Voigt function appear in the literature.[14]

The equivalent width of a molecular absorption line, $W = \int A(\nu)d\nu$, is ordinarily proportional to pressure. The pressure limit below which the equivalent width of a single line is no longer linearly proportional to pressure is reached when the contribution to W by the Doppler profile can no longer be ignored. An expression appears in the literature[16] for a single absorption line which gives the actual equivalent width in terms of that expected from a purely Lorentzian line:

$$W/W_L = 1 + \frac{6}{16\pi} a^{-2}z^{-2} + \frac{180}{512\pi^2} a^{-4}z^{-4} - \frac{12}{32\pi^2} a^{-2}z^{-4} + \ldots \quad (28)$$

Thus, if $W/W_L > 1$, the measured equivalent width is influenced by Doppler broadening. Table 2 presents values of W/W_L for the fundamental band $^1H^{35}Cl$ P(8) isotopic line for the experimental conditions reported in Ch. 4. Of all the doublets observed, this doublet is most likely to show Doppler influence. This table shows that such influence is negligible once pressures of 4 torr are reached. All experimental pressures exceed this value.

Because Lorentz line wings fall off <u>much</u> more slowly than those of the Doppler profile, the opacity is still determined by the Lorentz contour even when $\gamma_L = \gamma_D$. The influence of Doppler broadening on the equivalent width of a heavier molecule will be even less, because $\gamma_D \sim (T/M)^{1/2}$ (see Figs. 6 and 7 and Ref. 28).

§ 2.10 - Other Broadening Mechanisms

The causes of molecular line broadening are many and complex. Each line may have its own particular shape. Many molecules do not show a net displacement between their positive and negative charge clouds. However, forces of attraction still exist between these molecules which broaden their spectral lines.

Fluctuating dipole moments are induced by temporary interactions among the neutral species. These moments tend to anti-align. The attraction between these molecules is described by a potential $u(r) \sim -\alpha^2/r^6$ where α is the polarizibility of the molecule. This attraction is responsible for deviations of the behavior of gases from the ideal gas law. As these deviations were described by Van der Waals, the residual forces are called Van der Waals forces. London[6] has treated these forces quantum mechanically and has found that they are due to the perturbation of the repulsive ground state by the higher electronic states of the system of two interacting atoms or molecules. He has called these attractive forces dispersion forces because they depend upon the same quantities as the dispersion of light by the gas, namely the strengths of the transitions to all excited states. The London forces exist for every molecular state although in general they are overshadowed by the stronger valence forces.

As a result of dispersion forces, two H atoms with parallel spins or two He atoms, which in consequence of valence forces repel one another strongly at small distances, attract one another weakly at large distances.

However, these forces are weak and need not be considered further here. Because only the first several rotation states are populated at room temperature in most HCl molecules, studied in Chs. 3, 4 and 5, the effect of resonance interaction is far more important[12] to this discussion.

§ 2.11 - Resonance Interaction

Binary collisions between molecules often result in the net transfer of energy from one molecule to the next. If the target molecule has energy levels capable of completely utilizing the energy of collision as internal energy, the interaction is said to be resonant. The interaction potential is long range, $u(r) \propto 1/r^3$. Resonance lines appear often in astrophysical spectra.

The shape of collisionally broadened resonance absorption lines in vibration-rotation spectra is generally taken to be Lorentzian[15,16,20,29]. Spitzer[17] has shown for resonance lines that the $|\Delta\nu|$

> must not exceed 0.30 $P_f^{-1/2}$ angstrom units . . . if the broadening is to follow the impact laws with a relative error not greater than P. Since the oscillator strength f is nearly unity for such lines it is clear that impact broadening is relevant only to the core of the line . . .

The Lorentz shape is nearly exact when $|\nu-\nu_0| \leq 1$ cm^{-1} (Refs. 12 and 16) but deviates slightly from the observed contour in the wings of the line where the line shape is governed by the specific intermolecular forces between closely colliding molecules.[16]

Experimental results from Benedict et al.[12] for HCl, Herget et al.[30] for HF, Varanasi et al.[31,32] for HCl and HF in a CO_2 atmosphere and Abels and DeBall[33] for NO reveal more absorption in the wings than in a Lorentz line of the same half-width. But the results from Benedict et al.[34] for CO, Winters et al.[35] and Burch et al.[36,37] for CO_2 show less absorption in the wings than in a Lorentz line of the same half-width. These non-Lorentz wings may have a small but noticeable effect upon half-widths determined from equivalent width measurements[12] but contribute very little to the band strength at low pressures[16] (at least for HCl). For the 0→1 band of HCl, the non-Lorentz contribution to the band strength amounts to $\sim 0.025\ P_{atm}$[12]. Hence, these deviations do not invalidate the use of the Lorentz shape. In view of the usefulness of that profile in calculating the radiative heat balance of Earth's atmosphere,[27,38,39] it was chosen as the basis for the overlapping analysis of Ch. 3.

The experimentation of Ch. 3 was undertaken in the "long cell" region of the curve of growth. The long path

allows more absorption to accrue at low pressure than would shorter cells.

As the number of molecules in an absorption path increases, two closely spaced absorption lines start to blend. When two lines have no effect upon each other, their equivalent widths merely add: $W_i = W_1 + W_2$. When they coincide, $W_c = (W_1^2 + W_2^2)^{1/2}$. Usually, neither extreme case holds exactly.

In order to utilize measurements of blended lines to recover molecular line parameters or environmental information, investigators must be able to ascertain how the observed blended equivalent width relates to the actual equivalent widths of the lines involved. It was, in fact, just such a concern which led Sakai and Stauffer (see next Chapter) to examine the overlapping problem. Instead of being concerned with just one gas path, they were concerned with the formation of a blended doublet partly in the atmosphere of Venus and partly on Earth. Telluric H_2O absorption clouded the Doppler shifted Cytherian lines in which their laboratory was interested. Their complex analysis greatly extended earlier pioneering but restrictive works. To this, we will now turn our attention.

CHAPTER 3

There are very few absorption lines in vibration-rotation band spectra that are not at least partially overlapped by the broad wings of adjacent lines. Nearly every line in the complex H_2O bands at 1.9μ and 6.3μ shows some blending and many nearly coincide. This renders the problem of locating baselines even more uncertain and alters the interpretation of observed equivalent widths.

Equivalent width measurements do not yield precise $S\gamma$ values unless the line being measured is completely free from overlapping adjacent lines. And the practical problem of accurately locating baselines must be solved. W is quite sensitive to inaccuracies in locating the 0% and 100% transmission reference baselines.

Even when these baselines are precisely known, if overlapping occurs the equivalent width will be less than it would be if the two lines could be measured separately. This deficiency must be corrected for. For this reason, the deviation, Δ, of the aggregate equivalent width of two slightly blended absorption lines from the sum $W_1 + W_2$ (when taken independently) is formulated in this Chapter. The deviation of two nearly coincident lines from their exactly superimposed value $(W_1^2 + W_2^2)^{1/2}$ is also studied, using resonance lines. Application of these studies is dependent,

of course, on an assumption within the theory: that the line is Lorentzian.

In 1913 Ladenburg and Reiche[40] integrated the absorption curve due to a collision damped resonance for a single isolated, pressure broadened spectrum line to yield the equivalent width. This was extended by Reiche[41] in 1956 to two equal, overlapping lines. It was 1964 before Sakai and Stauffer[42] were able to present a correction term, Δ, that allowed estimation of the equivalent width of two unequal Lorentz lines that were not totally independent. Their rigorous result was unwieldy, but they were able to find an approximate solution that was tractable if overlapping was mild. However, Plass[43] soon demonstrated that their result should be used with caution if either absorption accrued in the square root region. More precise formulations for the combined equivalent width appear in his paper, but they strictly apply only when the two line centers coincide, or, alternatively, when they display equal half widths. Sakai[44] then revised Ref. 42 to more exactly represent W due to two superimposed lines in the linear region but the extent of its applicability in the square root region is unclear.

Consideration of two overlapping lines, when they are nearly coincident in frequency, or independent, is greatly simplified when both lines are in the strong mode, i.e., well into the square root region of the curve of growth. The Lorentz absorption coefficient is then able to assume a

particularly simple and useful form.

This simplification allows estimation of the correction, Δ, giving the 1, 2, 5, and 10% deviations of the equivalent width from that estimated if conditions of coincidence or independence were strictly fulfilled. The technique employed is far simpler than those presented previously, and allows identification of substantially isolated lines over a wide range of experimentally realizable parameters.

§ 3.1 - Modifying the Lorentz Shape

Following Strong[21] I express $k(\nu)$, the Lorentz contour, for collisionally or naturally damped lines, in terms of the parameters

$$Z = \frac{s'u}{\pi^2 \gamma_o (P_{torr}/760) SB} \quad \text{and} \quad x = (\nu-\nu_o)/\gamma Z \tag{29}$$

where s' is the line strength, $cm^{-1}/(g\ cm^{-2})$

ν_o is the line center frequency, cm^{-1}

ν is the frequency of interest, cm^{-1}

γ_o is the half-intensity half-width of a plot of $k(\nu)$ with frequency, cm^{-1}/atm ($\gamma = \gamma_o P_{torr}$)

P_{torr} is the experimental pressure, torr

SB is the self broadening factor

SB is equal to unity if self-broadened values for the line half-intensity half-widths are used.

A new value of the self-broadening factor must be measured for each type of foreign gas encounter, however. For example, the H_2O molecule is $\sim$ 5.49 times more effective at broadening its spectral lines than is atmospheric N_2.

u, the optical path length, may be calculated as follows:

$$u = \rho\ell = \frac{M\ell}{V_o} \frac{P}{P_o} \frac{T_o}{T} \tag{30}$$

where M is the molecular weight of the gas

ℓ is the absorption cell path length in cm

V_o is the molar volume, 22400 cm^3

P_o is the standard atmospheric pressure, 760 torr

T_o is the standard temperature, 273.16K

Other symbols retain their meanings above.

The parameter z specifies the region of the curve of growth in which an absorption lies.

Using these parameters, the Lorentz absorption profile may be written as

$$k(x)u = \frac{\pi}{x^2 + (1/z^2)} \tag{31}$$

Strong has demonstrated that lines in the square root region of the curve of growth have $k(x)u = \pi/x^2$ when z, which is independent of pressure and equal to the Ladenburg-Reiche function in this region, is $\geq\pi$ (see Fig. 8). Strong's approximation to the Lorentz contour introduces at most a

1.7% error in A. This occurs at the modified frequency scale value of $x \sim 1.4$. If lines are strong enough such that $z \sim \pi^2$, this error falls to 0.2% which declines to 0.02% if $z \sim \pi^3$.

In the 93.5m absorption path at this laboratory, when $s' \geq 1$, $z > \pi$ for square root water vapor lines. For the HCl experiment reported in the following chapter, absorption lines with $J \gtrsim 8$ have z between $\sim\pi^2$ and π^3.

In addition, $(\int A_{Str}dx - \int A_{Lor}dx)/\int A_{Lor}dx = (W_{Str} - W_{Lor})/W_{Lor} \leq 0.0009$. In this strong mode the equivalent width of a single line may be written

$$W = \gamma z \int (1 - e^{-\pi/x^2})dx \qquad (32)$$

where the integration is over the extensive Lorentz line. The great extent of a Lorentz absorption contour may be realized from the fact that integrating out to x = 20 still misses 5% of W. For example, if $\gamma = 0.1$ cm^{-1} with $z = \pi^4 \sim 97$, then x = 20 corresponds to $\nu - \nu_o \sim 195$ cm^{-1}. Because of such extensive wings there are serious overlapping difficulties in the analysis of observations, although these wings are often buried in the noise. Here, A(x) (see Eqn. 5) is taken to be precisely measurable and unhampered by noise. This theoretical situation assumes the existence of an established baseline against which absorptions may be precisely measured. Corrections will be applied to experimental equivalent widths in Chapter 4 to include unobservable signal buried within distant line wings.

Here I consider only two absorption lines. If they are sufficiently separated to be strictly independent, then the combined equivalent width is

$$W_i = W_1 + W_2. \tag{33}$$

If, in contrast, they are completely coincident, then

$$W_c = (W_1^2 + W_2^2)^{1/2}. \tag{34}$$

In general, neither case holds exactly. Taking W_p to be the predicted equivalent width when overlapping occurs, I define ε, the departure from either independence or coincidence, as follows:

$$\varepsilon = 100 \frac{W_p - W_{i,c}}{W_{i,c}} \%.$$

§ 3.2 - The Combined Equivalent Width

W_p is predicted from the combined gas transmittance of two strong infrared lines with aggregate transmittance

$$\exp \left[- \pi \left(\frac{1}{x^2} + \frac{1}{y^2} \right) \right] ; \tag{35}$$

where the variables

$$x \equiv \frac{\xi}{\gamma_1 z_1} \qquad \text{and} \quad y \equiv \frac{\eta}{\gamma_2 z_2}$$

are measures of the distances from the respective line centers tailored to the particular lines, as illustrated by Fig. 9. The symbols ξ and η denote $(\nu - \nu_o)$ in the two lines.

To evaluate ε we shall let the equivalent widths of the two lines be various multiples of one another: that is,

$W_2 = fW_1$.

Accordingly, since $\eta = (\nu-\nu_1^\circ) + (\nu_1^\circ - \nu_2^\circ) \equiv \xi + \Delta\nu$; the combined equivalent width, W_p, is (36)

$$W_p = \int_{-\infty}^{+\infty} \left\{ 1 - \exp\left[\frac{-\pi\gamma_1^2 z_1^2}{\xi^2} \left(1 + \frac{f^2}{\left(1 + \frac{\Delta\nu}{\xi}\right)^2} \right) \right] \right\} d\xi$$

In the above notation, the subscript "o" which denotes a line center value is written as a superscript whenever a second index is attached to the particular parameter.

§ 3.3 - Evaluation

The parameter f was varied from 0.06 to 1.0, the lower limit being large enough to allow W_p to vary at least 5% from either W_c or W_i. At each value of f, $\gamma_1 z_1$ assumed values between 0.01 and 10.0 such that coverage of a desired range of half-widths was obtained when $\pi^2 \leq z \leq \pi^5$. As such, we consider aggregate equivalent widths in excess of 0.10 cm^{-1}.

As an example of the scope of these parameters, when $z = \pi^4 \sim 100$, and γ_o, where $\gamma = \gamma_o P_{atm}$, is 0.10 cm^{-1}/atm, then $\gamma z = 0.01$ as above corresponds to a pressure of 10^{-3} atm whereas $\gamma z = 1.0$ implies a pressure of 10^{-1} atm, and

$\gamma z = 10.0$ means a pressure of 1 atm, for self-broadening.

To demonstrate the meaning of the variable $\gamma_1 z_1$, a single self-broadened H_2O absorption line with $z \tilde{=} \pi^2$ and $\gamma_1 = 0.05$ has a strength, $S = \int k(\nu)d\nu = 37.91$ cm^{-1}/(g cm^{-2}). If $z \tilde{=} \pi^4$ and $\gamma_1 = 0.10$, then $S = 7581.99$, when observed in our 93.5m absorption cell at 287.7 K.

However, it is not mandatory that we adhere to an upper limit in z of π^5. Any $\gamma_1 z_1$ product such that $z \geq \pi^2$ within the above range of $\gamma_1 z_1$ is considered here.

This range of parameters allows a comprehensive appraisal of the strong lines in the tabulation for water vapor by Benedict and Calfee[45] when it is reviewed to select lines that are close enough in frequency to be pressure broadened into coincidence, or separated sufficiently to be realizable as independent. In each case conditions are defined under which lines are suitably isolated to be experimentally investigated and theoretically interpreted.

Figs. 10, 11, 12, and 13, of variable ordinate scale, define zones of independence and coincidence for two absorption lines which fall completely within the passband of the spectrometer. These figures plot f as abscissa and the separation of the lines, $\Delta\nu$, as ordinate. Solid lines employ one-tenth of the printed $\Delta\nu$ scale and represent that wavenumber separation, for a particular ratio of equivalent widths, at the $\gamma_1 z_1$ dictated by the experimental conditions, beyond which the equivalent width of the two lines no longer coincides

with W_c to within ε*%; where $\varepsilon^* = 1$ in Fig. 10, $\varepsilon^* = 2$ in Fig. 11, $\varepsilon^* = 5$ in Fig. 12, and $\varepsilon^* = 10$ in Fig. 13.

Broken curves employ the printed ordinate, $\Delta\nu$, and present the $\Delta\nu$ beyond which W_p for the two lines is within ε*% of W_i. It is seen that two equal strong lines with $z = \pi^4 \sim 97$ and $\gamma_o = 0.10$ cm^{-1}/atm must be separated by 1.75 cm^{-1}, if $p = 10^{-2}$atm, and by 175 cm^{-1}, if $p = 1$ atm, before achieving independence to within 1%.

§ 3.4 - Polynomial Representation

A useful feature of this development arises when f is plotted as abscissa with $x' \equiv \Delta\nu / \gamma_1 z_1$ as ordinate. In this representation, all solid curves converge to a single line at each of the four considered percentages. The behavior of the broken curves is similar. These eight lines are described by polynomials that requre only knowledge of the individual line strengths, half-widths, and optical path length of the employed absorption cell (such that $z \geq \pi^2$) to be useful. Their form is

$$x' = \sum_{i=0} a_i f^i$$

where the a_i appear in Table 3. If this is multiplied by $\gamma_1 z_1$,

$$\Delta\nu_{\varepsilon^*} = \gamma_1 z_1 \sum_{i=0} a_i f^i \qquad (37)$$

This equation may be used to obtain values of $\Delta\nu$, accurate to two decimals, which must separate two lines in order for the various deviations from coincidence or independence to hold.

Table 4 demonstrates the usefulness of these equations in reproducing Figs. 10, 11, 12, and 13.

§ 3.5 - Correcting for Slight Departures

The deviation, Δ, is evaluated using Eqns. 33 and 34:

$$W_i = W_1 (1 + f) \tag{38}$$

$$W_c = W_1 (1 + f^2)^{1/2}. \tag{39}$$

where W_1 is the strongest line of the pair. These are used in the defining relation for ε. For example, when $W_p = W_1 + W_2 - \Delta = W_i - \Delta$, then

$$\Delta_i = (\frac{\varepsilon}{100}) W_i = (\frac{\varepsilon}{100})(1 + f) 2\pi \gamma_1 z_1. \tag{40}$$

Similarly,

$$\Delta_c = (\frac{\varepsilon}{100}) W_c = (\frac{\varepsilon}{100})(1 + f^2)^{1/2} 2\pi \gamma_1 z_1. \tag{41}$$

Predicted values for Δ from Eqns. 40 and 41 appear in Table 5. Where applicable, the expressions presented here are easier to employ than even the tractable solution of Sakai and Stauffer or Sakai which necessitate use of the Ladenburg-Reiche function, and are less restrictive than the results of Plass.

The result is applicable only to square root lines. When $\nu^\circ_1 = \nu^\circ_2$, the above Δ_c vanishes, and the formulation of W_c is completely equivalent to Eqn. 9 in Ref. 43 (see Table 6).

§ 3.6 - Applications

An opportune test of this procedure is afforded by the isotopic doublets in the 0→ 1 vibration-rotation band of HCl.

In this case, lines from identical transitions in the two isotopic species are separated by $\sim 2\ cm^{-1}$, while adjoining doublets lie $\sim 20\ cm^{-1}$ away. This is treated in Chapter 4.

The S and γ_o calculations of Benedict and Calfee for H_2O and CO_2 infrared lines represent an intricate mixture of molecular theory with experiment. Of these, many of the line parameters need further experimental verification since agreement is only fair between individual experimenters.[46] Three water vapor lines have been examined by many investigators, ν_o = 1429.96, 1447.98, and 1464.93 cm^{-1}, because these strong lines seem substantially isolated from their nearest strong (or square root) neighbors. Table 7 lists these lines together with strong lines to either side. Each of these may be examined for its influence upon the derived line parameters of the appropriate fundamental line. In particular, using the optical path and maximum pressure (3.5 torr) reported by Fridovich and Kinard[46], and the nitrogen broadened line parameters of Benedict and Calfee[45] adjusted to produce values for γ_o consistent with self-broadening, I find these three lines to be independent of all of their strong neighbors to better than 1%. The Doppler profile does not influence the line contour at these pressures. The wavenumber separations at which two lines of these parameters become independent to within ε = 1% are also given in Table 7, as well as the actual separation for comparison.

To stress the role of pressure, when two strong lines whose S and γ_o parameters are identical to those of ν^o_1 = 1447.98 and its neighbor at ν^o_2 = 1452.08 are examined at 3.5 torr, as above, then they must be separated by 1.06 cm^{-1} to be completely independent. If, however, p = 14 torr, the critical separation rises to 4.23 cm^{-1}. Thus, overlapping becomes important for this pair, physically separated by 4.10 cm^{-1} at pressures in excess of 13 to 14 torr.

Preliminary applications of these overlapping criteria to the 6.3μ water vapor band at multiple pressures, between 1400 and 1700 cm^{-1} (5.88μ to 7.14μ), reveals 70 lines independent of strong neighbors at p = 0.5 torr, 65 at p = 1 torr, 47 at p = 2 torr, with 14 remaining as the pressure is increased to 8 torr in our 93.5 m cell. These are tabulated in Table 8. Each of these remains to be examined for influence of weaker neighbors and no account has been taken of the recently found continuum absorption.[7] Such influence will decrease somewhat the above number of lines, particularly at higher pressures.

These procedures have been subjected to experimental analysis by measuring self-broadened absorption lines in the HCl fundamental band. This experiment is described next.

The results of these tests then suggest a further experiment whereby the accuracy of the Lorentz line shape assumption may be tested. In this instance, the validity of

employed S and γ values is already known. This is treated in Chapter 6 and is applicable to a variety of gas mixtures and interaction potentials.

CHAPTER 4

It is the purpose of this Chapter to verify experimentally the analysis of Chapter 3 using new absorption measurements of pure HCl gas in a 3.34 m path. Since S values for the HCl fundamental vibration-rotation band published by various experimenters do not agree, and additional purpose is to resolve that discrepancy (see Table 9). At the pressures and temperatures used in this experiment, only collision self-broadening is important. Room temperature Doppler widths are $\sim$ 0.003 cm^{-1} and even at the lowest pressures used here, $W/W_L \sim 1$ (Eqn. 28) for the weakest observed lines (1.008 at 4 torr for P(8)).

§ 4.1 - The Advantages of Using HCl

The HCl molecule has been extensively studied since its vibration-rotation spectrum consists of widely spaced, broad lines whose width depends upon the rotational quantum number. These lines are doublets due to the natural presence of two HCl isotopes. Contour measurements on the "outside" wings of these doublets are able to be made to relatively great distances from line centers.

The fundamental band lies in a region of the spectrum that is nearly free of overlapping atmospheric absorption bands and where sensitive photo-conducting detectors facilitate the use of high resolving power.

The isotopic rotation doublets from $^1H^{35}Cl$ and $^1H^{37}Cl$ are separated $\sim$ 2 cm^{-1}. They are shown in Fig. 14 at five pressures ranging from $\sim$ 2 torr to $\sim$ 1 atm. Each doublet contains lines from identical transitions in the separate isotopes. The ratio of their integrated fractional absorptances are uniquely calibrated by the chlorine abundance ratio. Fig. 15 shows the P(5) doublet observed in the detail necessary to record accurately the absorption contour. It typifies the quality of the spectra in this experiment.

Adjoining doublets lie $\sim$ 20 cm^{-1} ($\sim$ 10 times the internal doublet spacing) to either side. They do not influence one another in the 3.34 m path until pressures $\sim$ 0.1 atm at 300 K are achieved. Each spectrum of the band is run at one pressure and gives 17 individual blended doublets. Each of these may be compared directly with the analysis of Chapter 3 in the manner described below.

§ 4.2 - The Experiment

The aim of the experiment was to examine nearly independent lines. The amount of absorber present in each spectrum was increased so as to gradually pressure blend isotope lines within each rotation doublet. At each pressure, equivalent widths were measured for each doublet as a whole. These measurements progressively deviate from the sum $W_1 + W_2$ of two separated lines. The amount of this variation, as

well as the pressure at which a certain variation occurs, is predictable from Chapter 3. These predictions are based upon published S and γ values. As higher and higher pressures are considered, two theoretical lines would initially need to be more widely separated to maintain a specific deviation of W from $W_1 + W_2$. For an actual pair of HCl lines (see Eqn. 37), $\Delta\nu$ is defined and that pressure may be selected for a particular

$$\varepsilon = 100 \frac{W - W_i}{W_i} \% \tag{42}$$

which just causes the pair to blend by $\varepsilon^*\%$. Here W_m is the measured blended equivalent width of the entire doublet and $W_i = W_1 + W_2$. Pressures necessary to blend a doublet to $\varepsilon^* =$ 1, 2, 5 or 10% are found by using new coefficients a_n (see Table 3) in the power series,

$$\Delta\nu = \frac{u(p)}{2\pi}^{1/2} \sum_n a_n \frac{[S_{37}\ \gamma_{37}(p)]^{n/2}}{[S_{35}\ \gamma_{35}(p)]^{(n-1)/2}} \tag{43}$$

In this 3.34 m cell, the HCl lines ($J \leq 8$) were all absorbing in the square root region of the curve of growth. Comparison was then made between the measured doublet equivalent width of the R(7) line and predictions based upon Chapter 3, as a function of pressure. S and γ are fairly well established for this line[12,31,47] (see Table 9) and it therefore serves to test the merit of the analysis of Chapter 3. Once the validity of the procedure was established, the comparison was repeated for the remainder of the lines ($J \leq 8$)

in the P and R branches of the band, based upon different sets of S and γ. The predicted pressures depend upon the $(S\gamma)_{35,37}$ values used. These pressures are then used to predict alterations to $W_1 + W_2$ to account for blending. Comparison to experimental blended equivalent widths provides a test of the validity of each $S\gamma$ product.

§ 4.3 - Apparatus Details

The experimental apparatus is diagrammed in Fig. 16. A Pfund, triple pass cell, using ten-inch diameter f/4 perforated mirrors was used. These mirrors were made of quartz and were coated with gold. The cell length was directly measured by hand. Chopped radiation from a current stablized Nernst glower was directed onto the entrance slit of a Perkin-Elmer Model 210-B monochromator and subsequently onto the thermocouple detector. Fig. 17 demonstrates the available resolution.

The cross hatched area indicates the most often employed corrected slit width (see Fig. 18) corresponding to a spectral resolution, σ, which varies from $\sim$ 0.5 to 0.6 cm^{-1} across the band. Frequency calibration of the monchromator was accomplished by observing the fundamental bands of the H_2O and HCl molecules. Published frequencies of these lines[12,48] (see Fig. 19) were then assigned. The resolution, σ is small compared to the isotope separation but large compared to individual line half-widths. Although the resolution is not

competitive with the state of the art using large gratings, transform spectrometry or laser sources, it is sufficient to achieve the desired results.

Spectra were examined with the 210-B monochromator working in the first order of a 240 line/mm grating. A cut on, long pass filter eliminated higher order, shorter wavelength spectra. The readout was displayed on a Brown strip chart recorder.

Radiation paths external to the cell and the associated imaging optics were purged with dry air (< 1 ppm H_2O) to eliminate unwanted water vapor intrusion. No spectral indication of this gas was observed nor was there any spectral indication of impurity gases in the Linde electronic grade HCl. Absorption lines from H_2O have presented a problem in at least one prior study.[13]

All spectra from which equivalent widths were measured were recorded at 0.25 cm^{-1}/min using a single filter 30 sec time constant. This allowed at least four time constants per resolution element.

Temperatures were 300K $\pm$ 2. Pressures, measured with a 1μ to 5 torr McLeod gauge and a 1.5 atm absolute Hg manometer read by a cathetometer, ranged from 2 to 70 torr. A few scans of the band were made at pressures as high as 750 torr. At these higher pressures (see Fig. 14) the rotational structure of the lower J doublets completely disappeared. Only lines with $J \geq 10$ were measurable at $\sim$ 1/2 atm and $J \geq 14$ at $\sim$ 1 atm.

Prior to gas admission, the cell ($\sim 9.5 \times 10^4$ cm^3) was evacuated to a pressure of 30μ and maintained at that pressure for 24 hours to allow the system to outgas. HCl was then slowly admitted to the desired pressure and a scan of the R(7) line was made. Following a subsequent scan of the entire self-broadened band, the R(7) measurement was repeated. This technique monitored the reproducibility of the measured line contour. It also supplied extra data for the important R(7) line which was used to insure the validity of the analysis of Chapter 3.

Once this series of scans at one pressure had been accomplished, the HCl was evacuated through a liquid nitrogen trap and subsequently boiled away through a solution of NaOH. The brackish water was then discarded.

A list of possible impurities (none were spectroscopically detected) was supplied by the Linde Company. These appear in Table 10. Fig. 20 shows the vapor pressures of HCl and of these (possible) impurities as a function of temperature.

§ 4.4 - NaF Windows

Broad, apparently continuous "bands" in the 2800 to 2000cm^{-1} region have been observed when HCl is brought into contact with alkali chloride films deposited at low temperature onto polyethylene substrates. These presumably arise from adsorption. Evacuation at 190 K for 2 to 3 hours entirely removed these "bands"[49]. Although coated polyethylene

substrates are not used as windows, the interaction of HCl with the alkali chlorides is of considerable interest here. If adsorption occurred during an experiment, upper P branch baselines would be altered.

Adsorption of HCl to NaF produces quite different infrared spectra from the above. Once HCl adsorbs to the NaF substrate, the transmitted intensity actually rises relative to measurements made before gas contact. This has been interpreted as a reduction in the general scattering of the film above 2000 cm^{-1}.[49] Otherwise, there is no change introduced into the background spectrum over the frequency range of the HCl fundamental. "Bands" which do occur near 1600 cm^{-1} were more permanent than those involving alkali chloride films. Evacuation at 200 K for 6 hours had no effect.[49] Hence, if such bands were to appear using NaF windows in the frequency range of interest after longer contact times, they would have still been apparent after cell evacuation.

Disagreement among various investigators regarding line strength values, shown in Table 9, is greatest in the P branch. Accordingly, NaF was used as the window material. This material, 3 mm in thickness, has a high transmittance at the HCl frequencies.

Scans made before and after nearly 500 hours of gas-window contact at pressures as great as 1 atm confirmed the expected lack of adsorption from 2700 to 3100 cm^{-1}.

§ 4.5 - Baselines

Equivalent width measurements were not made when overlapping from adjacent doublets was observed. Estimating reference baselines in one of the most difficult problems in interpreting observed spectra. On a chart recorder trace of an absorption spectrum, the level corresponding to 0% transmission (see Fig. 3) may be found by observing chopped continuum radiation from a source whose temperature is identical to that of the chopper. It may also be found by examining the cores of opaque lines as done here, when the gas, chopper and source temperatures are the same. In the present experiment, the same level could be obtained simply by blocking radiation from falling on the thermocouple detector (50 nv sensitivity).

However, estimation of the 100% transmission level, necessary for fitting theoretical contours to actual lines or for measuring equivalent widths, can be more difficult. Errors in locating its height can greatly affect equivalent width measurements because spectral lines have their greatest width at the 100% line.

Often the desired frequency interval is scanned without any absorber present, as in marginal cases here. This is used as the 100% reference line for a subsequent spectrum. However, the shape of that baseline (both 100% and 0% levels are referred to as baselines here) may change in the interim due

to slight changes in the ambient (or chopper) temperature, source brightness or system noise level.

Alternatively, if there are not any nearby lines whose absorption overlaps the region of interest, if the line profiles are symmetric and if there is no continuous absorption in the line, then regions "far" from the line center may be connected by a curve whose shape (linear here) depends upon the "color" distribution of the source intensity (i.e., a blackbody) and upon the type of dispersive element being used. Techniques presented in Chapter 3 for Lorentz lines in the square root region allow the amount of blending by nearby lines to be assessed. And when a Lorentz profile may be used, symmetric profiles for isolated lines are reasonably assured.

Strong[21] has developed a technique for estimating the 100% transmission level for square root lines by convoluting a triangular slit function, $s(\nu-\nu')$ with a Lorentz absorption contour for a variety of half-intensity half-widths, γ, line strengths, S, and spectral resolutions, σ. By measuring the inflection point slope, $\alpha = \frac{d\bar{A}}{d\nu}$ (see Eqn. 7 for the meaning of $\bar{A}$), the experimental product $\alpha\sigma$ may be formed which directly yields the peak absorptance, $\bar{A}_o$ using Table III in Ref. 21. Then the actual measured distance between the 0% transmission line and the absorption line peak, d, defines the distance on the chart paper between the baselines, D by (see Fig. 3):

$$\frac{d}{1 - \bar{A}_o} = D \qquad (44)$$

for lines which are not opaque at their centers.

This procedure has recently been applied to the present HCl spectra with disappointing results. It is the purpose of the next three sections to reassess the procedures of Ref.21 and to identify instances when it may be useful.

§ 4.6 - Basis of the Procedure

Table III of Ref.21 was recalculated by directly convoluting the Lorentz absorption contour with a triangular slit function (and normalizing). This contrasts subtracting the normalized convoluted transmission from unity as in Strong's paper. The results appear in Fig. 21 and agree completely with the aforementioned table. The procedure for locating baselines is derived directly from simple mathematical relations. Because lack of agreement between predicted and measured baselines here could implicate the assumed line profile, slit function shape or conversion of slit separation to spectral resolution, the discrepancy has been explored. The absorption line depth, and d, are exceedingly sensitive to the slit function shape. Slight deviations from the assumed triangular form could seriously hinder the application of the Ref. 21 procedure to observed spectra.

§ 4.7 - Application to HCl Spectra

Three isotopic doublets from the HCl 0→1 band (3.2 to 3.7μ) are shown in Figs. 22 and 23. All three lines lie within the square root region of the curve of growth. Because the low pressure HCl spectrum consists of widely separated rotation doublets, the baseline for each doublet may be accurately drawn by connecting interdoublet 100% transmission levels. When HCl pressures $\leq$ 20 torr, even the intradoublet baseline for lines with ratational quantum numbers J $\geq$ 5 recovered to the level of $\sim$ 100% transmission. Thus, the slopes of $^{1}H^{35}Cl$ lines should barely be affected by the wings of the $^{1}H^{37}Cl$ member of the doublet and not at all by adjoining doublets. This is particularly true for the P(8) line in Fig. 22. These hand drawn baselines are straight lines and offer a good comparison for baselines derived from line slope measurements. These two figures show wide discrepancies among predicted baselines as well as between most predicted baselines and the hand drawn line. It was especially surprising that slope #1 which follows the line profile in Fig. 22 predicted such a low baseline. Comparison with Fig. 23 shows that the change in baseline placement is not solely a function of the magnitude of the error made in estimating the slope as implied by Fig. 4 in Ref. 21. It depends upon the line being measured. It is not apparent how one should draw the tangent line nor is it apparent where the inflection point lies in

some spectra. Hence, it appears that more uncertainties are introduced into the baseline prediction by measuring contour slopes than by other methods.

§ 4.8 - Sensitivity of Baselines to Slope Errors

Figs. 24 and 25 show theoretical $^{1}H^{35}Cl$ P(8) line contours plotted for the present experimental conditions as a function of x (see Eqn. 29) for two different values of the spectral resolution. ν_o is the line center frequency and γz equals the equivalent width divided by 2π in the square root region (see Ch. 3 for further notation). These contours are a convolution of a square root Lorentz absorption line and a triangular scanning function. The calculated slope at the inflection point is drawn in. It should be noted that this slope together with the indicated values for σ correctly predicts the calculated peak absorptance in these two theoretical cases. The difficulty arises in applying the procedure to the cases of practical interest for which it was designed.

Plots of $\frac{d\bar{A}}{dx}$ and $\frac{d^2\bar{A}}{dx^2}$ are also indicated with the slope $\alpha = \frac{d\bar{A}}{d\nu}$ on the chart paper related to the slopes on Figs. 24 and 25 by

$$\frac{d\bar{A}}{d\nu} = \frac{1}{\gamma z}\frac{d\bar{A}}{dx} . \qquad (45)$$

For the P(8) doublet in Figs. 22 and 24 (3.34m path at 18.55 torr), $\gamma z = 0.058\ cm^{-1}$ and

$$\alpha = 17.24\ \frac{d\bar{A}}{dx} \text{ and } \frac{d^2\bar{A}}{d\nu^2} = 17.24\ \frac{d^2\bar{A}}{dx^2}\ .$$

Two striking features emerge from the theoretical plots:

A. Over the region from $x \sim 4$ to 7, it is difficult to visually perceive any change in the slope of the line contour, A(x), while in fact the curve $\frac{d\bar{A}}{dx}$ changes. The change is sufficient to cause a 5% error in the value of $\bar{A}_o$ which would be derived (see Fig. 26) if we could accurately measure various slopes in this region misinterpreting many as inflection point slopes. However, errors in the measured slope are more likely determined by noise fluctuations and erratic averaging by the eye than by our ability to measure barely detectable contour changes in this region.

B. As the spectral resolution increases, the inflection point becomes experimentally more precisely defined (the second derivative curve crosses the x axis at a sharper angle), but less of an expanse of the actual line contour is then representative of the inflection point slope. How the appropriate tangent line is drawn is still not well defined. Even on Strong's Fig. 4, the tangent line crosses the line contour without actually following its sides for very long.

Hence, it would seem that Strong's method might only be usefully applied to low resolution spectra [for P(8),

$\sigma \gtrsim 0.7\ cm^{-1}$] where the second derivative curve is more nearly horizontal. This largely eliminates the need to precisely define the location of the inflection point. This is because the slope stays nearly equal to α_i for some measurable segment of the line contour defining a tangent line ($\sim 0.27\ cm^{-1}$ for P(8) when $\sigma = 0.7\ cm^{-1}$).

The more generalized Fig. 27 shows that this is true only when $\bar{A}_o \lesssim 75\%$ (as in Figs. 22 and 24). Once $x_o \lesssim 3.5$, the precision to which the inflection point is defined is no longer as important as the rapid decline ($\bar{A}_o \gtrsim 80\%$) of Fig. 21 (large slopes but a small x_o value, where x_o is defined in Eqn. 51). A large slope change barely affects the derived value for $\bar{A}_o$ here.

The varying sensitivity of Fig. 22 and 23 baseline predictions to a standardized slope error arises because an initial experimental estimate of the 0% → 100% baseline separation, D, must be made in applying Strong's method. This estimate allows the vertical component of the slope actually measured, Δv, to be converted to $\Delta\bar{A}$, where $\bar{A}$ runs from 0 to 1, but depends upon the background radiation intensity level which is usually changing (i.e. a blackbody) with frequency. Similarly, the horizontal component Δh must be converted to Δv by taking into account the dispersion δ (cm^{-1}/inch) which depends upon the chart speed. Hence

$$\alpha = \frac{\Delta\bar{A}}{\Delta\nu} = \frac{\Delta v}{\Delta h} \cdot \frac{1}{D\ (\text{inches})\ \delta\ (cm^{-1}/\text{inch})} . \qquad (46)$$

For the three $^{1}H^{35}Cl$ members of the doublets shown in Figs. 22 and 23.

$$\alpha = \frac{\Delta v}{\Delta h} \times \begin{cases} 0.1498 \text{ for R(7)} \\ 0.2244 \text{ for P(8).} \\ 0.2639 \text{ for P(5)} \end{cases} \qquad (47)$$

This means that if the same value of $\frac{\Delta v}{\Delta h}$ were measured for each of these three lines, their slopes (and baselines) would be different. If a constant measurement error were added to each of these, the change of slope would also be different:

$$\Delta\alpha_i \text{ R(7)} < \Delta\alpha_i \text{ P(8)} < \Delta\alpha_i \text{ P(5).} \qquad (48)$$

The magnitude of the variation in predicted baselines also differs:

$$\Delta \text{ base R(7)} < \Delta \text{ base P(8)} < \Delta \text{ base P(5)} \qquad (49)$$

assuming a constant value for σ. This is precisely what is observed in Fig. 23 for the P(5) doublet. The difference between 100% baselines predicted by slope #1 and #2 is not even definable because the $\alpha\sigma$ product of the erroneously drawn slope #2 exceeds every theoretically possible value in Fig. 21 or in Strong's Table III. Hence, the proper slope would lie intermediate to the two drawn slopes. The change $\Delta\alpha$ between that new slope and α for line #1 would be so small that it would be difficult to measure. Yet, the resultant variation in predicted 100% transmission levels is very significant. The three baselines in Fig. 23 are labelled according to the

$\Delta v/\Delta h$ values which would predict those baselines. A difference in $\Delta v/\Delta h$ of only 0.24 changes the derived central absorption value $\sim$ 9%.

The effect on α_i of errors in measuring $\Delta v/\Delta h$ can be minimized by using a full scale chart deflection (opening the slits) which also decreases the resolution and allows slopes to be more precisely measured. It can also be minimized by using a chart speed which adequately presents the changes in the convoluted profile. Thus, except in low resolution spectra, it seems nearly impossible to consistently produce reliable baselines by the slope method.

In spectra where $\bar{A}_o$ is near unity, any slight deviations from the triangular scanning function alter d. These deviations are severely magnified in the prediction of D (see Eqn. 44).

§ 4.9 - An Alternative

The initial strength of Strong's technique was that it was empirical. If we relax that requirement and theoretically specify α, using only lines that have been assigned values of S' and γ, his table may still be used to derive baselines to within a few percent.

The difficulty in locating the inflection point or in correctly drawing the tangent line is circumvented by employing the following polynomial for a square root Lorentz

line (assuming a triangular slit function):

$$\frac{d\bar{A}}{dx} = \sum_i \eta_i \, x_o^{\,i} \qquad (50)$$

where

$$x_o \equiv \frac{\pi\sigma}{\sqrt{S'u\gamma}} \qquad (51)$$

Other quantities are defined in Eqns. 29 and 30. The coefficients η_i appear in Table 11.

Once the predicted value $\frac{d\bar{A}}{dx}$ is multiplied by the x_o value used to predict it, the product may be directly inserted into Table III of Ref. 21 or Fig. 21 here to find $\bar{A}_o$.

Of course, circumventing an actual measurement of α_i is not admirable, but apparently necessary. And it does not depend upon an initial experimental estimate of the 0% → 100% transmission line separation for its application.

Other schemes could be developed to predict the chart paper distance from line center to the inflection point position as a function of various parameters which retain the measurement of α. But baselines then would depend upon accurate measurements of ν_o and the problem of actually drawing tangent lines would still exist.

§ 4.10 - Wing Corrections

The area of each spectral doublet was measured at least 5 times with a Keuffel and Esser polar planimeter. All measurements for a particular line were later averaged. When divided

by the baseline separation and multiplied by the dispersion, these averages constituted the uncorrected doublet equivalent widths W'. W' does not include signal in the distant line wings which is buried in noise and is unmeasurable. Hence, this inconspicuous area must be corrected for.

The correction was accomplished by convoluting two Lorentz profiles and performing a computer integration of the remaining area beyond the variable frequency cut-off, $|\nu'-\nu_o|$ of the measurements. It amounts to $\sim$ 5% increase in the measured value of W.

Comparison was then made to the analytic correction scheme, Eqn.17b in Ref. 16. The latter method applies to solely one line, symmetrically about line center. By that method, when correcting a blended doublet for additional wing absorption, each line must be corrected separately. The largest frequency, $|\nu'-\nu_o|$, to which one can measure, depends upon the degree of overlap even though measurements could be extended further on the unintruded side. Table 12 tabulates this comparison for three HCl lines, P(1), R(5) and R(7) at low pressures where a complete recovery of the chart recorder trace to the apparent 100 per cent transmission line was observed within the doublet.

The entire doublet is measured in this experiment. No area is neglected due to the symmetry of the correction scheme. Corrections to the measured equivalent widths for the three aforementioned lines derived from the two methods agree well.

CHAPTER 5

In this chapter, the results of the experiment are discussed.

§ 5.1 - The R(7) and R(8) Lines: Testing the Theory

Fundamental band HCl line strengths of Benedict et al.[12] and Toth et al.[47] generally agree well as do those of Varanasi et al.[31] and Babrov et al.[13] For the R(7) and R(8) doublets, S values from Refs. 12, 31 and 47 for each isotope are nearly identical (Babrov et al. did not measure R branch strengths). Accordingly, line strengths from Benedict et al. and Varanasi et al. are used separately with Ref. 12 half-widths (Varanasi et al. did not measure self broadened half-widths) in Ch. 3 to predict the blended equivalent width of these two doublets. This is done using Eqn. 40 at the four predictable pressures where ε = 1, 2, 5 and 10%. These pressures are found using Eqn. 37. If the analysis of Ch. 3 is accurate, predictions based upon $S_{Ben}\gamma_{Ben}$ and $S_{Var}\gamma_{Ben}$ should agree at each of the four pressures. And because the line strengths for these two doublets are established, if Ref. 12 half widths are accurate, these predictions should also be identical with the low pressure HCl measurements. For these measurements measureable absorption only extends to $|\nu - \nu_o| \sim 1$ cm^{-1}, a

region where the Lorentz contour is quite useful.

The results are shown in Fig. 28. Equivalent widths, whether the theorectical or corrected experimental value, are plotted as ordinates with pressure plotted as abscissa. Observations are represented by solid dots.

Predicted equvalent widths based upon S and γ values from Benedict et al. are points encased by circles. Results based upon S values from Varanasi et al. and γ values from Benedict et al. are enclosed by squares.

The solid line, which should pass through the origin, is a linear least squares fit to the observations. As mild overlapping commences ($\varepsilon \neq 0$), the predicted equivalent width (see Eqns. 38 and 40) is

$$W_p = W^o_i \ (p - \varepsilon p/100). \qquad (52)$$

Here, p is the pressure in torr ($W_i = W^o_i \ p$) and ε is defined by Eqn. 42.

Plots of $\varepsilon/100$ as abscissa and $p - \varepsilon p/100$ as ordinate are not linear once ε exceeds $\sim$ 5%. Hence, W_p will no longer be linearly proportional to the pressure. Deviations from the least squares line should be expected theoretically and experimentally above pressures at which ε reaches this value.

The expected agreement among predictions based upon line strengths from these two contrasting sources, as well as their agreement in concert with the experimental results,

is striking. Tables 13 and 14 investigate the effect upon the pressure predictions of deviations in the values of S_{35}, S_{37} and γ from the published values. The resulting change in the respective predicted pressures would be easily detectable. This strongly supports the validity of the analysis of Ch. 3 to specify the deficiency in the equivalent width of two slightly blended lines from $W_1 + W_2$. It also supports its ability to predict the pressure at which specified percentage deviations, ε^*, of the blended equivalent width from $W_1 + W_2$ occur.

§ 5.2 - The Remainder of the Band

The line strengths of Babrov et al.[13] agree well with those of Varanasi et al.[31] when the two are able to be compared in the P branch. Thus, predictions from Ch. 3 based upon S and γ values from Babrov et al. provide a continuing contrast to those of Benedict et al. across the fundamental band. This is true as long as the shift from Ref. 12 half-widths in the R branch to Ref. 13 half-widths in the P branch introduces no error.

Babrov et al. make no distinction in their tabulation between $^1H^{35}Cl$ and $^1H^{37}Cl$ half-widths. Rather, they list a weighted average (3 to 1) of the two where the weighting is determined by the chlorine abundance ratio. Table 15 presents these with similarly averaged values calculated from Ref. 12. These results

> . . .may be compared directly. . . . The self-broadened line widths are in very good agreement (well within the experimental error of the two experiments). (Ref. 13)

If the agreement among the half-widths is good enough, then any trend in the predicted equivalent widths, to best reproduce the observations based upon parameters from any one of these experimental groups would allow identification of the most accurate line strengths to date. However, as was shown earlier in Table 13 for the R(7) doublet, even small variations between γ_{Ben} and γ_{Bab} are significant in the theoretical placement of the predicted points. The effect of γ variations becomes more pronounced as ε increases. Hence, the effects of inaccurate values of S (ΔS_{37} has a greater effect upon the pressure predictions than does an equal ΔS_{35}) and γ upon these predictions can not be deconvolved here in the P branch. Nor can they be in the R branch, except for R(7) and R(8), unless half-widths from Benedict et al. are assumed to be correct.

The results for the remainder of the band are shown in Figs. 29 through 42. Predictions based upon S and γ values from Babrov et al. are encased by triangles. Other notation remains the same as in Fig. 28. Equivalent widths per unit pressure for these lines are listed in Table 16.

The deviation of the predicted equivalent width of the entire doublet from the extention of the linear least squares fit is evident beyond $\varepsilon \sim 5\%$ in most of the

figures. This may especially be seen in Figs. 31, 32, 34 and 42 for the R(4), R(3), R(1) and P(8) doublets respectively. It may also be seen in the experimental equivalent widths when they are examined carefully. If the four predictions based upon S and γ from Babrov et al. (triangles) are examined in Fig. 41, a distinct downward deviation may be seen from the least squares line which is closely followed by the experimental points.

A permanent depression in the R(3)→R(4) interdoublet baseline was noted before any HCl gas was allowed to enter the system (perhaps due to the interference filter). Accordingly, most measurements of W for these doublets were unacceptable.

While R branch isotope lines within each doublet are more widely spaced than in the corresponding P branch lines, respective doublets are more closely spaced. Because of this, the pressures necessary to blend these lines to $\varepsilon^* = 10\%$ are sufficient to render baselines uncertain. This is due to the growing influence of the wings from adjoining doublets. Hence, for the R(8), R(7), R(6), R(5), R(1) and R(0) doublets in Figs. 28, 29, 30, 34 and 35, there are no experimental points with which to confirm this behavior at pressures such that $\varepsilon^* > 5\%$. This is also true for the P(7) and P(8) line pairs in Fig. 42.

§ 5.3 - Discussion

Equivalent widths predicted from Ch. 3, based upon the S and γ values from Benedict et al. closely predict the experimental doublet growth for all doublets within the R branch and for the P(2), P(4), P(5) and P(8) doublets. These are shown in Figs. 28 through 35, 37, 39, 40 and 42. As outlined in Table 17, seven doublets are equally well predicted by the S and γ values from Benedict et al. as by the S and γ values of Babrov et al. or by the S values of Varanasi et al. with γ values from Ref. 12. Even the growth of the P(1) doublet in Fig. 36 is best predicted by Ref. 12 parameters. Because of the paucity of experimental points for the latter doublet, the deviation between experiment and theory may not be as acute as it at first seems. These results confirm the accuracy of the $S\gamma$ products published by Benedict's group, with the possible exception of the P(1) and P(6) pairs.

In the R branch the same (but not necessarily correct) values of the half width are used with the Benedict et al. and Varanasi et al. S values separately. Clearly, the agreement of equivalent widths predicted by Ch. 3 using Benedict et al. line strengths does not negate Varanasi et al. S values. This follows because these predictions depend upon $S\gamma$ products. If the line strength measurements in Ref. 12 made in the linear region of the curve of growth

were in error, the Benedict et al. $S\gamma$ measurements in the square root region would yield <u>different</u> values for γ. The product $(S\gamma)_{Ben}$ would not change, but $(S_{Var}\gamma_{Ben})$ would! Hence, a distinction between S values is not possible in the R branch either. Table 18 lists the ratio S_{37}/S_{35} calculated from Refs. 12 and 31 for each doublet. This ratio is utilized by the analysis of Ch. 3 to predict pressures where various deviations from independence occur. When this ratio nearly agrees among these two investigators, predicted pressures for $\varepsilon^* = 10\%$ are more widely separated. They are more distinguishable than when these ratios more widely differ. Fig. 42 demonstrates both of these instances using the P(8) and P(7) doublets respectively. Even the P(4) doublet which appears in Table 9 to show the greatest disparity among the S_{35} measurements from the various experimental groups, displays this behavior. The respective equivalent width predictions are separated on the pressure axis of Fig. 39, but not as widely as might at first be expected. This trend may be seen in the other doublets, as well.

Equivalent widths have been predicted only at four pressures for each doublet. These pressures were predicted from Eqn. 37 using a different set of coefficients to predict the pressure responsible for each deviation $\varepsilon^* = 1$, 2, 5 and 10% from independence. However, the theory of Ch. 3 is applicable at any percentage ε once the pressure which causes that deviation is known. For

HCl, these pressures are predictable by interpolating Table 19 which assumes S and γ values from Ref. 12 and a 3.34m path.

Sporadic doublet equivalent widths at pressures $\sim$ 1/7, 1/2 and 1 atm have been measured at room temperature for lines with $9 \leq J \leq 15$. These are tabulated per unit pressure in Table 20. Figures have not been prepared for these doublets because they barely absorb in the square root region. Unlike Table 16, these values are <u>not</u> corrected for unmeasureable signal within the distant line wings, but the limits to which W has been measured are indicated.

CHAPTER 6

The practical merit of studies of vibration-rotation line shapes, line strengths and half-widths lies in obtaining more accurate representations of the infrared opacity of the atmosphere. This is of considerable use in meteorological, astronomical, environmental and geological studies, military weaponry and communications technology.

The difficult problem of calculating the equivalent width of a band of overlapped lines has been treated in the past by forcing all lines to have equal spacings and strengths[50], or by superimposing many such bands, each with its own internally constant spacing and line strengths.[51,52] It has also been treated by using a statistical distribution of spacings and line strengths.[53,54] But they do not provide analytic corrections to individual line equivalent widths nor do they specify the degree of blending by adjacent lines.

The procedure of Ch. 3 enables investigators to select accurate $S\gamma$ products for two square root lines whose strengths and widths have already been measured, but are not necessarily well known. Once many line strength values are known within a band, an accurate value of the band strength may be derived.[12] In the

special case where either the strength or half-width is well known, the value of the other may be specified.

For small equivalent width ratios, i.e. $f \leq 0.4$, ε doesn't exceed $\sim$ 24%. Here, slightly blended absorption lines may be ovserved as they coalesce due to pressure broadening. The pressures necessary for various stages of blending may be predicted assuming the formulations for nearly coincident lines to be valid as well.

When $f > 0.4$, lines may overlap by an amount whereby they are neither nearly independent nor coincident. The amount of influence at line center of line i by the wing of line j may be estimated by (see Ref. 21, section III-c):

$$A_{\text{wing at } \nu_o} = \pi \left[\frac{\sigma \bar{A}_{o,j}}{(\nu_j - \nu_o)} (6.154 - 3.9\, \bar{A}_{o,j}) \right]^2 \qquad (53)$$

where $\bar{A}_{o,j}$ is the instrumentally modified peak absorptance of line j.

The procudure outlined in Ch. 3 could be reworked and broadened to encompass the linear and transition regions of the curve of growth. The reasons for initially choosing the square root region were:

a) the particularly simple expression in that region for the equivalent width of a single, isolated absorption line, $W = 2\sqrt{S\gamma u}$,

b) Strong's[21] simplification of the Lorentz contour in that region, demonstrated here in Figs. 8 and 9.

The expressions for the equivalent width which appear at the outset of § 2.6 are specific examples of the more general relation $W = 2\pi\gamma f(\zeta)$. This applies to a single pressure broadened Lorentz absorption line in any region of the curve of growth. The function $f(\zeta)$ is called the Ladenburg-Reiche function and is plotted in Fig. 43. As it requires the use of low order Bessel functions for its application, L. Stover has published a convenient tabulation of the function in the literature[55].

A polynomial representation of Stover's table would allow further computer analysis of blended lines in other regions of the curve of growth. It would allow predicted equivalent widths to be monitored as in § 3.2 and 3.3 which used Eqn. 32 initially. Hence, blending among two absorption lines could be followed regardless of the absorption path length employed or the strength and half-width of the lines.

Such a polynomial was found and appears below. It also may be used in Sakai's[44] analysis. Coefficients d_i are listed in Table 21 where

$$P \equiv \ell n_e f(\zeta) = 2.309 \sum_{i=0}^{7} d_i (\log_{10}\zeta)^i \qquad (54)$$

and

$$W = 2\pi\gamma e^P. \qquad (55)$$

Here, $f(\zeta)$ is given by e^P.

In the square root region, $\zeta = \pi z^2/2$. Table 22 compares selected results from this polynomial with Stover's tabulation. Table 23 lists coefficients for a less precise representation of W, accurate to $\sim$ 2%.

§ 6.1 - Future Experiments

HCl overtone bands lie at higher vibrational frequencies in the near infrared. Line parameters are available for the lower bands. The 0→2 band at 1.77 μ provides an excellent extension to this work. In a 3.34m cell, the lowest 7 or 8 lines within the P and R branch of that spectrum absorb in the square root region of the curve of growth.

The wavenumber separation of the isotopic lines within each doublet is twice as large as in the fundamental band. For a given slit separation, using the present monochromator, the spectral resolution is roughly twice as poor at these shorter wavelengths, but the ratio of line separation to spectral resolution is maintained.

Higher pressure will be needed to blend these doublets to $\varepsilon^* = 10\%$ from $W_1 + W_2$. Even though higher pressures are utilized, only slightly overlapping lines are considered. The theory has been experimentally verified here for just that case. It is at these higher pressures that deviations from the Lorentz contour become more acute.

Accordingly, deviations may be searched for using lines whose S and γ values are known from low pressure measurements. This is done by searching for the conformity, or lack thereof, of predicted doublet equivalent widths to those experimentally measured.

The 0→2 band is of considerable interest since it has been detected in absorption in the scattering-absorbing Cytherean atmosphere.[56] Various interpretations have arisen concerning its origin.[57] As HCl is liberated from Earth's mantle by volcanic eruption, its presence on Venus may indicate past volcanic activity on that planet. Volcanic craters on the moon and the huge volcano on Mars[58] indicate such activity is not restricted to our planet.

When higher resolution is available, the isotope spectrum of HBr can be examined. Isotope lines in its fundamental are separated by 0.4 cm^{-1}, one-fifth that of the HCl fundamental. These lines may be pressure broadened until the isotope lines are completely superimposed ($W_p = (W_1^2 + W_2^2)^{1/2}$) at pressures low enough for the Lorentz assumption to be useful. The suitability of the analysis in Ch. 3 to describe nearly completely blended lines has been theorectically demonstrated earlier (see Table 6). However, it has never been <u>experimentally</u> tested for this extreme. The necessary precautions for using HBr as well as the interaction with NaF windows are similar to HCl.

The experiment here has confirmed the value of the self broadened half-width for the R(7) doublet since prior agreement among investigators for the line strengths in that doublet is excellent (see § 5.1). A final experiment may be constructed to test the validity of the Lorentz line profile as a function of various interaction potentials. This consists of pressure broadening only the R(7) doublet in a cell whose length is long enough to place the doublet absorption within the square root region. Otherwise, it is as short as possible so as to minimize the influence from the adjacent R(6) and R(8) doublets. Measured doublet equivalent widths can be compared to predicted values at $\varepsilon^* = 1$, 2, 5 and 10% exactly as done here, but including deviations from coincidence as well. This would use S values from Ref. 12 and half widths[59]

$$\gamma = \gamma_o p_{HCl} + \gamma_F p_F \ . \qquad (56)$$

Every time the experiment is performed, a new foreign gas is introduced to broaden the HCl line. Notation above is as follows: γ is the Lorentz half-width to be used in Ch. 3, γ_o is the (Benedict) self broadened half-width of either the $^1H^{35}Cl$ or $^1H^{37}Cl$ line, p_{HCl} is the HCl partial pressure, γ_F is the half width of the HCl line due to foreign gas broadening (per unit atmosphere) and p_F is the foreign (non absorbing) gas partial pressure. Values for γ_F are available for selected gases [12,29,31] in the

fundamental band and for a variety of gases in the P branch.[13] If these become generally available for gases of astrophysical interest for the R(7) doublet, the pressure "cut-off" of the ability of the Ch. 3 Lorentz predictions to portray experimentally blended equivalent widths may then be observed. This should be done for a variety of types of molecular interactions and will be indicative of the usefulness of the Lorentz line shape assumption in studies of these gases at various pressures. Recent evidence suggests that nearly every H_2O and CO_2 line may have its own unique shape.[60] Many of these profiles are now known to be asymmetric and hence slightly non-Lorentzian.

§ 6.2 - Epilogue

For spectra able to be examined in the square root region without appreciable influence from more than one additional line, and without influence from weaker, non square root lines, a selection of isolated absorption lines is now possible. The equivalent width of blended doublets is predictable when blending is present to a predictable degree.

The realizable benefit to spectra such as water vapor will be lessened due to the complexity of its line and continuum spectrum. However, if the analysis of Ch. 3 were extended to encompass the entire curve of growth and perhaps to more than two lines (or alternatively used in

conjunction with Ref. 44), application to more complex molecular spectra would be facilitated.

And further application to astronomy should be possible in the theory's present form. For example, the procedure could find application to size or abundance determinations in comets. This would involve directing the light from a comet through a laboratory absorption cell (or through the atmosphere) which contained the gas of interest within the comet. If the comet approached a segment of Earth's orbit which had not yet been traversed, its absorption lines would be Doppler shifted relative to the corresponding line in the laboratory cell. The magnitude of this shift would decrease to zero as the comet crossed our orbit.

The observed effect would be to produce a spectral doublet. One doublet line would arise in the comet. The other would result from the laboratory or atmospheric path of known length. As the Doppler shift decreases, the doublet would coalesce.

This technique, used in conjunction with other existing techniques which provide necessary input to the theory of Ch. 3 (i.e. abundance→pathlengths in the comet) could provide a valuable investigative tool. The greatest promise of the procedures of Ch. 3 though, lies in line shape studies in the laboratory.

TABLE 1.--Independence of the equivalent width of a single absorption line upon the monochromator resolving power for a square root line. Data are reproduced from Reference 12.

Slit Width (cm^{-1})	Equivalent Width (cm^{-1})	
	R(5) - $^{1}H^{35}Cl$	R(5) - $^{1}H^{37}Cl$
0.24	0.525	0.322
0.29	0.546	0.306
0.34	0.564	0.327
0.41	0.560	0.319
0.47	0.566	0.322
0.71	0.538	0.314
1.02	0.536	0.308

TABLE 2.--The effect of the Doppler Profile on W for the P(8) line of $^{1}H^{35}Cl$ (γ_o=0.13 cm^{-1}/atm) as a function of pressure. This is determined by Equation 28 for a 3.34 meter pathlength at 298.86 K.

P_{torr}	W/W_L
760.0	1.000
100.0	1.000
50.0	1.000
20.0	1.000
15.0	1.001
10.0	1.001
9.0	1.002
8.0	1.002
7.0	1.003
6.0	1.004
5.0	1.005
4.0	1.008
3.0	1.015
2.0	1.036
1.5	1.068
1.0	1.177
0.75	1.376
0.50	2.239
0.25	14.45

TABLE 3.--This table presents suitable coefficients, a_i, for use with the power series $\Delta\nu_{\varepsilon^*}=\gamma_1 z_{1i}\sum_{i=0} a_i f^i$. These polynomials predict the wavenumber separation at which the equivalent width of two absorption lines departs from W_c or W_i by ε^* = 1, 2, 5, and 10%. The series are applicable from $0.10 \leq (f = W_2/W_1) \leq 1.0$ except for the coincidence 5% and independence 10% cases, where the lower limit rises to 0.15, and the coincidence 10% polynomial which extends from 0.20 to 1.0.

i	a_i for 1%	a_i for 2%	a_i for 5%	a_i for 10%
		Coincident Case		
0	1.739	2.037	2.790	4.024
1	-7.502	-8.235	-8.636	-10.859
2	20.996	25.330	18.401	18.682
3	-31.724	-42.682	-13.297	-11.213
4	24.627	36.392	-11.358	-1.128
5	-7.537	-12.002	23.811	2.624
6	0.0	0.0	-10.302	0.0
		Independent Case		
0	1.955	1.103	.066	-1.140
1	42.236	33.501	25.788	24.416
2	-96.273	-96.069	-83.202	-68.044
3	183.756	226.032	204.633	114.042
4	-201.283	-307.176	-294.091	-95.546
5	105.880	213.337	220.017	31.073
6	-18.770	-58.539	-65.821	0.0

TABLE 4.--Presented are the theoretical wavenumber separations necessary for the equivalent width of two strong absorption lines to approach W_c or W_i to within 1, 2, 5 and 10%. These numbers are generated by the polynomial representations of Table 3 for four ratios of $f = W_2/W_1 = (S_2\gamma_2/S_1\gamma_1)^{1/2}$. Column labels, followed by percent deviation from that precise condition, are I for independent, and C for coincident.

$\gamma_1 z_1$	C1	C2	C5	C10*	I1	I2	I5	I10
				f = 0.15				
.05	.05	.06	.09		.33	.23	.13	.07
.25	.25	.31	.47		1.66	1.15	.66	.33
1.25	1.24	1.56	2.33		8.31	5.74	3.28	1.66
4.00	3.96	4.98	7.44		26.60	18.36	10.48	5.32
7.00	6.94	8.72	13.02		46.55	32.13	18.34	9.31
10.00	9.91	12.45	18.60		66.50	45.90	26.20	13.31
				f = 0.4				
.05	.03	.04	.07	.10	.55	.38	.23	.15
.25	.16	.22	.34	.49	2.77	1.92	1.16	.73
1.25	.78	1.09	1.68	2.44	13.83	9.60	5.78	3.64
4.00	2.48	3.49	5.36	7.80	44.24	30.72	18.48	11.64
7.00	4.34	6.11	9.38	13.65	77.42	53.76	32.34	20.37
10.00	6.21	8.73	13.40	19.50	110.61	76.80	46.20	29.10
				f = 0.7				
.05	.03	.04	.06	.10	.73	.51	.31	.20
.25	.14	.19	.32	.48	3.66	2.56	1.54	1.00
1.25	.68	.96	1.58	2.38	18.29	12.78	7.70	5.01

TABLE 4.--*Continued.*

$\gamma_1 z_1$	C1	C2	C5	C10*	I1	I2	I5	I10
4.00	2.16	3.06	5.05	7.60	58.54	40.90	24.64	16.03
7.00	3.78	5.35	8.84	13.31	102.44	71.57	43.13	28.06
10.00	5.41	7.65	12.63	19.01	146.34	102.24	61.61	40.08
				f = 1.0				
.05	.03	.04	.07	.11	.88	.61	.37	.24
.25	.15	.21	.35	.53	4.38	3.05	1.85	1.20
1.25	.75	1.05	1.76	2.66	21.88	15.24	9.24	6.00
4.00	2.40	3.36	5.64	8.52	70.00	48.76	29.56	19.20
7.00	4.19	5.88	9.86	14.91	122.51	85.32	51.73	33.61
10.00	5.99	8.40	14.09	21.30	175.01	121.89	73.90	48.01

*The coincident polynomial for 10% does not apply at f = 0.15.

TABLE 5.--This table presents corrections (cm^{-1}) to the equivalent width of a blended absorption doublet when the two lines are neither exactly coincident nor independent, for three different ratios of W_2/W_1. The label I denotes independent; C denotes coincident. Numbers following these letters give the percent deviation of the equivalent width from that derivable if the lines were strictly separate or coincident in frequency.

$\gamma_1 z_1$	C1	C2	C5	C10	I1	I2	I5	I10
				f = 0.1				
.02	.001	.003	.006	.013	.001	.003	.007	.014
.20	.013	.025	.063	.126	.014	.028	.069	.138
2.00	.126	.253	.631	1.263	.138	.276	.691	1.382
10.00	.631	1.263	3.157	6.315	.691	1.382	3.456	6.911
				f = 0.5				
.02	.001	.003	.007	.014	.002	.004	.009	.019
.20	.014	.028	.070	.140	.019	.038	.094	.188
2.00	.140	.281	.702	1.405	.188	.377	.942	1.885
10.00	.702	1.405	3.512	7.025	.942	1.885	4.712	9.425
				f = 1.0				
.02	.002	.004	.009	.018	.003	.005	.013	.025
.20	.018	.036	.089	.178	.025	.050	.126	.251
2.00	.178	.355	.889	1.777	.251	.503	1.257	2.513
10.00	.889	1.777	4.443	8.886	1.257	2.513	6.283	12.566

TABLE 6.--This compares Plass' formulation (Equation 9, Ref. 43) of the overlapped equivalent width with that obtained here for 1% and 5% departures from complete coincidence. Numbers from Plass' expression, strictly valid only when the line centers coincide, appear at the top of each block. Parenthetically enclosed numbers are the critical wavenumber separations necessary for the indicated deviations from coincidence, for the two equal, square root absorption lines.

P_{atm} \ Z	π^2	π^3	π^4
	1% Departure		
10^{-3}	.05 .05 (.00)	.15 .15 (.01)	.48 .48 (.03)
10^{-2}	.48 .48 (.03)	1.51 1.53 (.10)	4.75 4.80 (.32)
10^{-1}	4.84 4.86 (.33)	15.13 15.28 (1.02)	47.52 47.99 (3.20)
	5% Departure		
10^{-3}	.05 .05 (.01)	.15 .16 (.02)	.48 .50 (.08)
10^{-2}	.49 .51 (.08)	1.52 1.59 (.24)	4.75 4.99 (.75)
10^{-1}	4.94 5.06 (.76)	15.17 15.88 (2.40)	43.53 49.90 (7.54)

TABLE 7.--Application of Equation 37 to three strong absorption lines in the 6.3μ water band at p = 3.5 torr and T = 287.7K. The cm^{-1} separation, $\Delta\nu$, of the indicated line pairs is also given.

Reference Line Frequency	Strong Neighbor	$\lvert\Delta\nu\rvert$	Overlap Criteria Imply
1429.96	1423.72	6.24	Ind $\leq$ 1% if $\Delta\nu$=1.26
	1424.12	5.84	Ind $\leq$ 1% if $\Delta\nu$=1.12
	1428.26	1.70	Ind $\leq$ 1% if $\Delta\nu$=0.69
	1432.05	2.09	Ind $\leq$ 1% if $\Delta\nu$=0.58
	1433.29	3.33	Ind $\leq$ 1% if $\Delta\nu$=0.78
1447.98	1452.08	4.10	Ind $\leq$ 1% if $\Delta\nu$=1.06
1464.93	1456.85	8.08	Ind $\leq$ 1% if $\Delta\nu$=3.14
	1458.24	6.69	Ind $\leq$ 1% if $\Delta\nu$=2.39
	1459.27	5.66	Ind $\leq$ 1% if $\Delta\nu$=1.94
	1471.72	6.79	Ind $\leq$ 1% if $\Delta\nu$=1.30

TABLE 8.--Frequencies of independent square root absorption lines between 1400 and 1700 cm-1 in the 6.3μ water vapor band. These lines are independent (using Equation 37) when observed at 300 K over a 93.5m path at the five pressures indicated below but take no account of non-square root lines or continuous absorption.

p=0.5 torr	1.0 torr	2.0 torr	4.0 torr	8.0 torr
1405.01	1405.01	1405.01	1405.01	1405.01
1411.49	1411.49	1411.49	1411.49	1411.49
1416.11	1416.11	1416.11	1416.11	1416.11
1418.92	1418.92	1433.29	1433.29	1433.29
1423.72	1423.72	1435.60	1435.60	1447.98
1424.12	1424.12	1447.98	1447.98	1452.08
1433.29	1433.29	1452.08	1452.08	1464.93
1435.60	1435.60	1454.60	1464.93	1481.26
1447.98	1447.98	1455.28	1481.26	1501.81
1452.08	1452.08	1464.93	1486.15	1594.51
1454.60	1454.60	1481.26	1487.35	1601.19
1455.28	1455.28	1486.15	1501.81	1603.34
1464.93	1464.93	1487.35	1510.54	1609.46
1473.52	1473.52	1490.86	1514.95	1640.32
1481.26	1481.26	1496.26	1531.65	
1486.15	1486.15	1501.81	1535.48	
1487.35	1487.35	1510.54	1554.40	
1490.86	1490.86	1514.95	1564.89	
1496.26	1496.26	1523.64	1594.51	
1501.81	1501.81	1527.34	1596.27	
1505.60	1505.60	1528.58	1601.19	
1506.64	1510.54	1531.65	1603.34	
1510.54	1514.95	1535.48	1609.46	
1514.95	1516.29	1538.29	1616.72	
1516.29	1516.71	1543.51	1627.84	

TABLE 8. *Continued.*

p=0.5 torr	1.0 torr	2.0 torr	4.0 torr	8.0 torr
1516.71	1523.64	1544.41	1640.32	
1523.64	1525.47	1554.40	1661.35	
1525.47	1527.34	1564.89	1662.80	
1527.34	1528.58	1594.51	1690.13	
1528.58	1531.65	1596.27		
1531.65	1533.21	1601.19		
1533.21	1535.48	1603.34		
1535.48	1538.29	1609.46		
1538.29	1540.31	1616.72		
1540.31	1543.51	1622.56		
1543.51	1544.41	1623.57		
1544.41	1550.20	1627.84		
1550.20	1554.40	1640.32		
1554.40	1564.89	1661.35		
1559.70	1568.92	1662.80		
1560.26	1569.80	1668.30		
1564.89	1594.51	1679.82		
1568.92	1596.27	1680.47		
1569.80	1601.19	1687.88		
1594.51	1603.34	1688.36		
1596.27	1609.46	1690.13		
1601.19	1616.72	1697.53		
1603.34	1622.56			
1609.46	1623.57			
1616.72	1627.84			
1622.56	1640.32			
1623.57	1645.98			
1627.84	1647.40			
1634.97	1648.30			
1635.64	1661.35			

TABLE 8. *Continued.*

p=0.5 torr	1.0 torr	2.0 torr	4.0 torr	8.0 torr
1640.32	1662.80			
1645.98	1668.30			
1647.40	1679.82			
1648.30	1680.47			
1661.35	1683.16			
1662.80	1684.00			
1668.30	1687.88			
1679.82	1688.36			
1680.47	1690.00			
1683.16	1697.53			
1684.00				
1687.88				
1688.36				
1690.13				
1697.53				

TABLE 9.--Experimental line strengths for the HCl fundamental band (in cm^{-2}/atm., from Reference 31).

	$^{1}H^{35}Cl$				$^{1}H^{37}Cl$			
Line	Ref. 31 295K	Ref. 12 300K	Ref. 13 300K	Ref. 47 300K	Ref. 31 295K	Ref. 12 300K	Ref. 13 300K	Ref. 47 300K
P(8)	1.44	1.30	1.41	1.32	0.48	0.427	0.463	0.433
P(7)	2.59	2.46	2.70	2.40	0.90	0.918	0.883	---
P(6)	4.52	4.16	4.54	4.17	1.54	1.44	1.48	1.34
P(5)	6.73	5.79	6.72	--	2.18	1.93	2.19	2.04
P(4)	9.00	7.58	8.91	--	2.93	2.48	2.90	2.73
P(3)	9.41	8.49	9.32	--	3.02	3.10	3.04	2.79
P(2)	8.20	7.46	8.16	--	2.72	2.54	2.66	2.54
P(1)	5.00	4.56	4.96	--	1.61	1.54	1.61	1.55
R(0)	5.25	4.71	--	4.90	1.72	1.61	--	1.61
R(1)	8.98	8.52	--	--	2.90	2.95	--	2.96
R(2)	10.20	9.61	--	--	3.09	3.13	--	3.42
R(3)	10.00	9.43	--	--	3.40	3.46	--	3.25
R(4)	7.92	7.65	--	--	2.61	2.47	--	2.71
R(5)	6.60	5.98	--	--	2.20	2.03	--	1.98
R(6)	4.24	3.69	--	3.74	1.40	1.40	--	1.25
R(7)	2.10	2.11	--	2.12	0.68	0.661	--	0.701
R(8)	1.07	1.07	--	1.09	0.44	0.418	--	0.359

TABLE 10.--Electronic grade HCl batch analysis supplied by the Linde Division of the Union Carbide Company. The notation ND means "not detected." The quoted value is the detection threshold of the mass spectrometric detection technique. Results are presented for both the liquid and gas phase.

Contents	Reported	
	Gas	Liquid
Nitrogen	270 ppm	ND < 10 ppm
Oxygen	40 ppm	ND < 10 ppm
Argon	ND < 10 ppm	ND < 10 ppm
Carbon dioxide	ND < 10 ppm	ND < 10 ppm
Hydrogen	150 ppm	ND <100 ppm
Helium	ND < 10 ppm	ND < 10 ppm
Hydrogen sulfide	ND < 20 ppm	ND < 20 ppm
Total* hydrocarbon	ND < 10 ppm	ND < 10 ppm
Hydrogen chloride	Balance	Balance

*Hydrocarbons present in lower grades are often confined to the following: ethylene, 1, 1-dichloroethane and ethyl chloride. Vapor pressures for these gases appear on Figure 20.

TABLE 11.--Coefficients used to calculate the inflection point slope, α_i, between $x_o = \frac{1}{z}\left(\frac{\sigma}{\gamma}\right) = 0.2$ and 10.0 for square root absorption lines. For these lines, $z \geq \pi$. Maximum error occurs at $x_o = 0.6$ and equals 9.8×10^{-3}.

i	η_i
0	0.487563
1	-0.125019
2	0.013356
3	-0.000531

TABLE 12.--Comparison of two methods for including unmeasurable contributions to the equivalent width buried by noise in the distant wings of two blended lines. The first main block of data results from measuring separate isotope lines. The final block results from measurements made on the entire doublet.

Line	P (torr)	Isotope Uncorrected W' (cm^{-1})	Summed Uncorrected W' (cm^{-1})	Δ (cm^{-1})	Isotope Corrected W_1 (cm^{-1})	Summed Corrected W_1 (cm^{-1})
R(7)	10.35	0.0986 (37)	0.3466	0.002 (37)	0.101 (37)	0.358
		0.2480 (35)		0.009 (35)	0.257 (35)	
R(5)	4.50	0.1181	0.3160	0.003	0.121	0.325
		0.1979		0.006	0.204	
P(1)	4.45	0.1103	0.2957	0.002	0.113	0.304
		0.1854		0.005	0.191	
R(7)	10.35		0.3481		0.008	0.356
R(5)	4.50		0.3155		0.004	0.319
P(1)	4.45		0.2933		0.004	0.297

TABLE 13.--Variations in the predicted pressure necessary to blend the R(7) doublet to within $\varepsilon^* = 1$, 2, 5 and 10% of $W_1 + W_2$ due to slight changes in each half width simultaneously.

Half Intensity Half Width	Deviation from Independence			
	1%	2%	5%	10%
γ_{Ben}-0.02 cm^{-1}	49.43	70.88	117.78	183.73 torr
γ_{Ben}-0.01	47.18	67.63	112.38	175.30
$\gamma_{Benedict}$	45.18	64.80	107.65	167.95
γ_{Ben}+0.01	43.43	62.28	103.50	161.43
γ_{Ben}+0.02	41.88	60.05	99.75	155.63

TABLE 14.--Variations in the R(7) predicted pressures (in torr) necessary to blend that doublet to within ε = 1, 2, 5 and 10% of $W_1 + W_2$ due to slight changes in <u>either</u> S_{35} or S_{37} separately.

Line Strengths [$cm^{-1}/(g\ cm^{-2})$] from Ref.12	Deviations from Independence			
	1%	2%	5%	10%
S_{35}-100, S_{37}	46.03	65.98	109.63	170.55
S_{35} , S_{37}	45.18	64.80	107.65	167.95
S_{35}+100, S_{37}	44.43	63.73	105.88	165.58
S_{35} , S_{37}-100	48.20	69.23	114.93	180.80
S_{35} , S_{37}	45.18	64.80	107.65	167.95
S_{35} , S_{37}+100	42.98	61.60	102.35	158.43

TABLE 15.--Weighted averages (3 to 1 ratio) of the $^{1}H^{35}Cl$ and $^{1}H^{37}Cl$ self broadened half-intensity half-widths (cm^{-1}/atm) in the fundamental band P branch at the temperature 300K.

Line	Ref. 12	Ref. 13	Difference Ref. 12 - Ref. 13
P(1)	0.216	0.207	0.009
P(2)	0.221	0.233	-0.012
P(3)	0.249	0.231	0.018
P(4)	0.244	0.227	0.017
P(5)	0.231	0.207	0.024
P(6)	0.193	0.171	0.022
P(7)	0.152	0.145	0.007
P(8)	0.132	0.124	0.008

TABLE 16.--Corrected isotopic doublet equivalent widths per unit pressure for low rotation HCl lines. Cell pressure varied from 2 to 70 torr for these observations.

Line	$\bar{W}^{o}$ (cm^{-1}/torr)*	Number of Observations Averaged
P(8)	0.026	10
P(7)	0.042	8
P(6)	0.062	11
P(5)	0.079	11
P(4)	0.097	8
P(3)	0.102	10
P(2)	0.092	6
P(1)	0.070	4
R(0)	0.075	6
R(1)	0.102	7
R(2)	0.111	12
R(3)	0.115	3
R(4)	0.097	4
R(5)	0.075	8
R(6)	0.054	7
R(7)	0.035	12
R(8)	0.025	6

*Cell length = 3.34 m. Corrections ($\sim$ 5%) use Benedict *et al.* S,γ.

TABLE 17.--The ability of blended doublet equivalent widths predicted by using published S and γ values in Chapter 3 to reproduce low pressure fundamental band HCl absorption measurements.

P Branch	Circumstance of the Predictions	R Branch
P(2), P(4), P(8)	Exact using S,γ from Benedict *et al.* only	R(0), R(5), R(6)
P(1), P(5)	Closest using S, γ from Benedict *et al.*	--
P(3)	Equally good using S, γ from Benedict *et al.* and Babrov *et al.*	--
P(6)	Exact using S,γ from Babrov *et al.* only	--
--	Exact using S from Varanasi *et al.* and γ from Benedict *et al.*	--
P(7)	All of the employed S, γ combinations equally good	--
--	Equally good using S from Varanasi *et al.* with γ from Benedict *et al.* and Sγ from Benedict *et al.*	R(1), R(2), R(3), R(4), R(7), R(8)

TABLE 18.--Ratio of previously measured isotopic line strengths in the HCl fundamental band. The theoretically expected value determined by the chlorine abundance ratio is 0.3257.

S_{37}/S_{35} (Ref. 12)	Line	S_{37}/S_{35} (Ref. 31)
0.329	P(8)	0.333
0.373	P(7)	0.347
0.346	P(6)	0.340
0.333	P(5)	0.323
0.327	P(4)	0.325
0.365	P(3)	0.320
0.340	P(2)	0.331
0.337	P(1)	0.322
0.341	R(0)	0.327
0.346	R(1)	0.322
0.325	R(2)	0.302
0.366	R(3)	0.340
0.322	R(4)	0.329
0.339	R(5)	0.333
0.379	R(6)	0.330
0.313	R(7)	0.323
0.390	R(8)	0.411

TABLE 19.--Pressures (in torr) necessary to blend HCl fundamental band isotopic doublets by $\varepsilon^* = 1$, 2, 5 and 10% from complete independence ($W_1 + W_2$) and coincidence [$(W_1^2 + W_2^2)^{1/2}$] based upon S and γ values from Reference 12 (for a path length of 3.34m).

Line	Deviations from Coincidence				Deviations from Independence			
	1%	2%	5%	10%	1%	2%	5%	10%
P(8)	1041.13	734.33	457.03	309.20	160.70	103.25	61.13	43.35
P(7)	729.63	515.15	317.53	213.40	107.40	69.33	41.70	29.10
P(6)	505.15	356.43	221.03	149.18	76.58	49.30	29.65	20.68
P(5)	397.50	280.38	174.38	117.93	61.18	39.33	23.65	16.50
P(4)	344.60	243.03	151.40	102.48	53.43	34.30	20.63	14.40
P(3)	331.10	233.70	144.33	97.13	49.18	31.70	19.08	13.30
P(2)	377.25	266.13	165.28	111.65	57.58	37.03	22.28	15.55
P(1)	498.03	351.33	218.30	147.53	76.25	49.00	29.50	20.58
R(0)	499.20	353.20	218.63	147.68	76.05	48.93	29.45	20.53
R(1)	378.60	267.15	165.65	111.83	57.40	36.95	22.23	15.50
R(2)	335.43	236.55	147.40	99.80	52.10	33.45	20.13	14.05
R(3)	352.58	248.90	153.63	103.38	52.28	33.70	20.28	14.15
R(4)	412.58	290.93	181.43	122.90	64.30	41.28	24.83	17.33
R(5)	518.55	365.83	227.23	153.50	79.20	50.95	30.65	21.38
R(6)	735.28	519.20	319.65	214.70	107.65	69.53	41.83	29.20
R(7)	1063.63	749.88	468.80	318.08	167.95	107.65	64.80	45.18
R(8)	1646.13	1162.68	714.00	478.73	238.05	153.95	92.63	64.65

TABLE 20.--Blended doublet equivalent widths, uncorrected for wing absorption, of high rotation lines per unit pressure. Observations were made over a 3.34 m path at 300K. The frequency extent of the measurements is also indicated. Cell pressures range from 32 to 750 torr for these observations.

Line	$\bar{W}^o$ (cm^{-1}/torr)	P_{torr}	$\lvert\nu-\nu_o\rvert$	
			Red	Blue
P(15)	0.0003	713.5	2.06	1.02
P(14)	0.0007	280.3	2.22	0.85
P(13)	0.0019	714.9	3.20	3.23
	0.0024	281.2	2.83	1.97
P(12)	0.0035	715.7	4.28	4.62
	0.0037	282.2	4.00	2.28
	0.0034	132.9	2.39	0.76
	0.0036	68.15	2.18	0.66
P(11)	0.0055	716.3	6.63	5.30
	0.0063	283.0	4.11	3.20
	0.0056	133.4	2.35	1.25
	0.0063	68.25	2.46	0.89
P(10)	0.0105	133.8	3.33	1.46
	0.0114	68.35	2.49	0.95
	0.0108	31.8	2.46	0.86
P(9)	0.0155	284.8	7.07	5.19
	0.0176	134.2	4.44	2.90
	0.0182	68.45	2.90	1.43
	0.0182	32.0	2.57	1.08
R(9)	0.0144	35.45	3.39	1.20
	0.0153	72.25	3.99	1.86
R(10)	0.0107	140.0	4.71	3.53
	0.0086	47.15	3.60	1.02
R(11)	0.0052	140.2	4.04	1.34

TABLE 20.--(*Continued.*)

Line	$\overline{W}°$ (cm^{-1}/torr)	P_{torr}	$\lvert\nu-\nu_o\rvert$	
			Red	Blue
R(12)	0.0029	140.3	3.45	1.45
R(13)	0.0015	299.3	3.45	1.30
R(14)	0.0006	718.8	3.37	1.22
R(15)	0.0001	719.1	0.85	0.88

TABLE 21.--Polynomial fit to ℓn_e of the Ladenburg-Reiche function from $\zeta = 0.04$ to $\zeta = 20.0$ ($z = 0.16$ to $z = 3.57$). It reproduces the natural logarithm exactly over this range to the third decimal.

i	d_i
0	-0.1717
1	0.6890
2	-0.1870
3	0.0347
4	0.0600
5	-0.0214
6	-0.0134
7	0.0060

TABLE 22.--Examples of the accuracy of the polynomial representation of the Ladenburg-Reiche function given in Table 21.

ζ	Stover Table Ref. 55	Polynomial
0.25	0.2223	0.2223
0.50	0.4007	0.4014
0.75	0.5483	0.5486
1.00	0.6737	0.6734
1.25	0.7828	0.7823
1.50	0.8797	0.8792
1.75	0.9673	0.9669
2.00	1.0476	1.0475
2.50	1.1916	1.1921
3.00	1.3195	1.3204
3.50	1.4357	1.4367
4.00	1.5430	1.5440
4.50	1.6432	1.6439
5.00	1.7376	1.7381
7.50	2.1477	2.1469
10.00	2.4910	2.4900
12.5	2.7923	2.7917
15.0	3.0641	3.0639
17.5	3.3137	3.3134
20.0	3.5457	3.5450

TABLE 23.--Approximate polynomial fit to the Ladenburg-Reiche function for the same region covered in Table 21. The accuracy of the polynomial fit to $\ell n_e f(\zeta)$ is $\sim$ 2%.

i	P_i
0	-0.1758
1	0.6723
2	-0.1315
3	0.0331

Fig. 1

Schematic energy levels for vibration-rotation transitions in a molecule, demonstrating the origin of the P, Q and R branches.

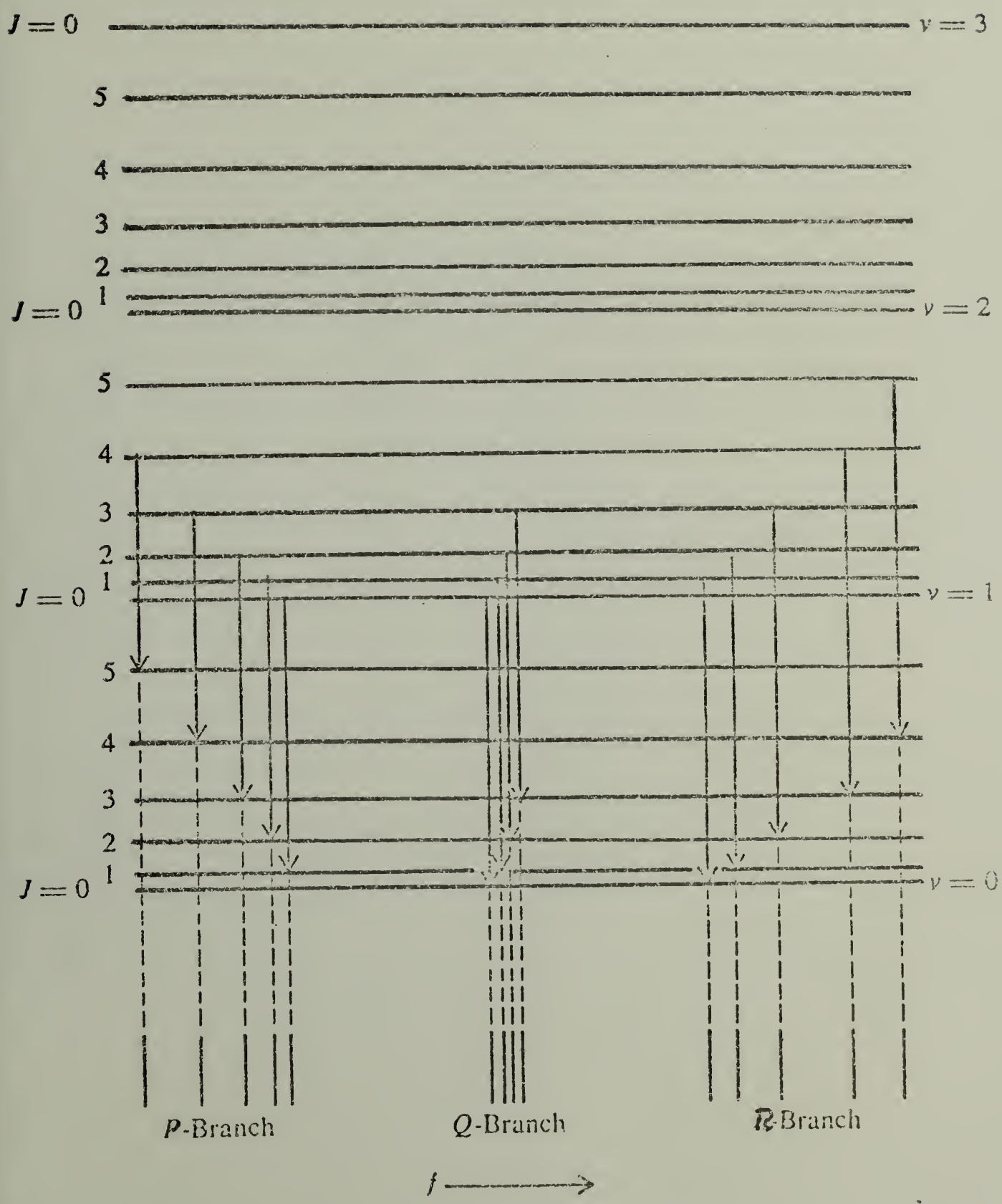
J = 0
v = 3
5
4
3
2
1
J = 0
v = 2
5
4
3
2
1
J = 0
v = 1
5
4
3
2
1
J = 0
v = 0
P-Branch
Q-Branch
R-Branch
J

Fig. 2

Experimental spectra of NO mixed with H_2O. This illustrates the severity of line blending in infrared vibration-rotation line spectra.

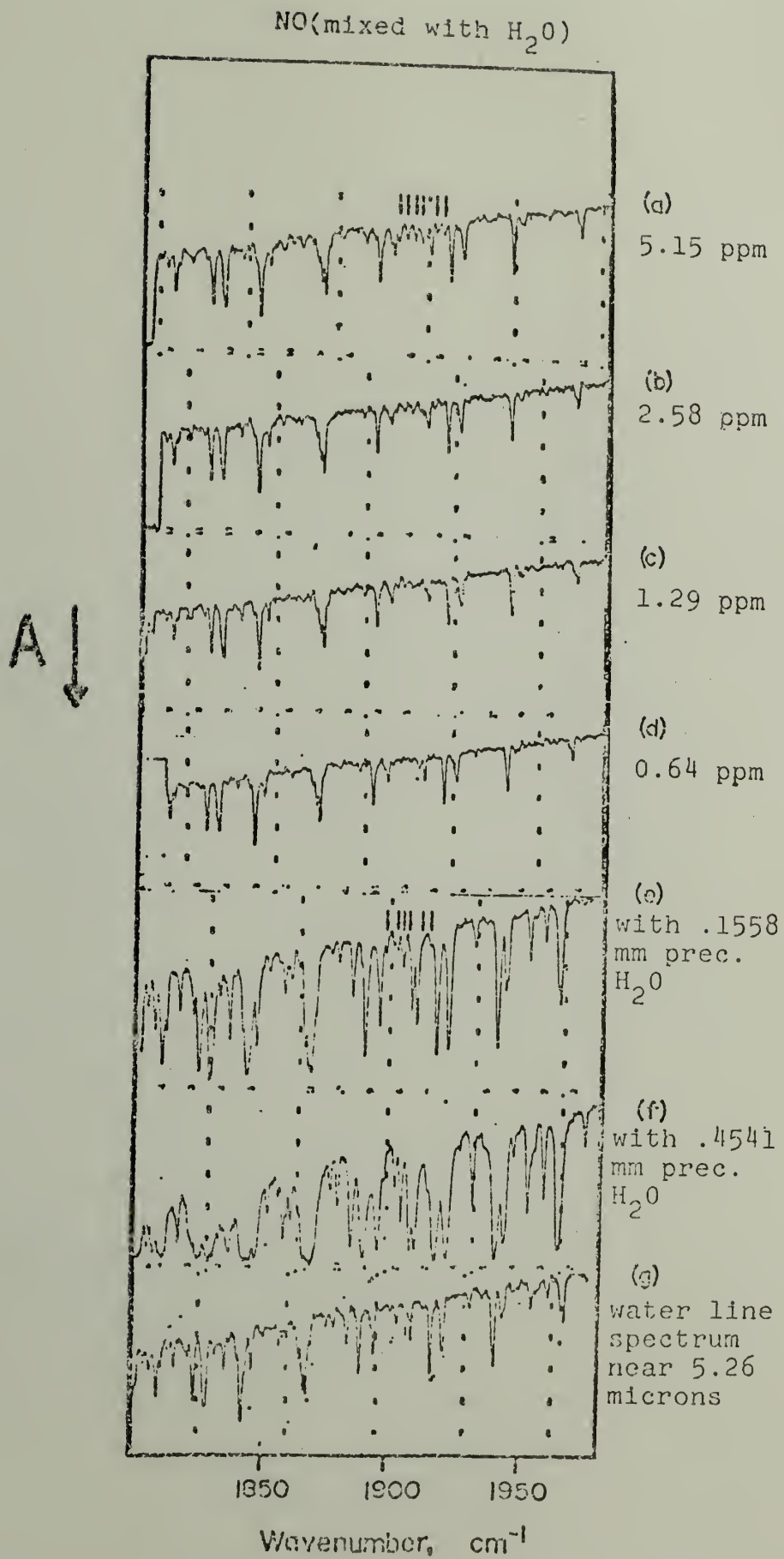
NO(mixed with H_2O)
(a)
5.15 ppm
(b)
2.58 ppm
(c)
1.29 ppm
(d)
0.64 ppm
(e)
with .1558
mm prec.
H_2O
(f)
with .4541
mm prec.
H_2O
(g)
water line
spectrum
near 5.26
microns
A
1850
1900
1950
Wavenumber, cm^{-1}

Fig. 3

Demonstration of the procedure employed to calculate the uncorrected equivalent width of an isolated absorption line. Here, g is the separation in cm^{-1} from ν_o to ν', where ν' is the frequency at which measureable absorption disappears (modified reproduction from Ref. 11).

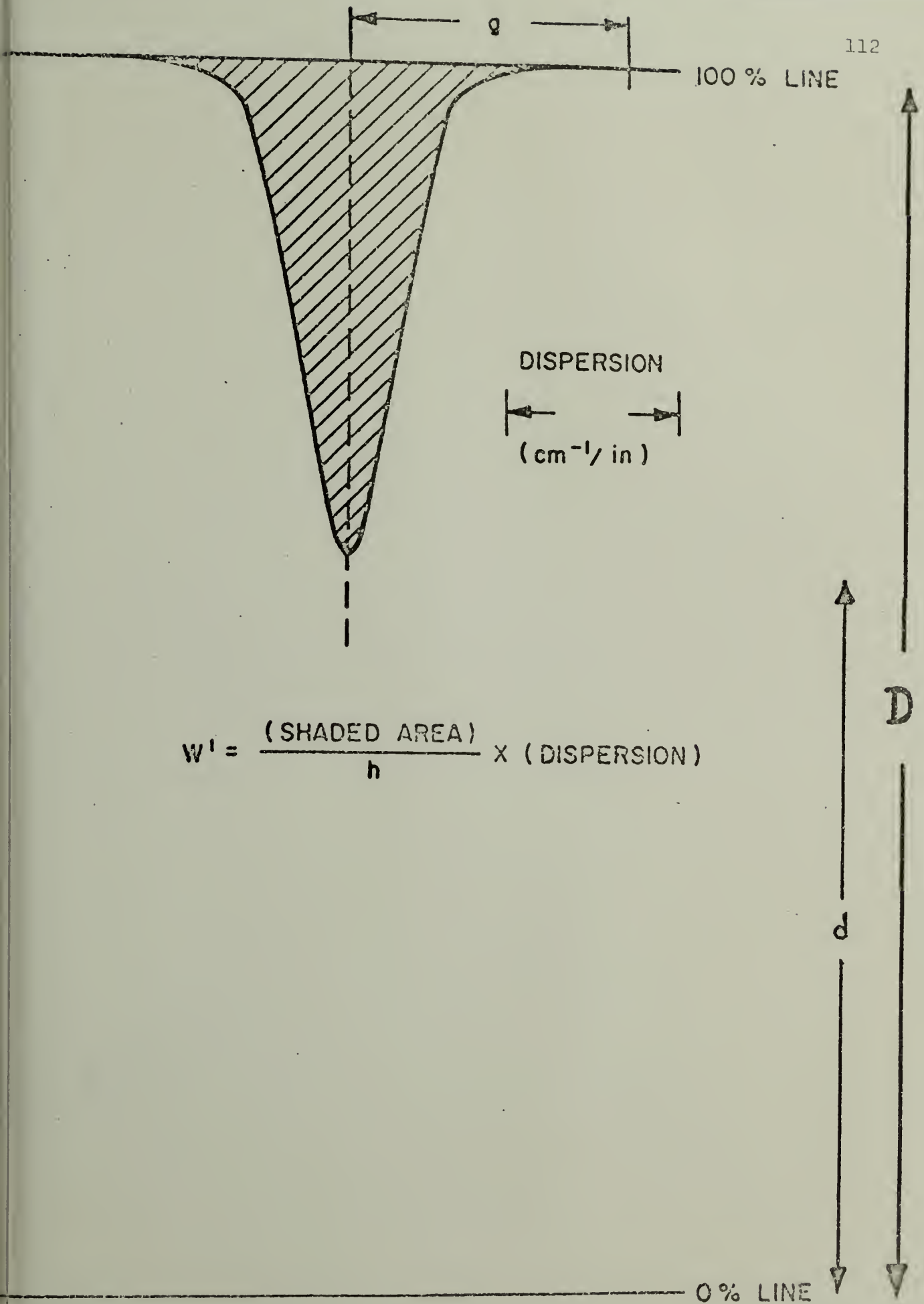

$$W' = \frac{(\text{SHADED AREA})}{h} \times (\text{DISPERSION})$$

Fig. 4

Dependence of the peak transmittance of the 1464.93 cm^{-1} water vapor absorption line upon the resolution, σ. The same line is viewed with three different resolutions in curves A, B and C.

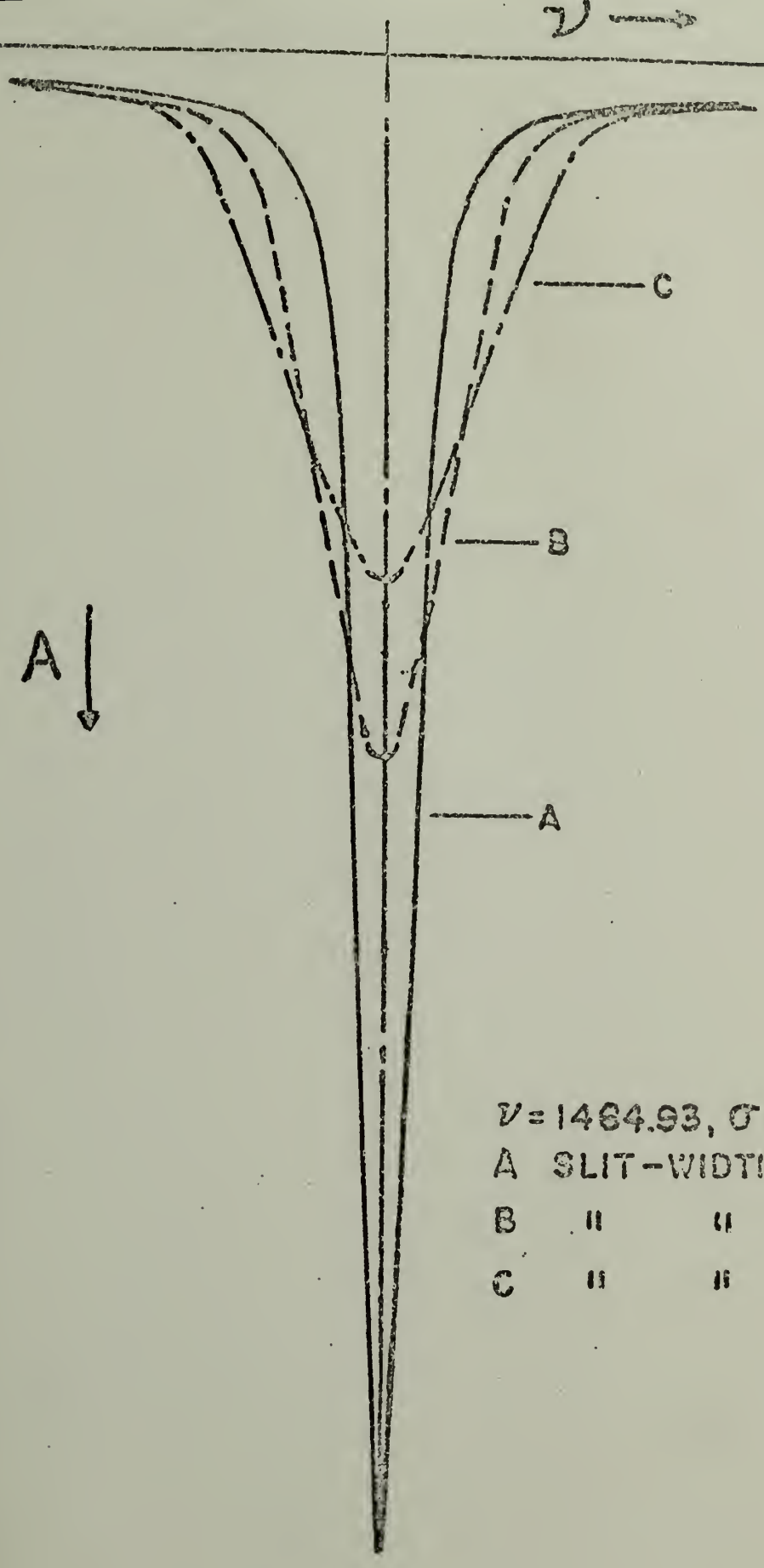

$\nu = 1464.93$, $\sigma = 0.1064\ cm^{-1}$

A SLIT-WIDTH = 0.338 "

B " " = 1.352 "

C " " = 2.028 "

Fig. 5

A curve of growth. Two interesting regions are noticeable: the linear region where $\log W_o \propto \log \ell$ and the square root region where $\log W_o \propto (\log \ell)^{1/2}$. The intersection of the two asymptotes occurs at $W = 4\gamma_o$ for a Lorentz line.

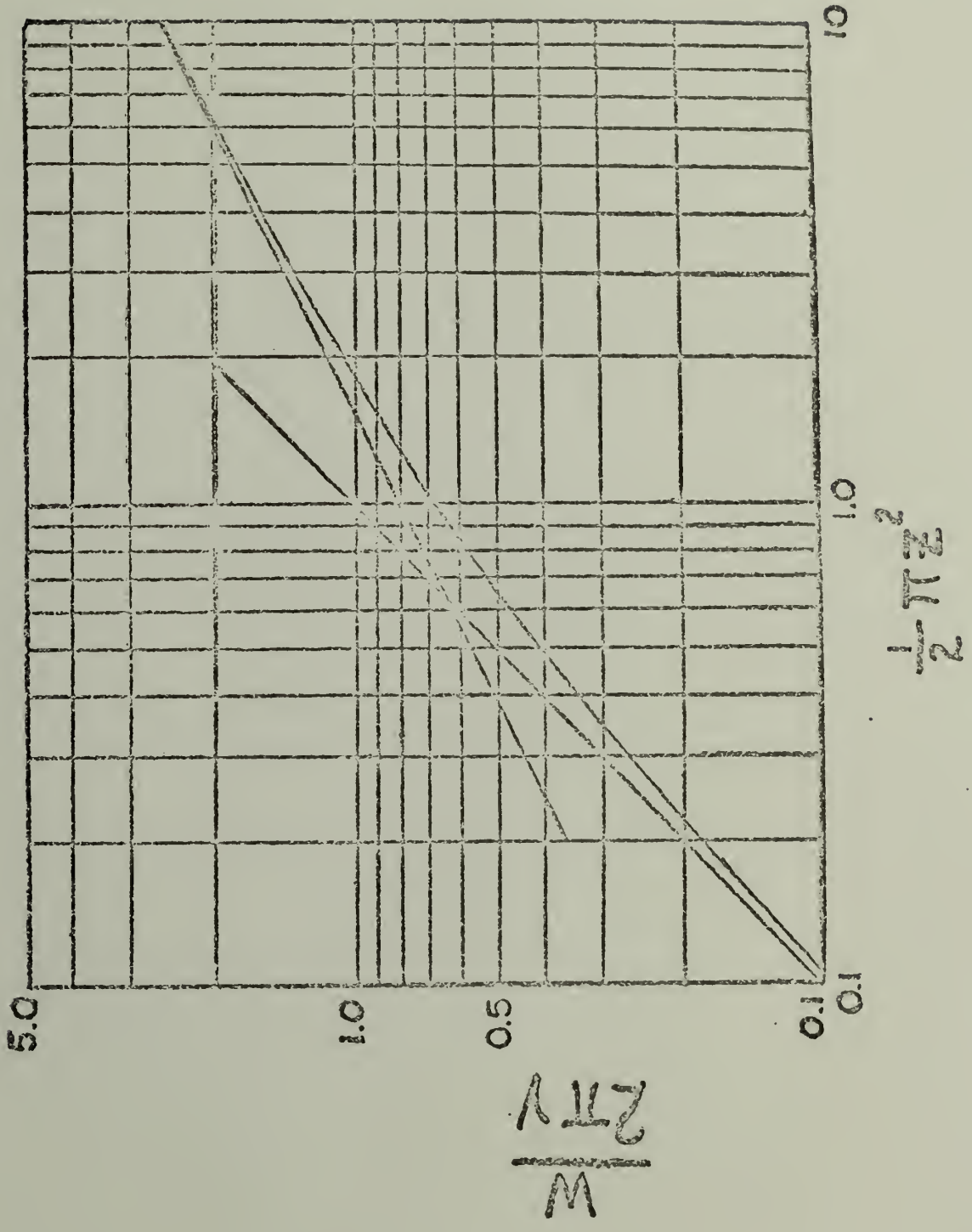
5.0
1.0
0.5
0.1
0.1
1.0
10
W / 2πV
½ πz²

Fig. 6

Half-width of a Doppler line of H_2O as a function of frequency for 6 temperatures. The bottom curve is calculated for T = 10 K while curves progressively higher represent T = 50, 100, 200, 300 and 400 K respectively. Calculations are based upon Eqn. 27.

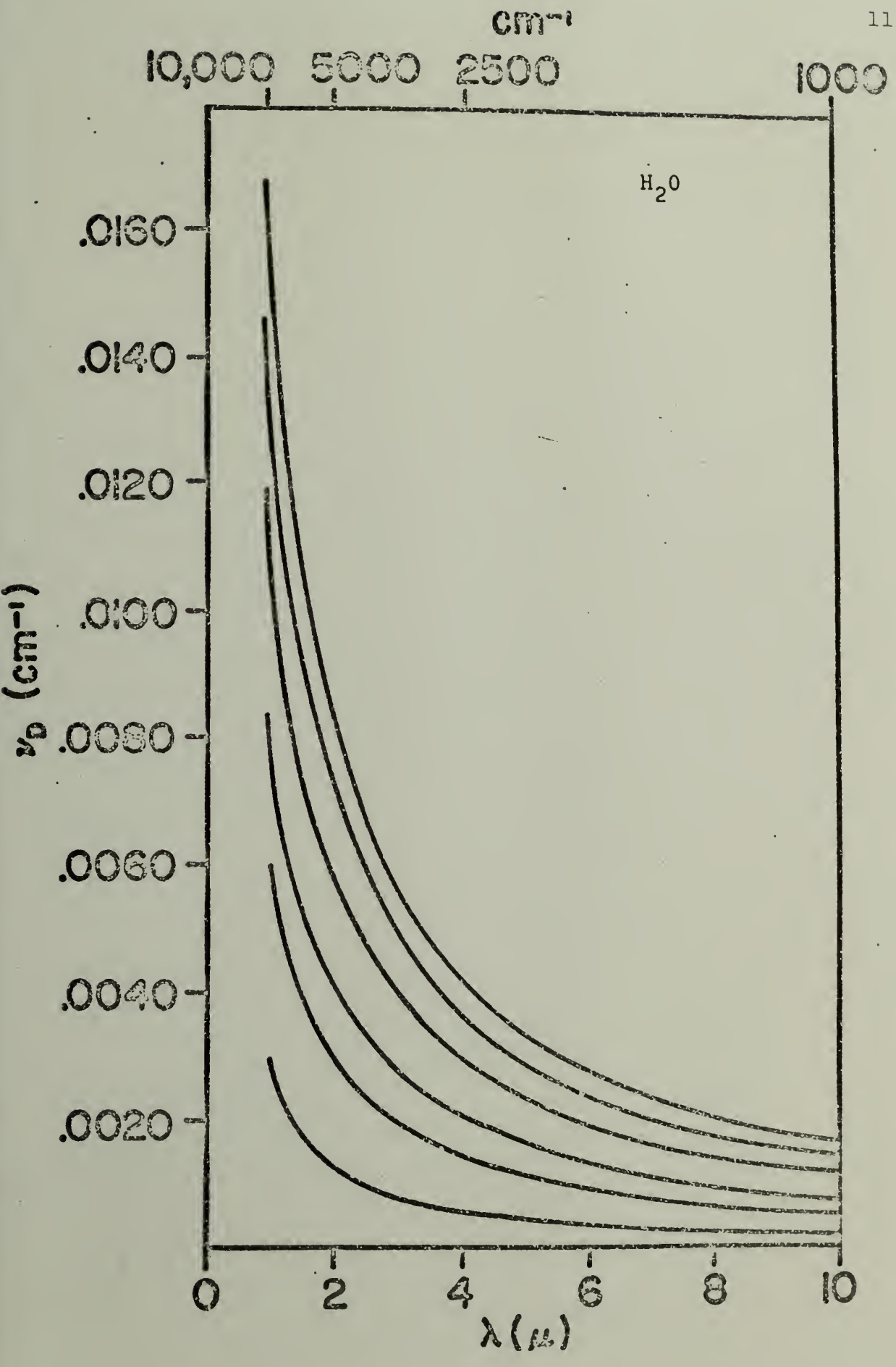
cm⁻¹
10,000
5000
2500
1000
H2O
.0160
.0140
.0120
.0100
.0080
.0060
.0040
.0020
κp (cm⁻¹)
0
2
4
6
8
10
λ(μ)

Fig. 7

Half-width of a Doppler line of HCl as a function of frequency. Temperatures are identical to those in Fig. 6. Notice the reduction in the Doppler width for this molecule which has a higher molecular weight than H_2O.

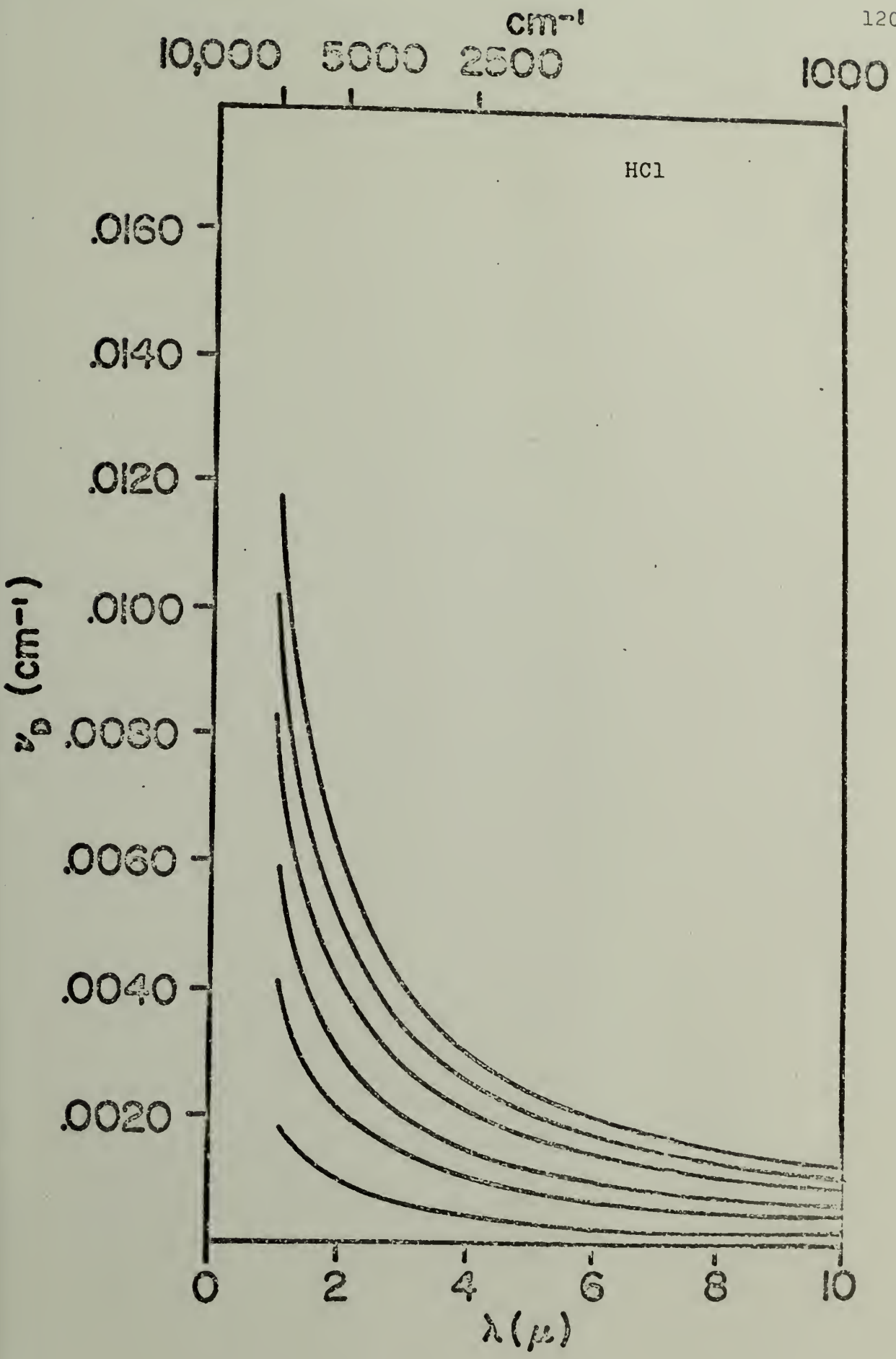
cm⁻¹
10,000
5000
2500
1000
HCl
.0160
.0140
.0120
.0100
.0080
.0060
.0040
.0020
ν_0 (cm⁻¹)
0
2
4
6
8
10
λ(μ)

Fig. 8

Normalized absorption contours calculated from Eqn. 31 for a single, isolated Lorentz line. Here, x is plotted as abscissa and the normalized absorption as ordinate. The lowest curve corresponds to $z = \pi^{-2}$ and successively higher curves correspond to $z = \pi^{-1}$, π^{o} and $z \geq \pi$.

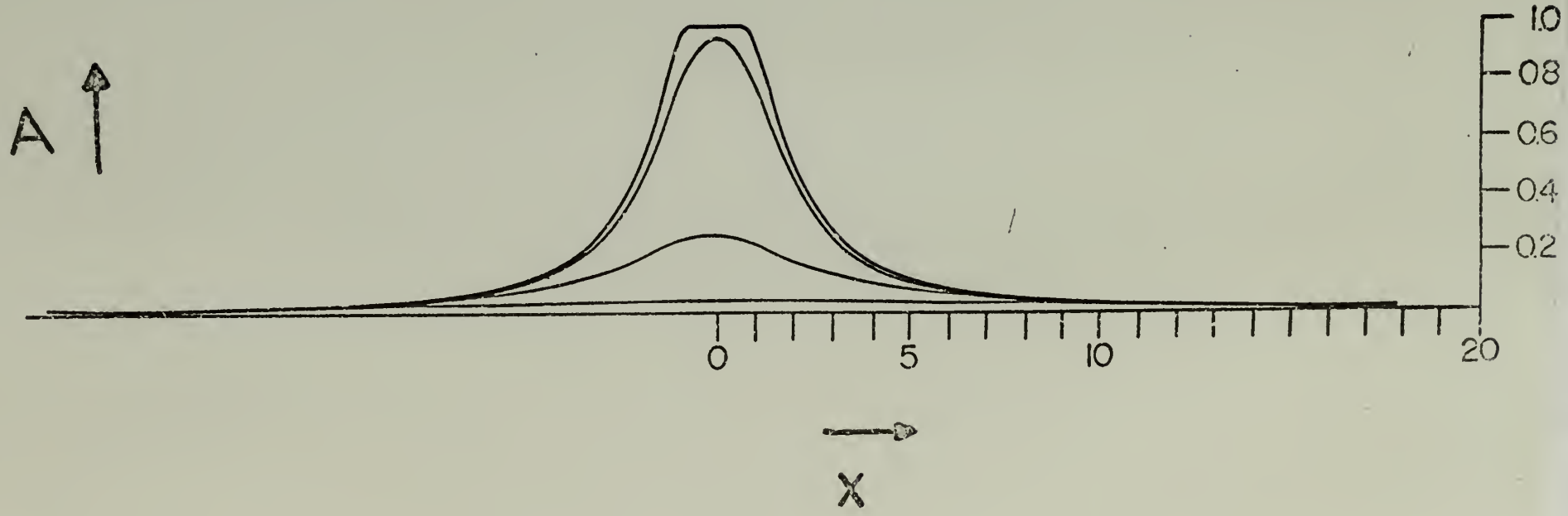
A
1.0
0.8
0.6
0.4
0.2
0
5
10
20
X

Fig. 9

This figure demonstrates the interrelationship of line parameters for two strong Lorentz lines of strengths S_1 and $2S_1$. The contours are calculated from Eqn. 31 for square root lines.

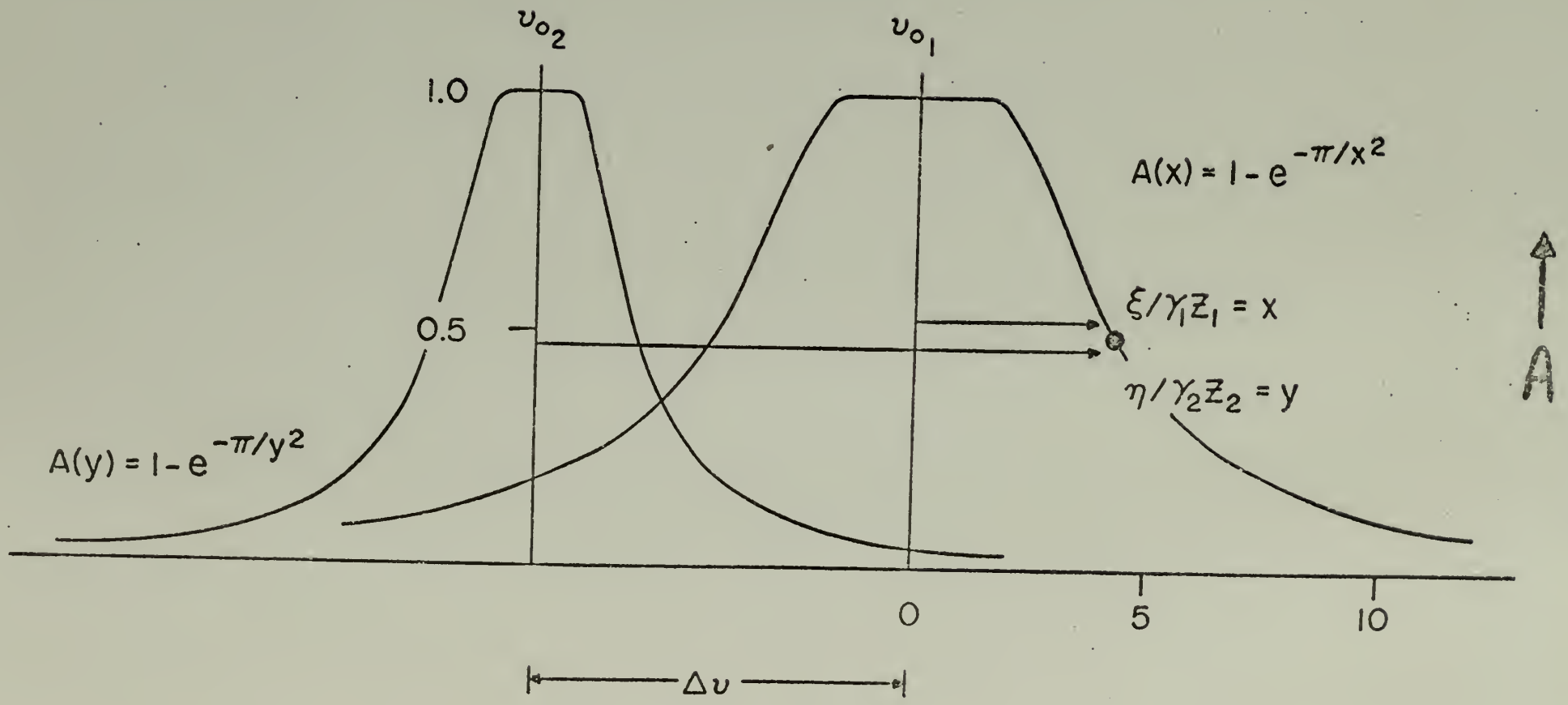
υ_{o_2}
υ_{o_1}
1.0
0.5
$A(x) = 1 - e^{-\pi/x^2}$
$\xi/\gamma_1 z_1 = x$
$\eta/\gamma_2 z_2 = y$
$A(y) = 1 - e^{-\pi/y^2}$
A
0
5
10
$\Delta\upsilon$

Figs. 10, 11, 12 and 13

Each figure presents semi-logarithmic curves at eight values of $W_1/2\pi = \gamma_1 z_1$ for that wavenumber separation below which the equivalent width of two strong Lorentz lines is within 1% in Fig. 10, 2% in Fig. 11, 5% in Fig. 12, and 10% in Fig. 13 of W_c. These are solid lines employing one-tenth of the printed ordinate. They also indicate that separation above which these lines are independent (broken curves using the printed ordinate) displaying the results as a function of $f = W_2/W_1$. $\gamma_1 z_1$ labels are for the broken curves, but the same progression applies to the solid set.

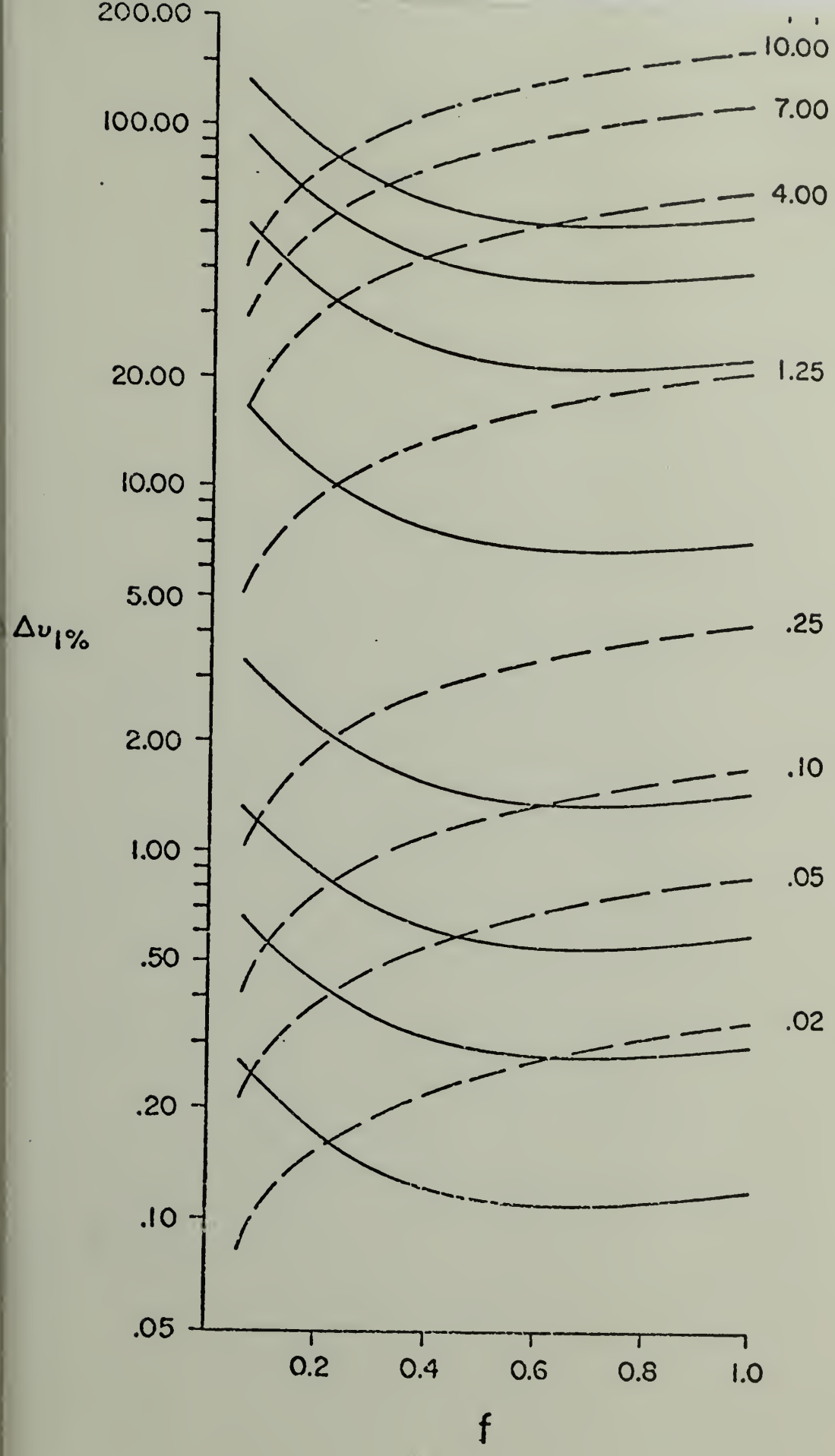
200.00
100.00
20.00
10.00
5.00
2.00
1.00
.50
.20
.10
.05
$\Delta v_{1\%}$
0.2
0.4
0.6
0.8
1.0
f
10.00
7.00
4.00
1.25
.25
.10
.05
.02

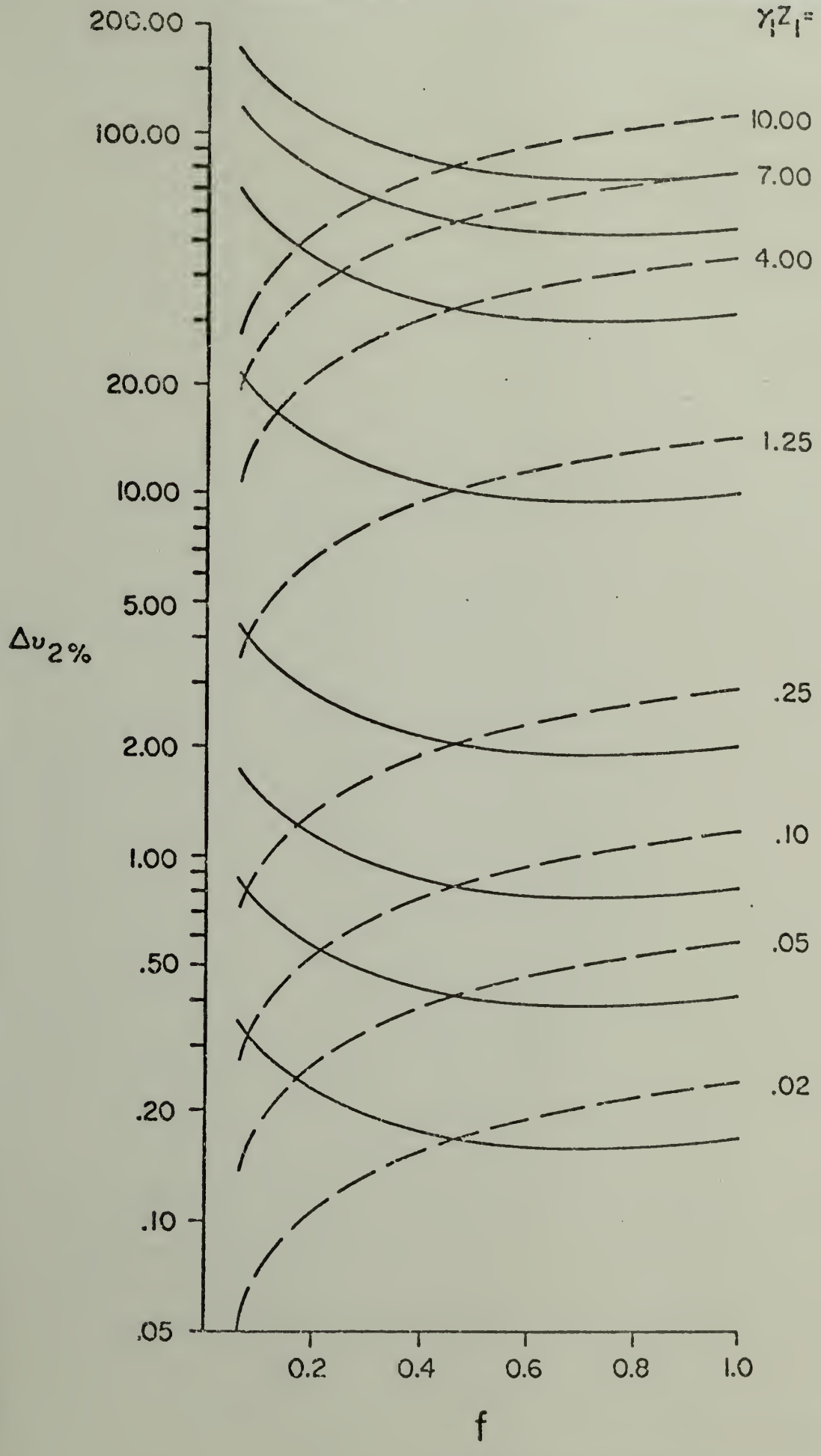
200.00
100.00
20.00
10.00
5.00
2.00
1.00
.50
.20
.10
.05
$\Delta v_{2\%}$
$Y_1Z_1=$
10.00
7.00
4.00
1.25
.25
.10
.05
.02
0.2
0.4
0.6
0.8
1.0
f

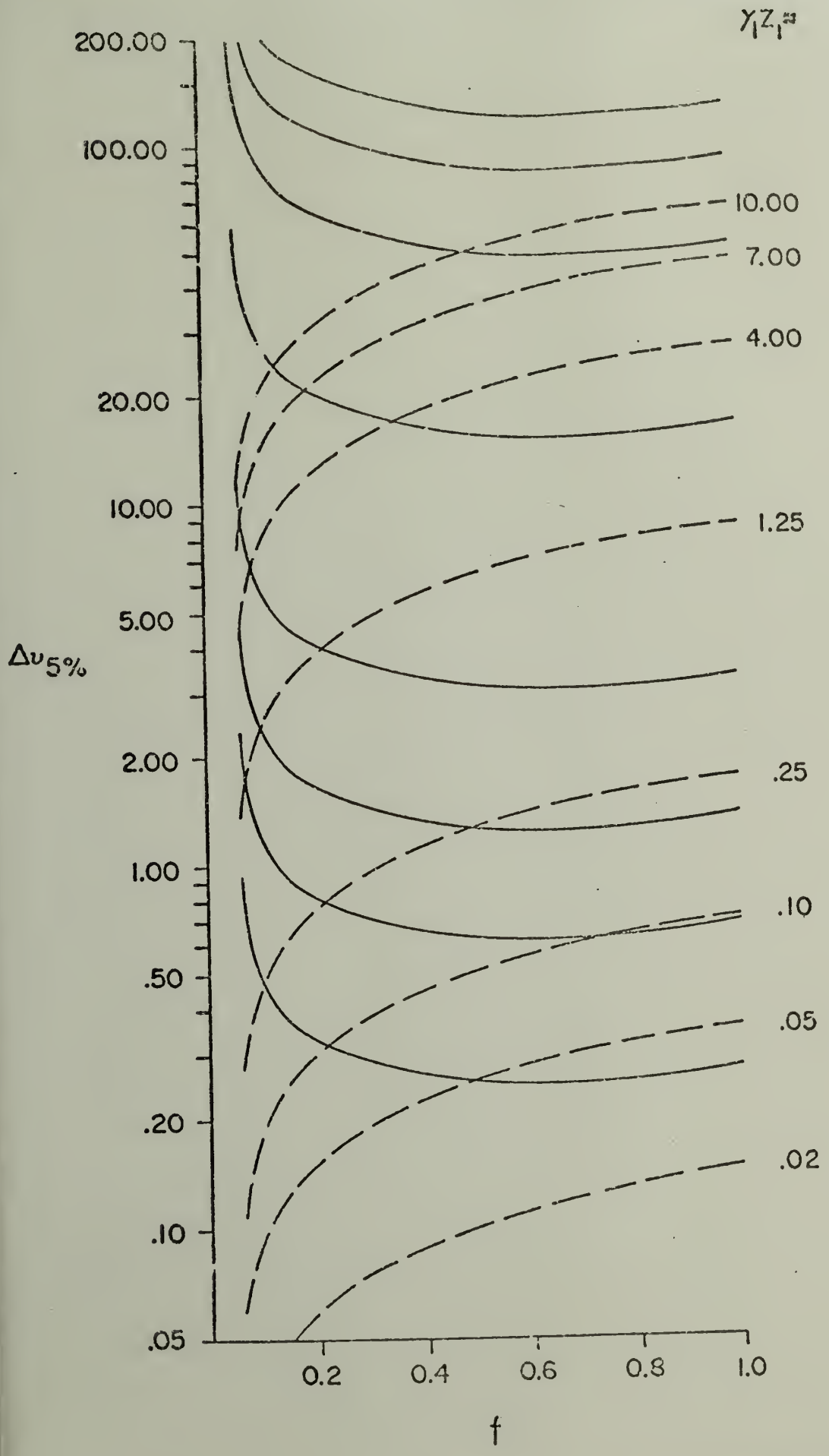
Y_1Z_1
200.00
100.00
20.00
10.00
5.00
2.00
1.00
.50
.20
.10
.05
$\Delta v_{5\%}$
10.00
7.00
4.00
1.25
.25
.10
.05
.02
0.2
0.4
0.6
0.8
1.0
f

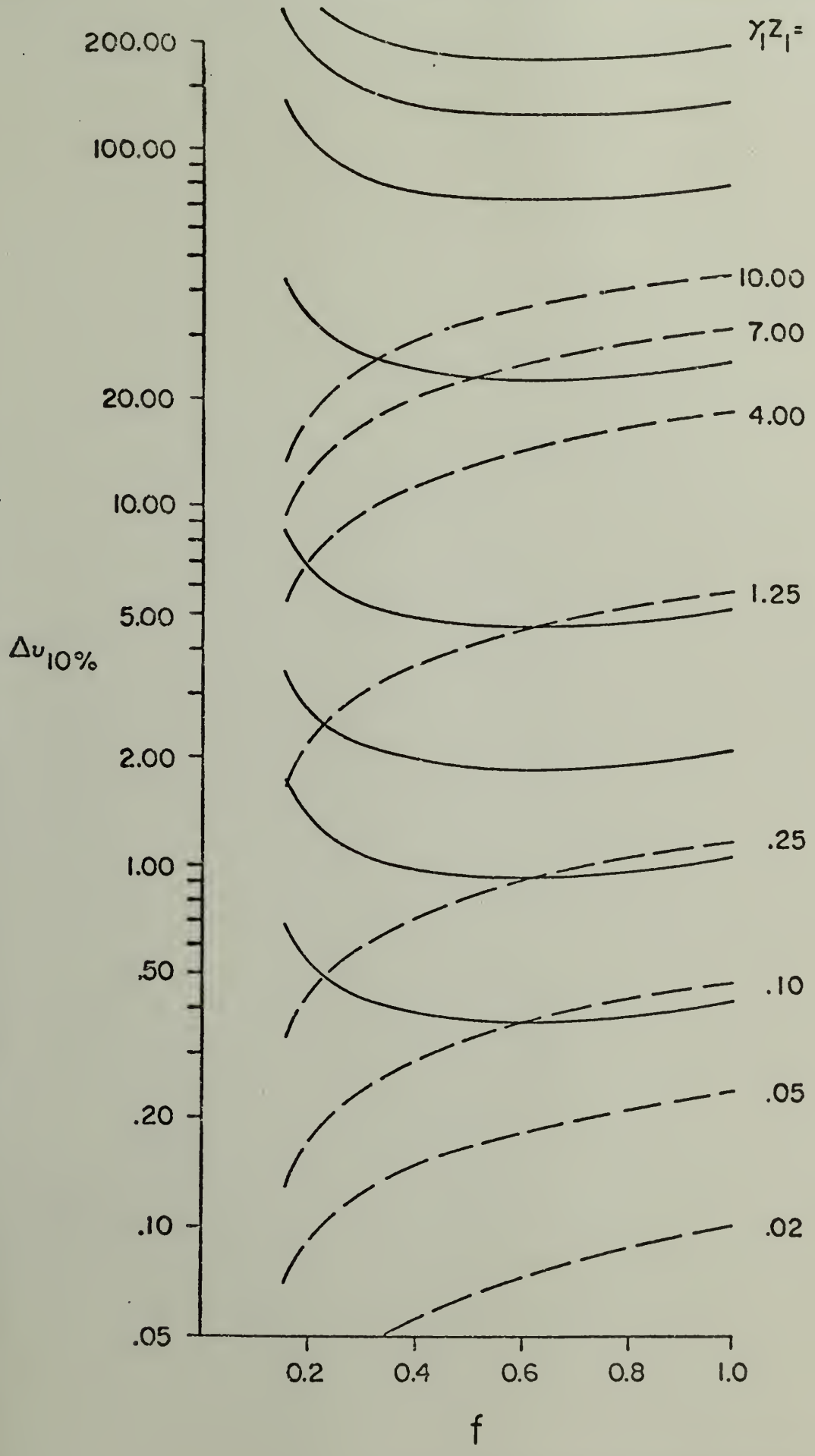
Y_1Z_1=
200.00
100.00
10.00
7.00
20.00
4.00
10.00
1.25
5.00
$\Delta v_{10\%}$
2.00
.25
1.00
.50
.10
.20
.05
.10
.02
.05
0.2
0.4
0.6
0.8
1.0
f

Fig. 14

The fundamental vibration-rotation band of the HCl molecule viewed from 3.2 to 3.7μ at five different pressures. The pathlength is 3.34m. The monochromator spectral resolution varied from ∿ 0.45 cm^{-1} at 2600 cm^{-1} to 0.65 cm^{-1} at 3100 cm^{-1}.

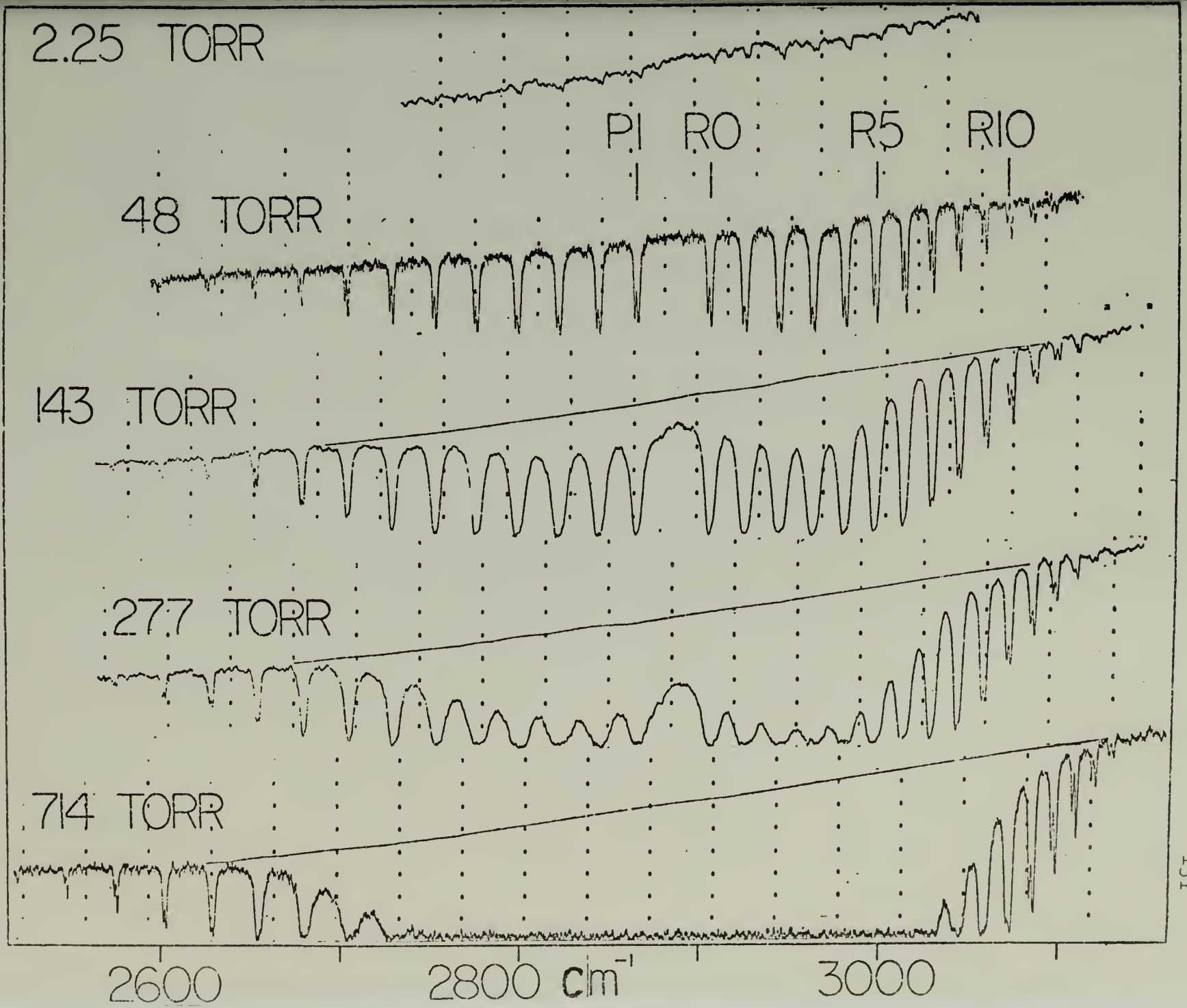
2.25 TORR
P1
R0
R5
R10
48 TORR
143 TORR
27.7 TORR
714 TORR
2600
2800 cm⁻¹
3000

Fig. 15

The P(5) isotopic doublet observed with a slower tracing speed at 18.65 torr. The quality of this spectrum is typical of spectra from which equivalent width measurements were made.

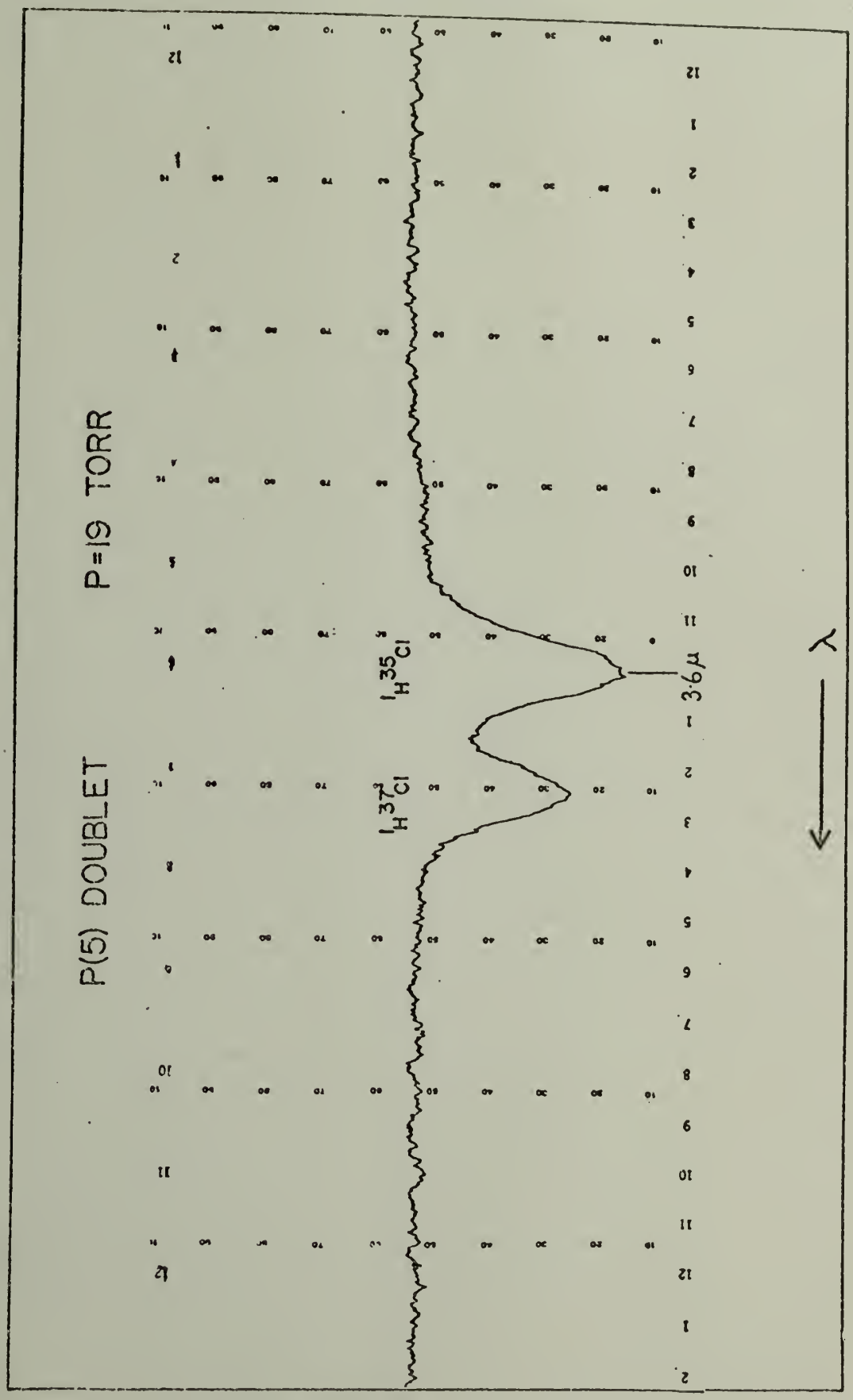
P(5) DOUBLET
P=19 TORR
$I_H{}^{35}Cl$
$I_H{}^{37}Cl$
3·6μ
λ

Fig. 16

Schematic representation of the experimental design described in Ch. 4.

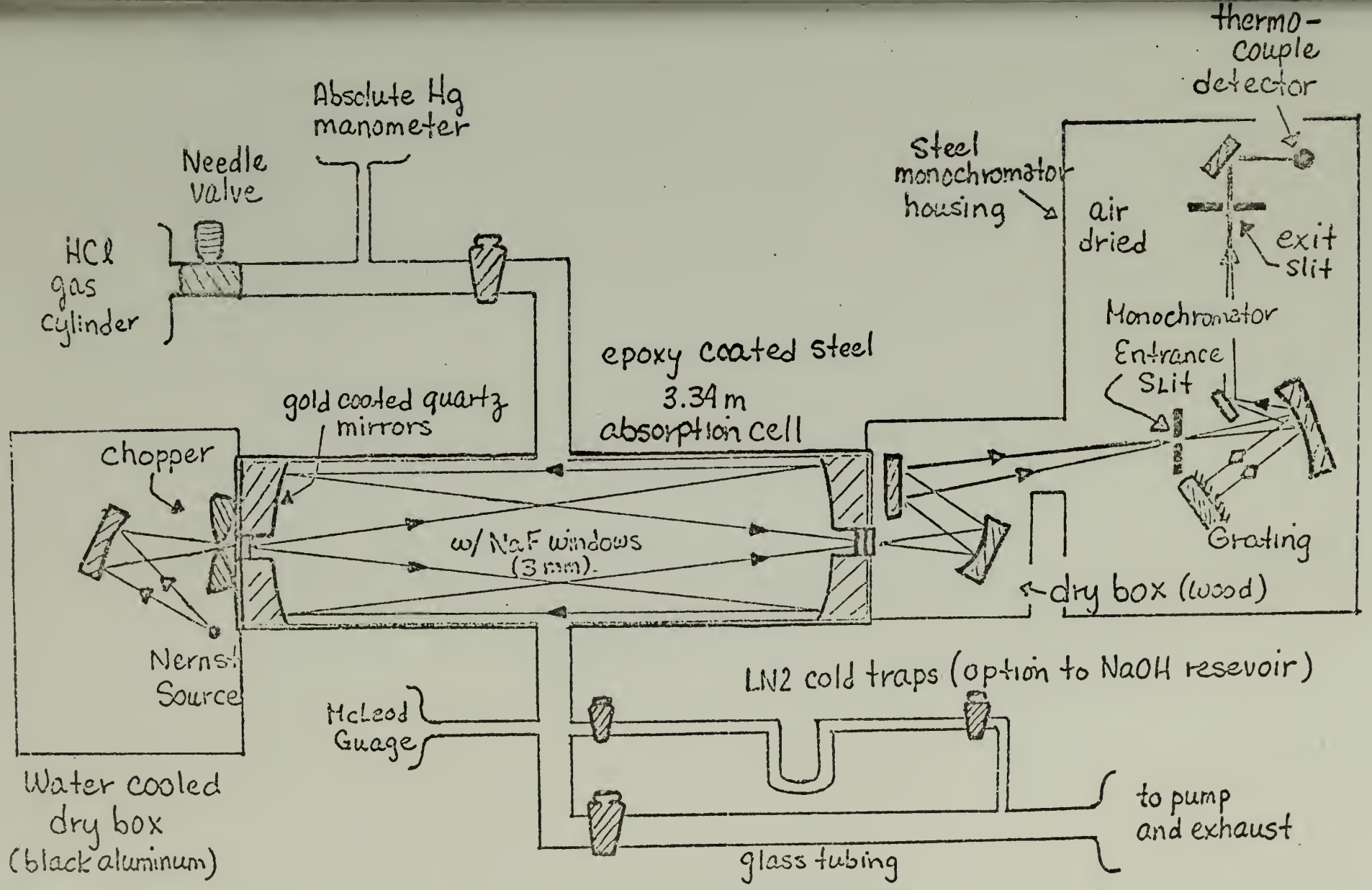

Experimental Apparatus
winter 1972-73

Fig. 17

Spectral resolution as a function of wavenumber in the HCl fundamental band using a Perkin-Elmer Model 210-B monochromator. The corrected slit width is indicated in microns next to each curve. The cross hatched area indicates the slit widths and frequencies most often used.

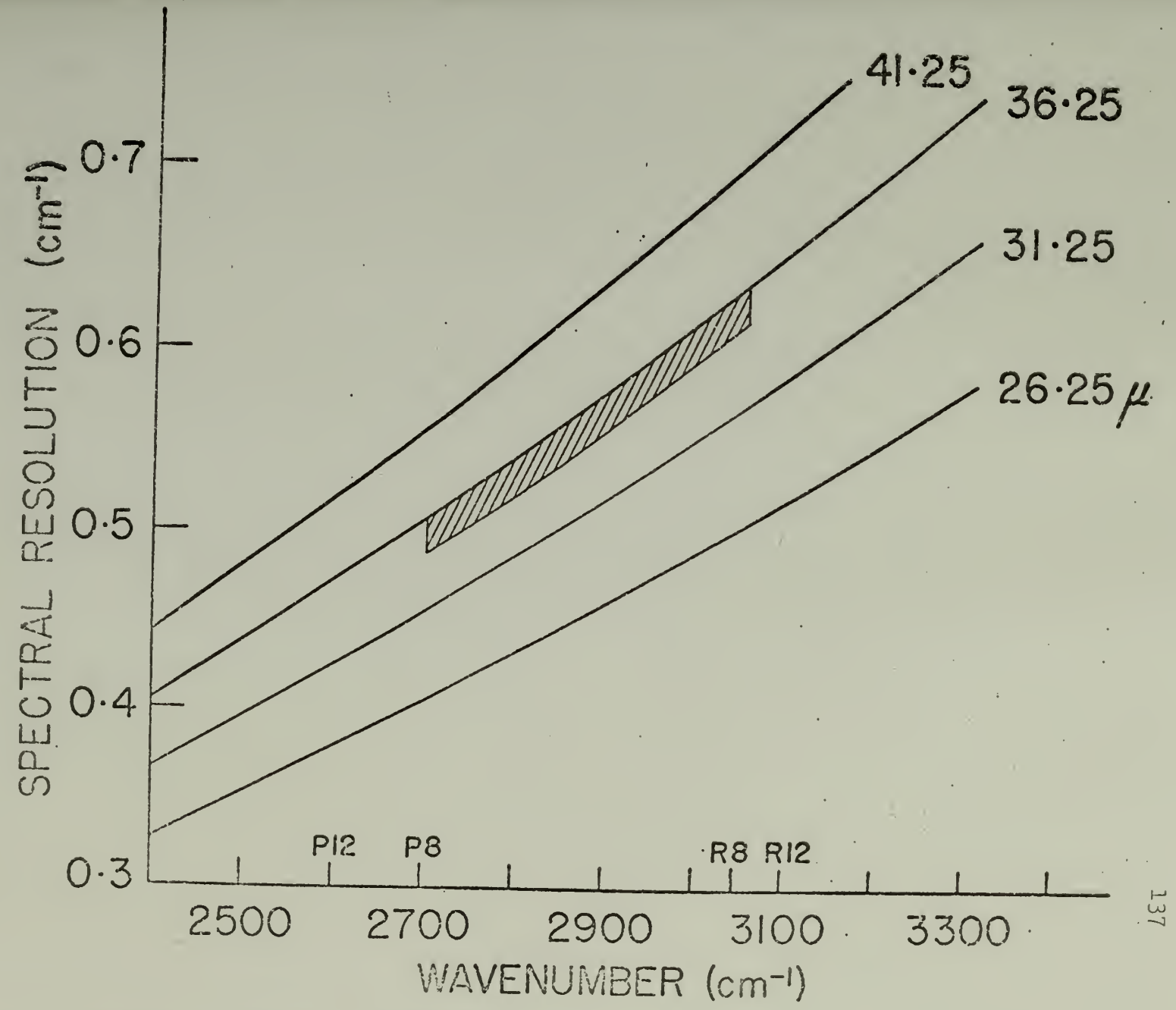
41·25
36·25
31·25
26·25 μ
SPECTRAL RESOLUTION (cm⁻¹)
0·7
0·6
0·5
0·4
0·3
P12
P8
R8
R12
2500
2700
2900
3100
3300
WAVENUMBER (cm⁻¹)

Fig. 18

Plot of the square root of the chart pen deflection (∝ intensity) as ordinate and the measured slit width on the monochromator micrometer dial as abscissa. The diagram illustrates the necessity for a "zero-point" adjustment to directly read slit width values of 23.75μ.

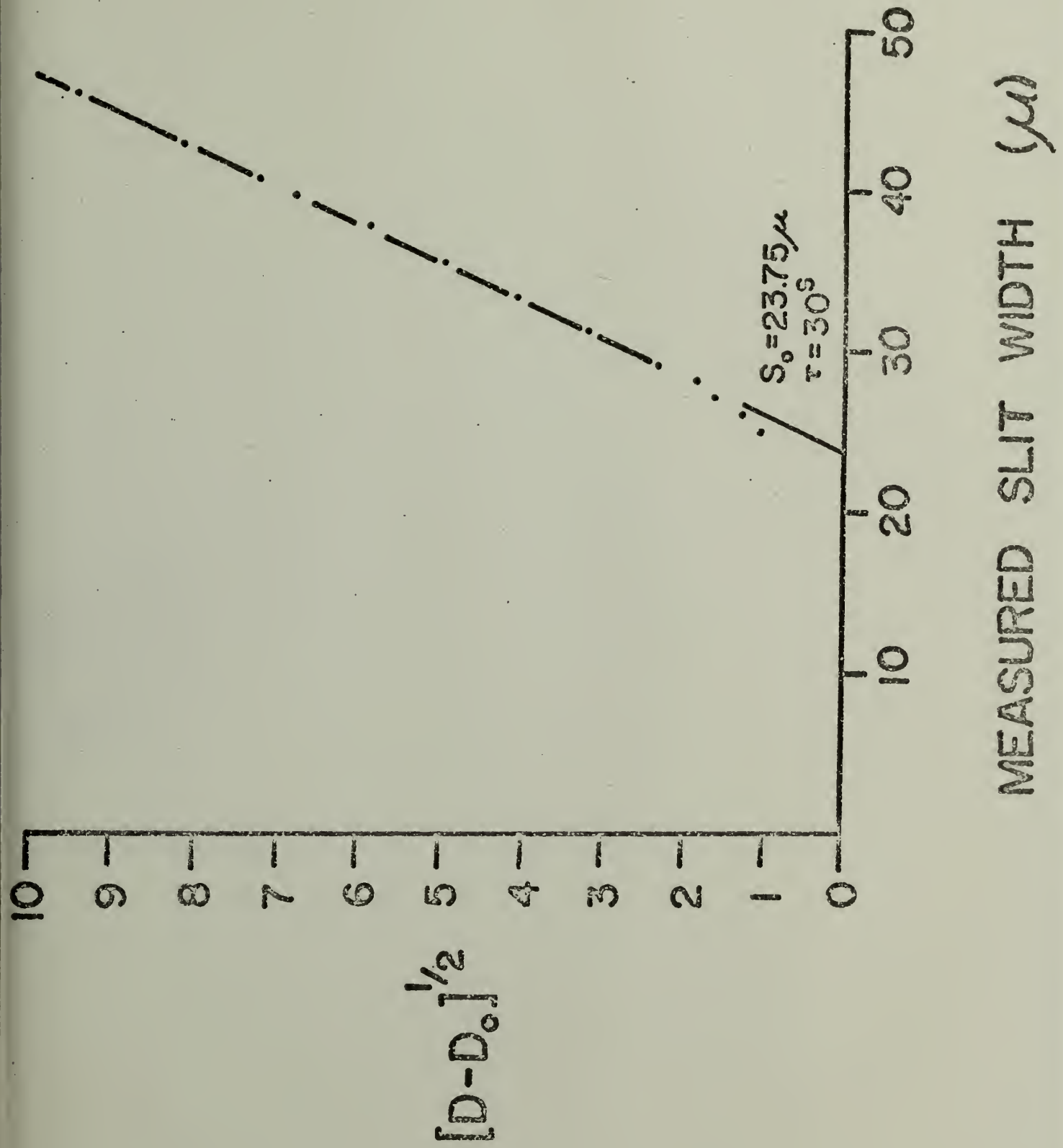
$[D-D_0]^{1/2}$
0
1
2
3
4
5
6
7
8
9
10
10
20
30
40
50
MEASURED SLIT WIDTH (μ)
S_0=23.75μ
τ=30^s

Fig. 19

Calibration of the grating angle of the Littrow mounted grating (or the associated drum number) in terms of frequency (in cm^{-1}).

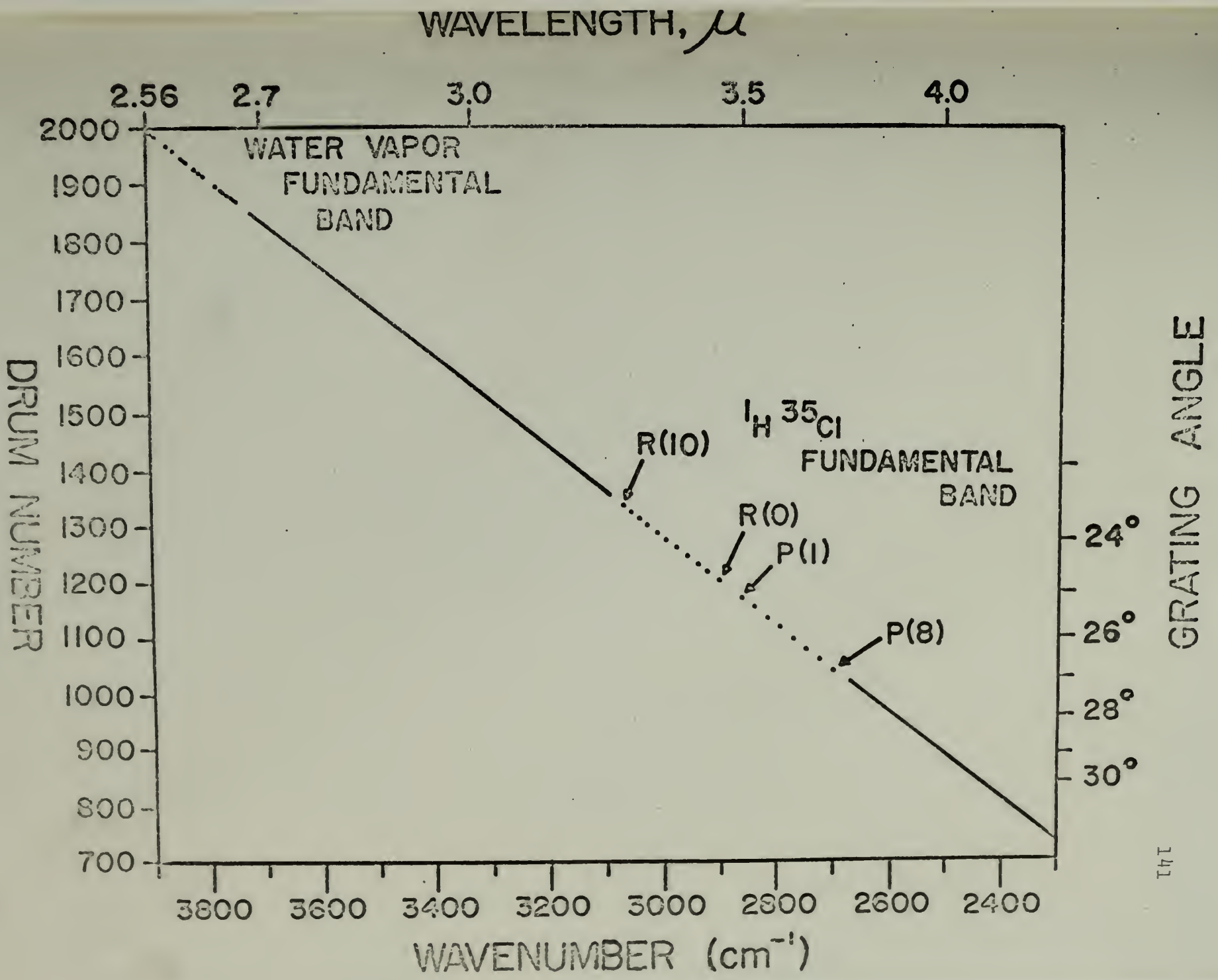
WAVELENGTH, μ
2.56
2.7
3.0
3.5
4.0
2000
1900
1800
1700
1600
1500
1400
1300
1200
1100
1000
900
800
700
DRUM NUMBER
WATER VAPOR
FUNDAMENTAL
BAND
R(10)
$^1H^{35}Cl$
FUNDAMENTAL
BAND
R(0)
P(1)
P(8)
24°
26°
28°
30°
GRATING ANGLE
3800
3600
3400
3200
3000
2800
2600
2400
WAVENUMBER (cm^{-1})

Fig. 20

Vapor pressures for all possible impurity gases within the HCl gas sample and for Mercury, Water, HCl and HBr. The latter was used in a calibration experiment. The ability of dry ice and liquid nitrogen to remove these impurities using entrance traps may be evaluated by noting their respective temperatures along the abscissa. When the gas partial pressure exceeds the vapor pressure, condensation occurs.

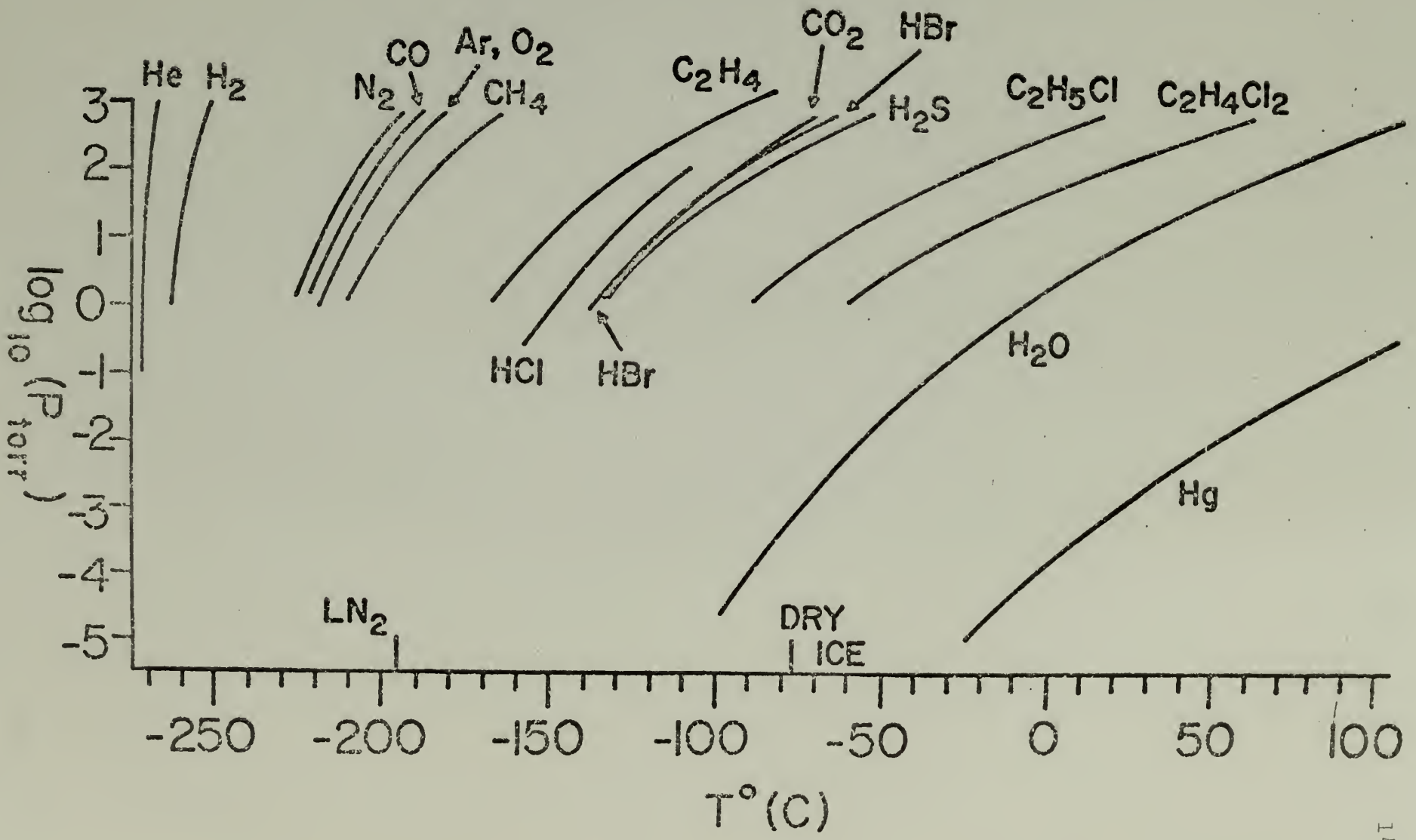
He
H_2
CO
N_2
Ar, O_2
CH_4
C_2H_4
CO_2
HBr
H_2S
C_2H_5Cl
$C_2H_4Cl_2$
HCl
HBr
H_2O
Hg
LN_2
DRY ICE
3
2
1
0
-1
-2
-3
-4
-5
$\log_{10}(p_{torr})$
-250
-200
-150
-100
-50
0
50
100
T°(C)

Fig. 21

Line center or peak absorptance, $\bar{A}_o$, as a function of $x_o \frac{d\bar{A}}{dx} = \alpha\sigma$ for a Lorentz absorption line convoluted with a triangular scanning function. Here, $\alpha = \frac{d\bar{A}}{d\nu}$ is the inflection point slope of the line contour and σ is the spectral resolution.

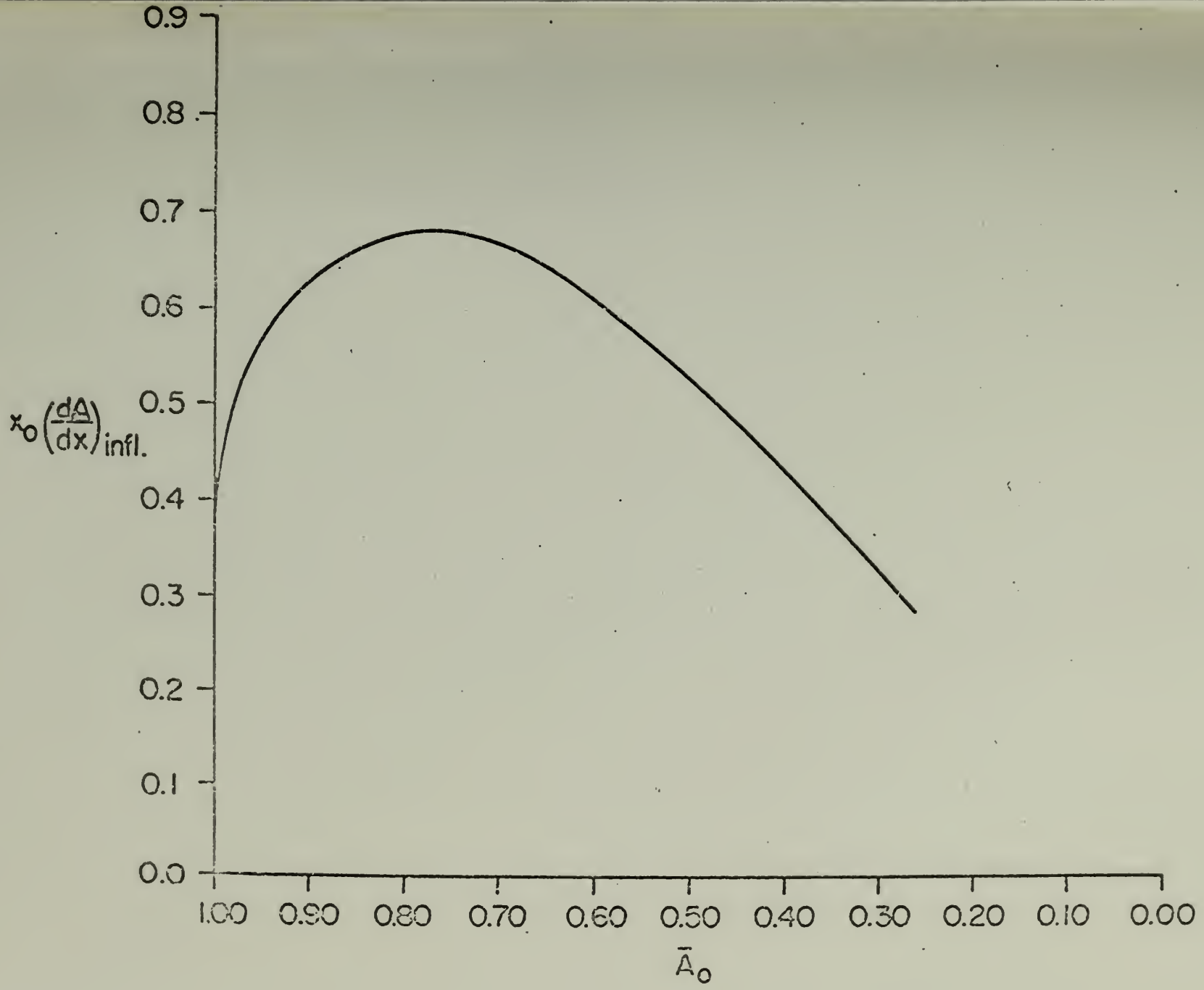
0.9
0.8
0.7
0.6
0.5
0.4
0.3
0.2
0.1
0.0
$x_o\left(\frac{d\bar{A}}{dx}\right)_{infl.}$
1.00
0.90
0.80
0.70
0.60
0.50
0.40
0.30
0.20
0.10
0.00
$\bar{A}_o$

Fig. 22

Experimental spectra of the HCl fundamental band R(7) and P(8) isotopic doublets recorded at 19.5 torr (σ = 0.632 cm^{-1}) and 18.55 torr (σ = 0.509 cm^{-1}) respectively using a 3.34m path. Three separate estimations of the inflection point slope are shown for the $^{1}H^{35}Cl$ line together with baselines derived from these estimates. The calculated value of the otherwise estimated inflection point position is shown by the middle arrow for P(8).

The slope of the $^{1}H^{35}Cl$ profile within the P(8) doublet approximates its inflection point slope for only $\sim$ 0.04 cm^{-1} (such that a $\Delta\alpha \rightarrow \Delta\bar{A}_o \leq 1\%$). On the original spectra, the distance from $\bar{A}_o$ to the point where $\bar{A} \sim 0$ is $\sim$ 1 cm^{-1} $\sim$ 1.25 inches. Hence, 0.04 cm^{-1} amounts to $\sim$ 1/25 inches and is nearly impossible to measure accurately. The two outermost arrows indicate the extent of the segment where α would approximate α_i if $\sigma \sim 0.7$ cm^{-1}.

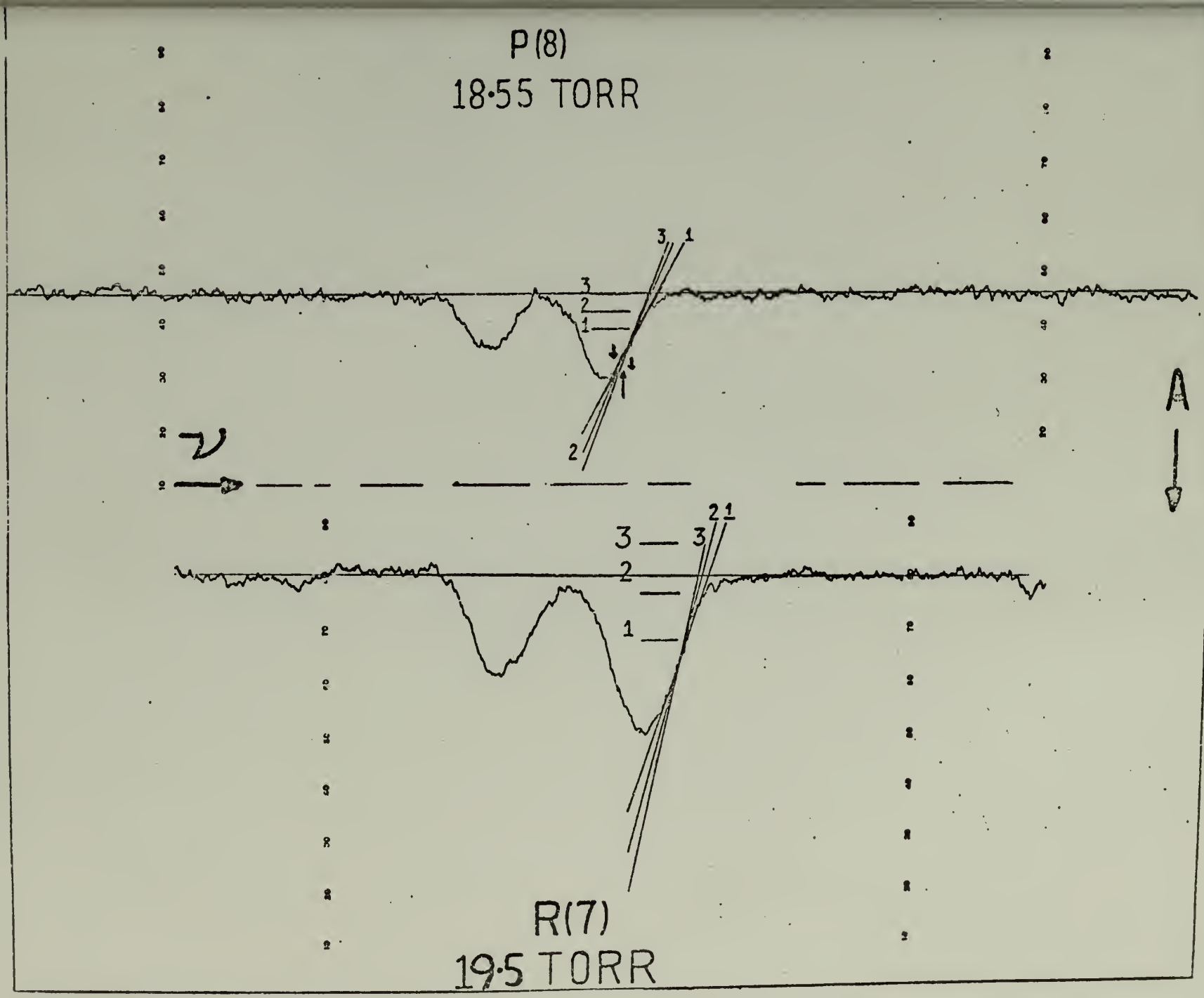
P(8)
18·55 TORR
3
2
1
3
2
1
ν
A
3
2
1
3
2
1
R(7)
19·5 TORR

Fig. 23

The P(5) isotopic doublet experimental contour from the same experiment (Ch. 4) on HCl gas. Here, σ = 0.535 cm^{-1} and p = 18.65 torr. Note the large variation in baseline placement produced by a very small error in locating the tangent line. Values of $\Delta v/\Delta h$ measured on the chart recorder trace are indicated next to the drawn baselines.

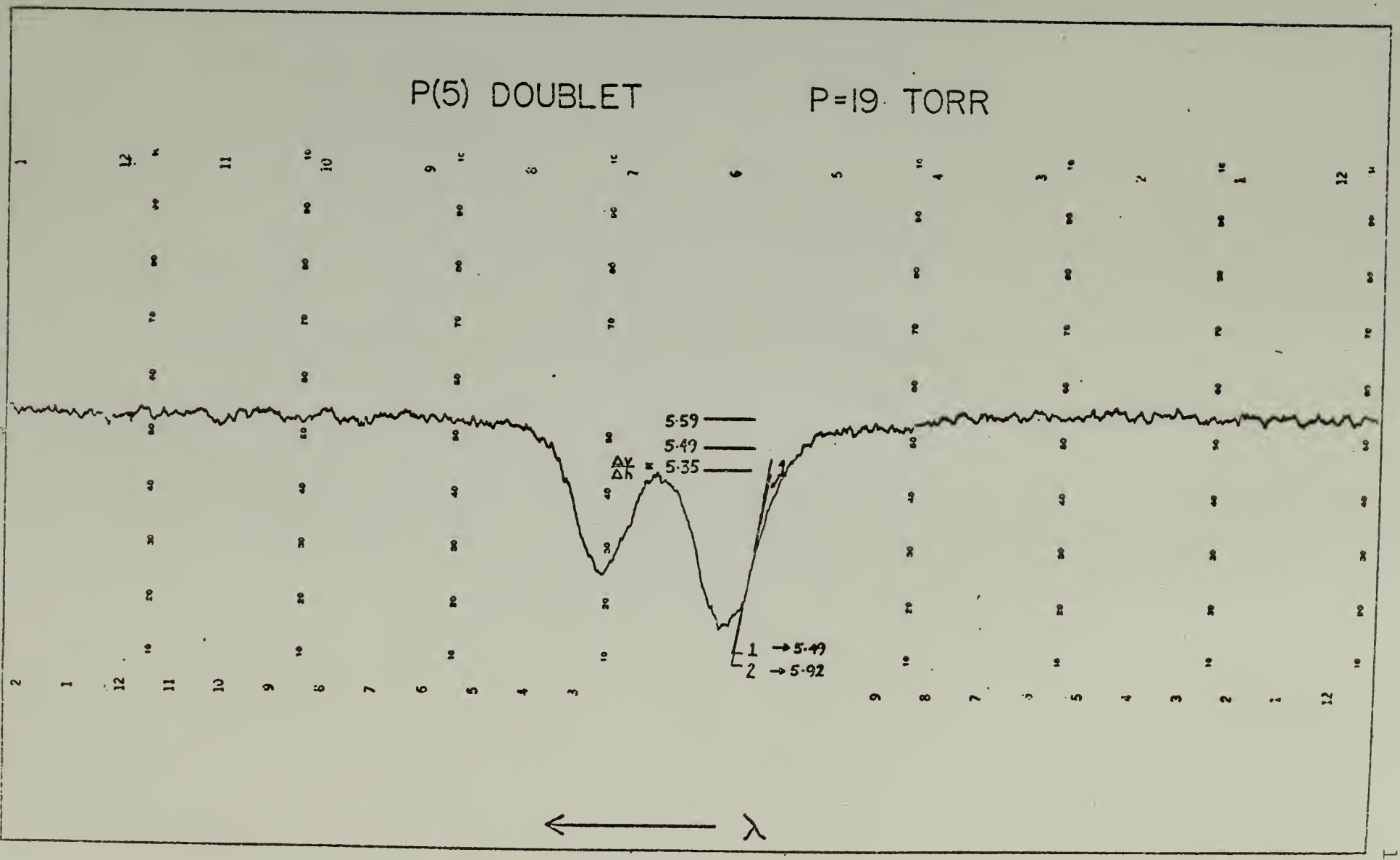
P(5) DOUBLET
P=19 TORR
5·59
5·49
Δν/Δh = 5·35
1 → 5·49
2 → 5·92
λ

Fig. 24

Theoretically convoluted absorption line contour (vertical scale multiplied by ten) as a function of x for the $^{1}H^{35}Cl$ member of the P(8) doublet using the experimental conditions of Fig. 22. This is a Lorentz line distorted by a triangular slit function (σ = 0.509 cm^{-1}). The conversion from x to $(\nu-\nu_o)$ is listed along the top of the figure. Plots are given of $\frac{d\bar{A}}{dx}$ which peaks at x $\sim$ 5 and of $d^2\bar{A}/dx^2$ which intersects the x axis at the inflection point (vertical scale) to indicate the ease with which the inflection point (indicated by the arrow) and its correct slope may be identified. The inflection point slope is drawn intersecting the line contour at x $\sim$ 5.

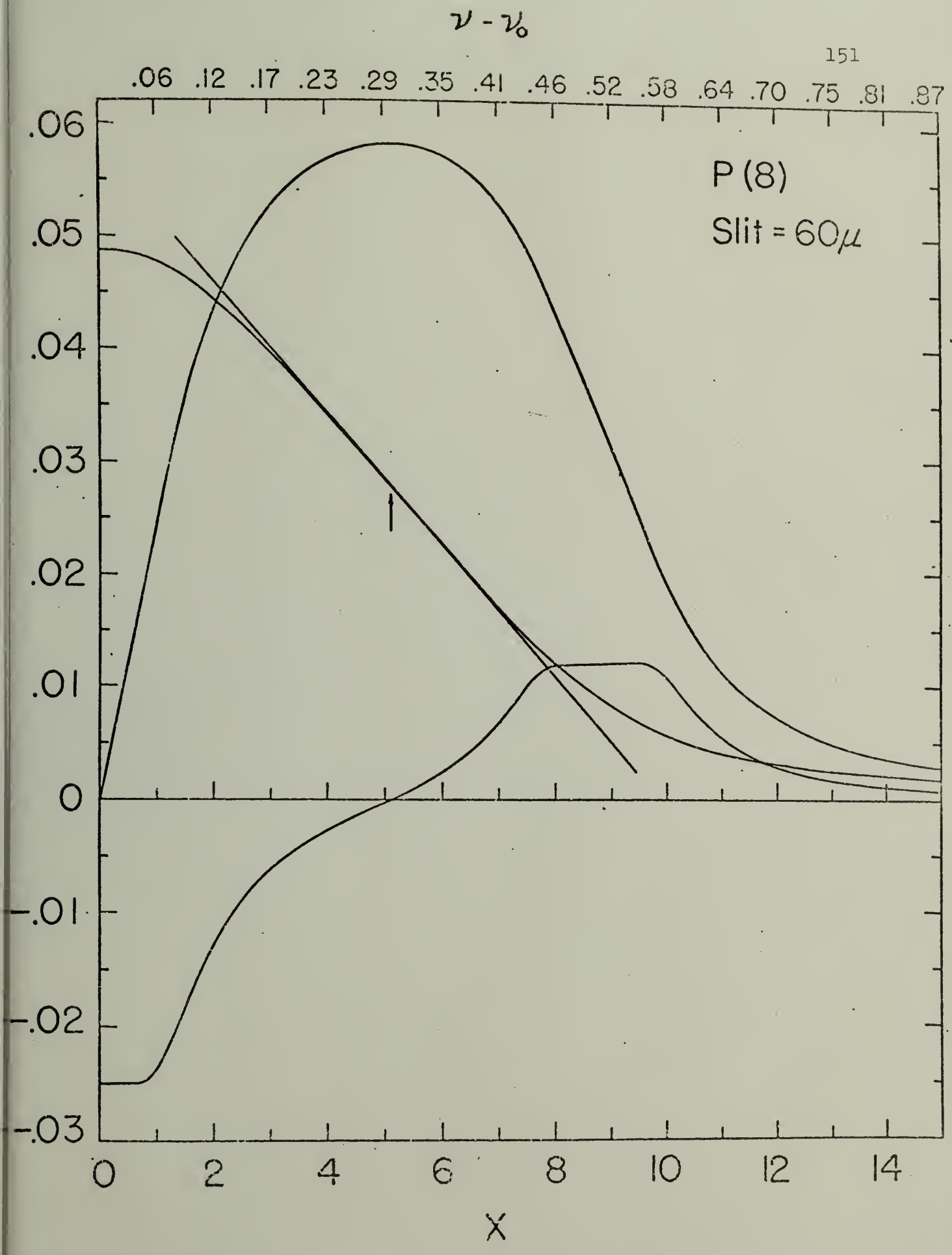
ν - ν₀
.06 .12 .17 .23 .29 .35 .41 .46 .52 .58 .64 .70 .75 .81 .87
.06
.05
.04
.03
.02
.01
0
-.01
-.02
-.03
P (8)
Slit = 60μ
0 2 4 6 8 10 12 14
X

Fig. 25

The P(8) line of Fig. 24 viewed at a poorer resolution (σ = 0.559 cm^{-1}). Note the smaller angle that the second derivative curve makes in crossing the x axis. Poorer resolutions force the slope to approximate the inflection point value for a greater portion of the line contour. Here, $\alpha \sim \alpha_i$ for $\nu-\nu_i \sim 0.1$ cm^{-1} ($\sim$ 1/8 inch on Fig. 22 if this resolution had been employed).

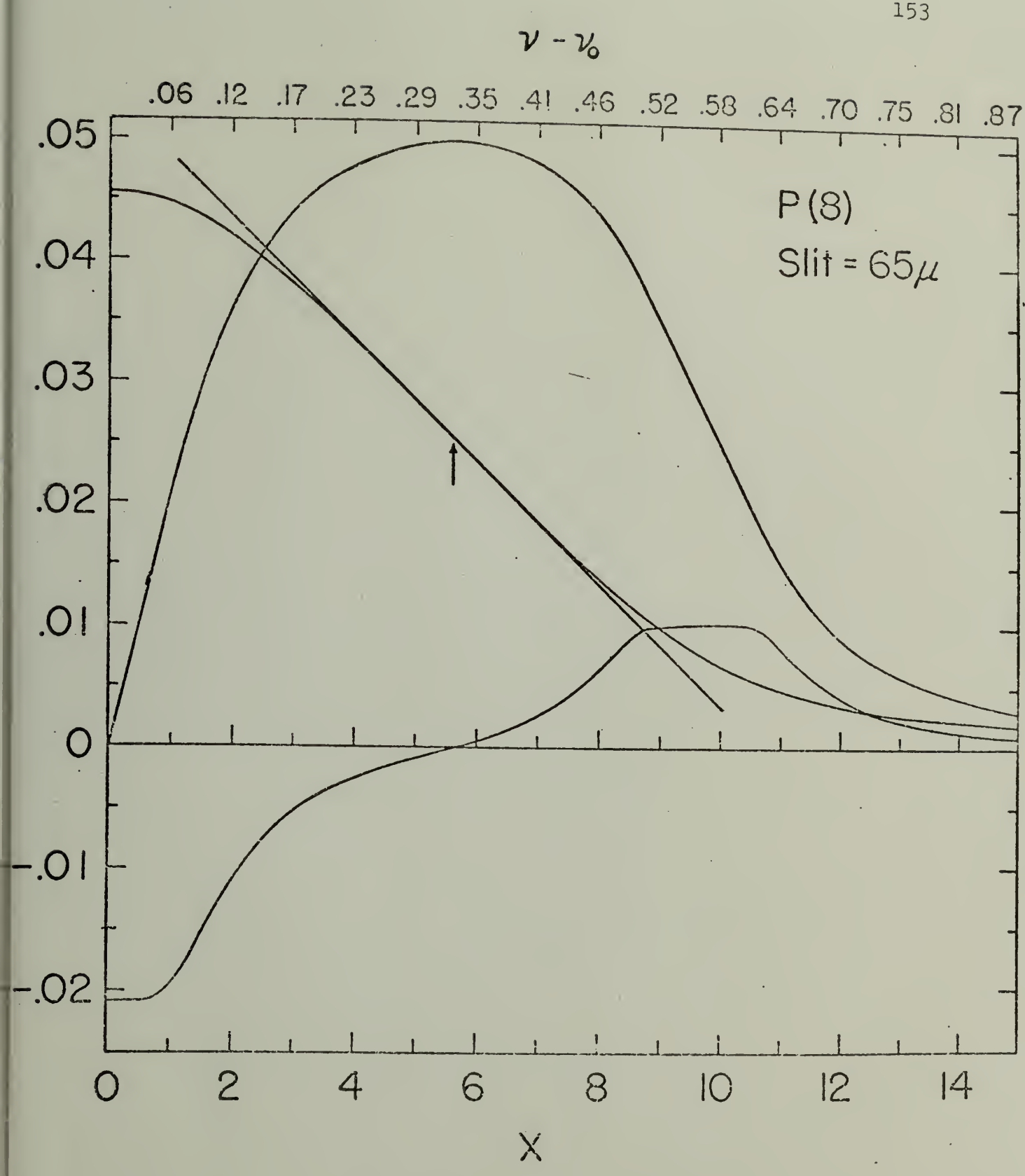
ν - ν₀
.06 .12 .17 .23 .29 .35 .41 .46 .52 .58 .64 .70 .75 .81 .87
.05
.04
.03
.02
.01
0
-.01
-.02
P(8)
Slit = 65μ
0 2 4 6 8 10 12 14
X

Fig. 26

Variation in the predicted peak absorptance when slopes are precisely measured at $x - x_i \neq 0$ and taken to be inflection point slopes by mistake. The top curve is derived from Fig. 25 ($\sigma = 0.559$ cm^{-1}) and the bottom curve from Fig. 24 ($\sigma = 0.509$ cm^{-1}).

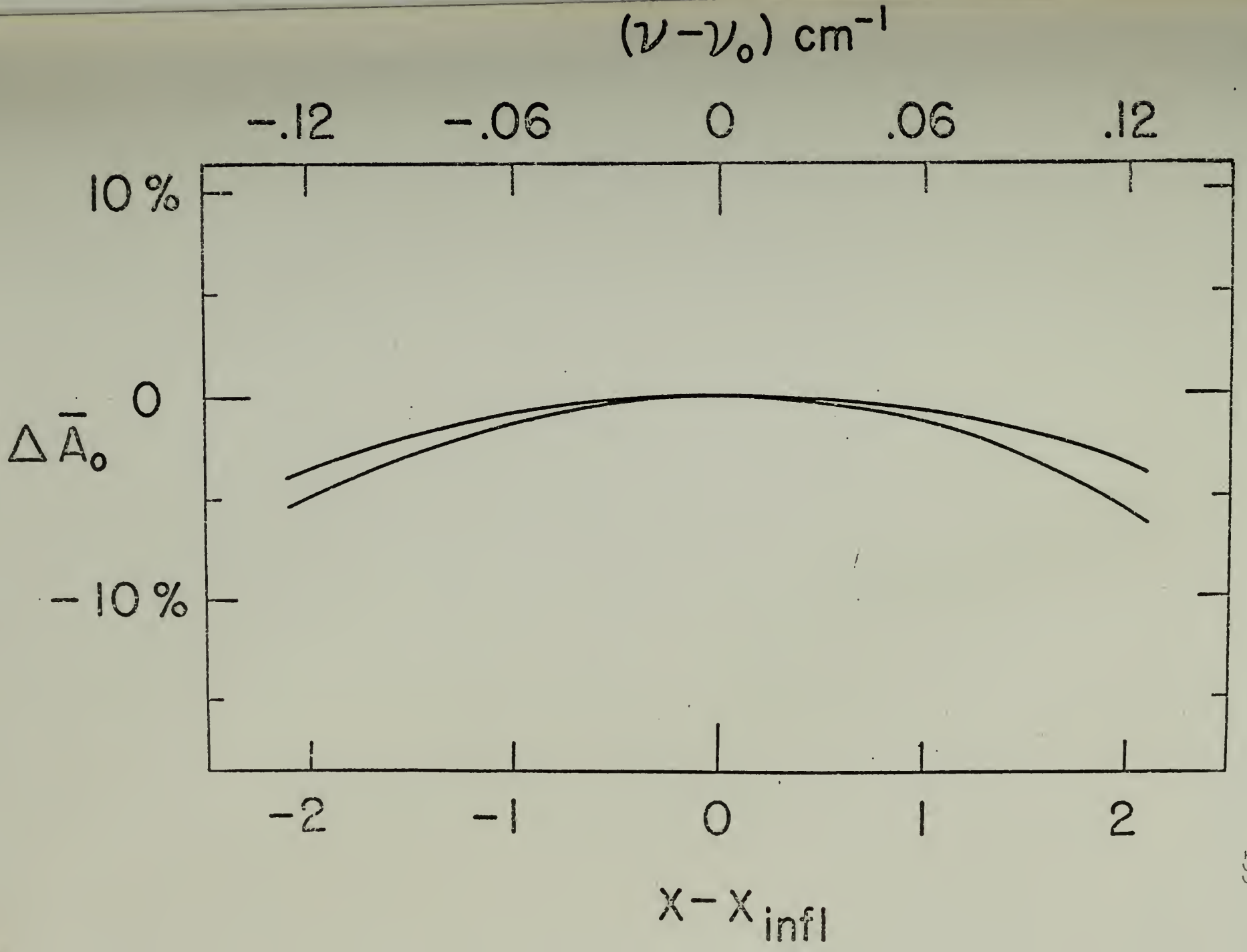
$(\nu - \nu_0)$ cm^{-1}
-.12
-.06
0
.06
.12
10 %
0
$\Delta \bar{A}_0$
-10 %
-2
-1
0
1
2
$X - X_{infl}$

Fig. 27

Plot of the second derivitive of a Lorentz absorption contour, $\frac{d^2\bar{A}}{dx^2}$ as ordinate with $x = \frac{\nu-\nu_o}{\gamma z}$ as abscissa for a variety of square root lines and spectral resolutions, σ. x_o is given by $\sigma/\gamma z$ where z indicates how deeply into the square root region the line absorbs. For a given line, the slope approximates that at the inflection point over a greater segment of the line contour as the resolution becomes poorer (σ and x_o increase). Alternatively, by specifying the resolution, narrower or weaker lines produce the same effect. When $\sigma = 0.509$ cm^{-1} (as for the P(8) results in Figs. 22 and 24), the extent in x about the inflection point may be identified (in this Figure, by solid lines which run horizontally just above the x axis) over which measured slopes deviate from the inflection point slope α_i by an amount which causes $\Delta\bar{A}_o \leq 1\%$.

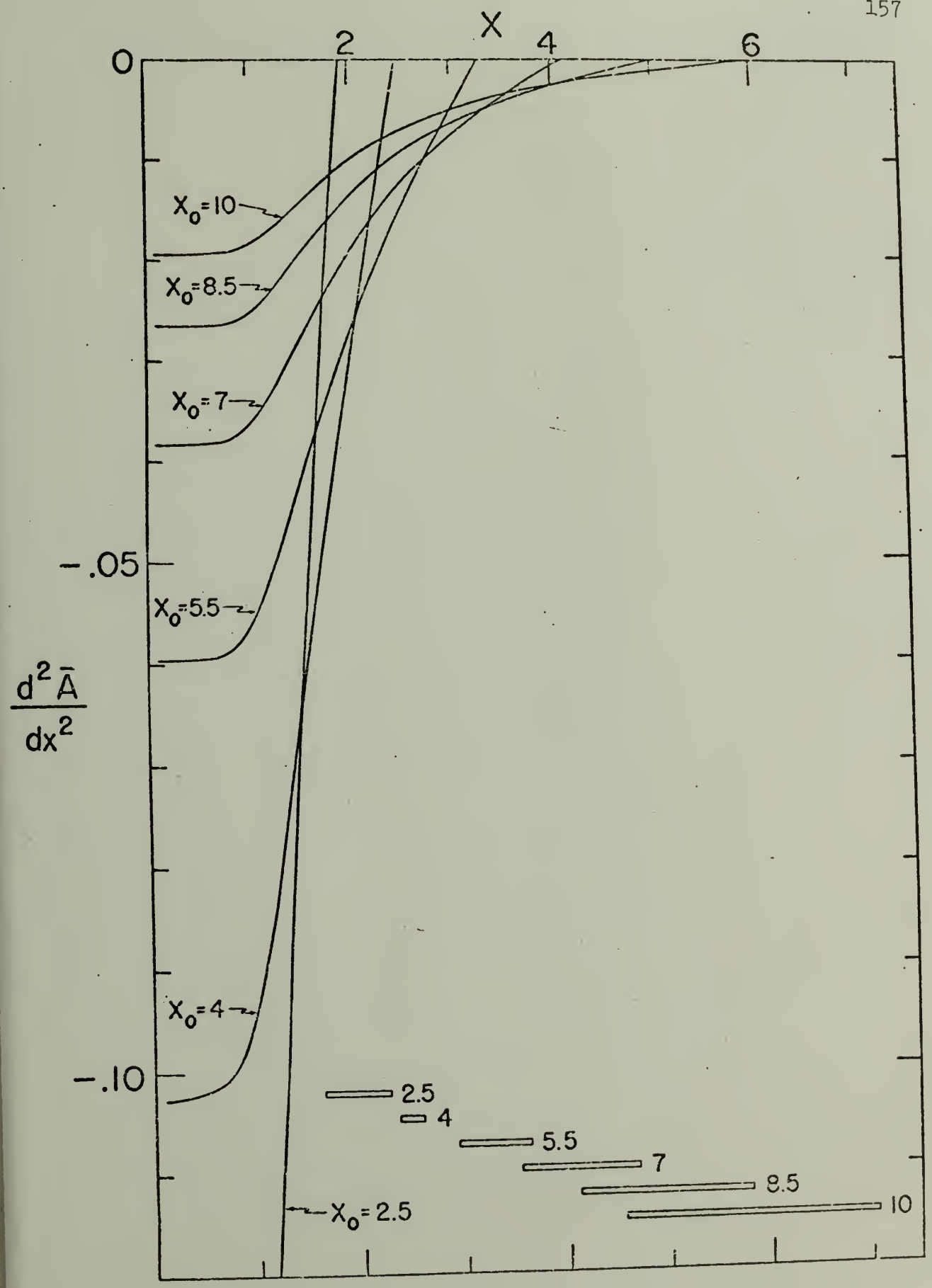
X
0
2
4
6
-.05
-.10
$\frac{d^2\bar{A}}{dx^2}$
X_0=10
X_0=8.5
X_0=7
X_0=5.5
X_0=4
X_0=2.5
2.5
4
5.5
7
8.5
10

Fig. 28

Predicted and experimental equivalent widths plotted as a function of pressure for the R(7) and R(8) isotopic doublets. Observed values have been corrected for unobservable absorption in the line wings and are plotted as solid dots. The straight line is a linear least squares fit to these observations and only applies at pressures such that $\varepsilon \leq 5\%$. Because all experimental points arise from Lorentz lines, W should vanish at $p = 0$ and the line should pass through the origin.

Equivalent widths predicted from Ch. 3 using S values published in Refs. 12 and 31 (using Ref. 12 values of γ) are enclosed by circles and squares respectively, at each (the large numbers directly below these predictions) of the indicated values for ε. The agreement between each prediction and the observational least squares fit is striking and strongly supports the accuracy of the analysis in Ch. 3.

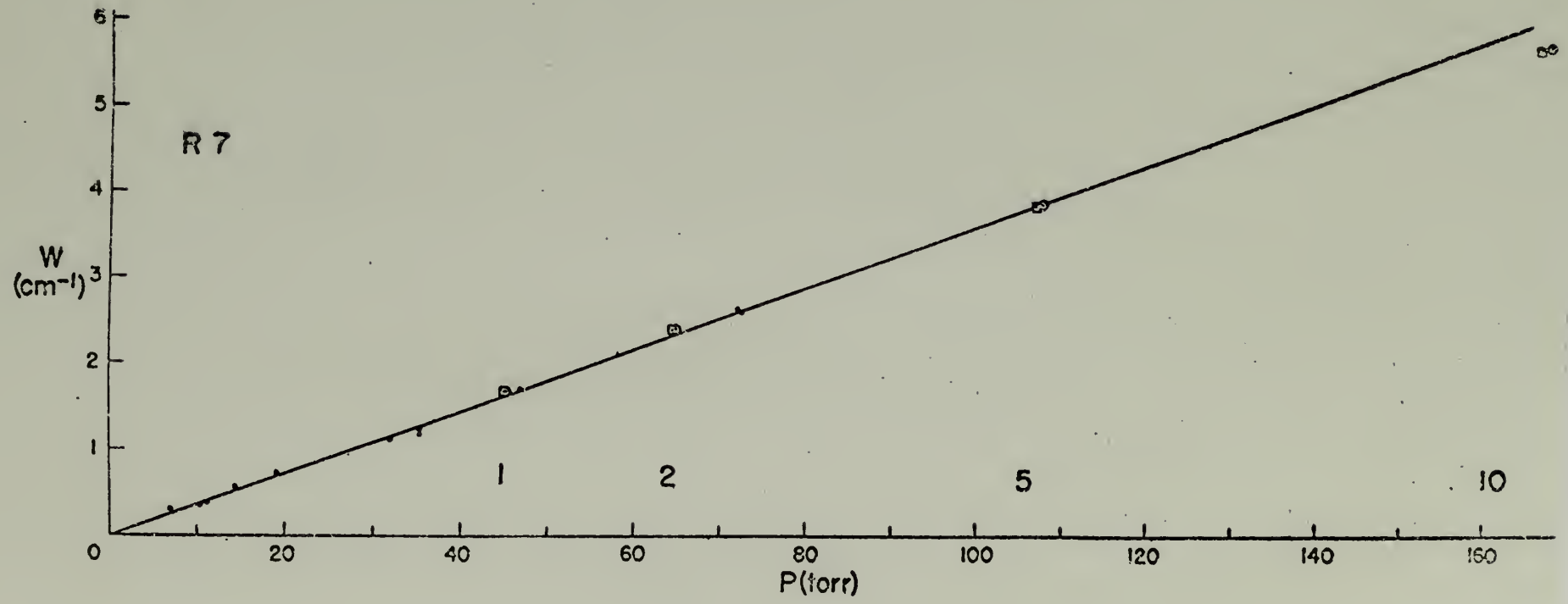
R 7
W
(cm⁻¹)
P(torr)
1
2
5
10

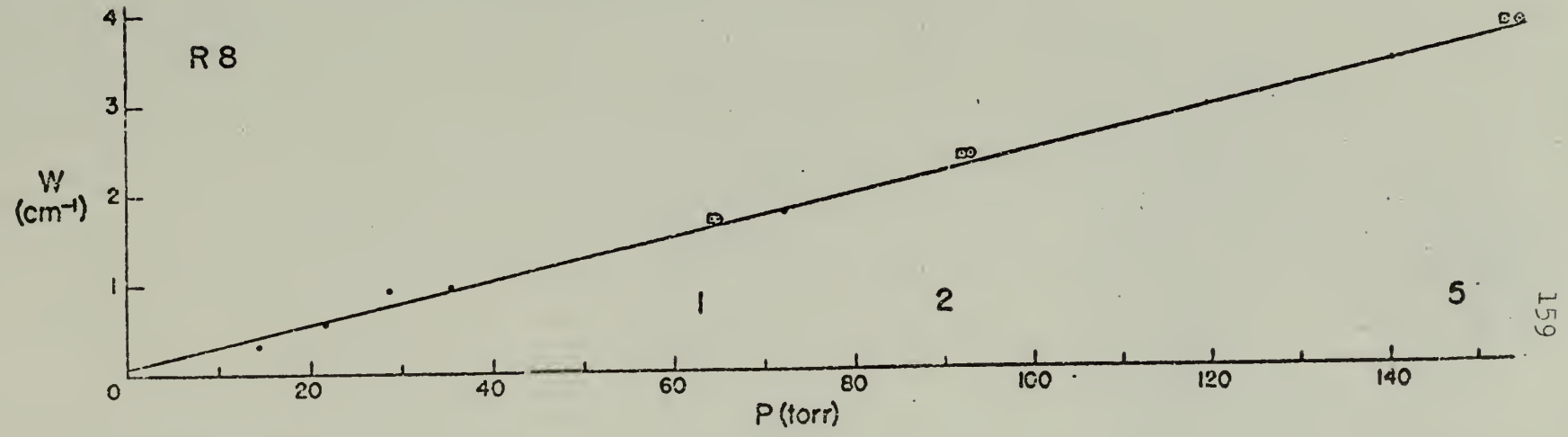
R 8
W
(cm⁻¹)
P (torr)
1
2
5

Figs. 29 through 42

Results for the remainder of the band from R(6) to P(8). Notation follows that in Fig. 28 with the exception that predictions based upon $S\gamma$ values from Ref. 13 have been added in the P branch and are enclosed within triangles. The agreement between predictions from the verified analysis of Ch. 3 using S and γ values from Benedict et al.[12] is, in general, quite good.

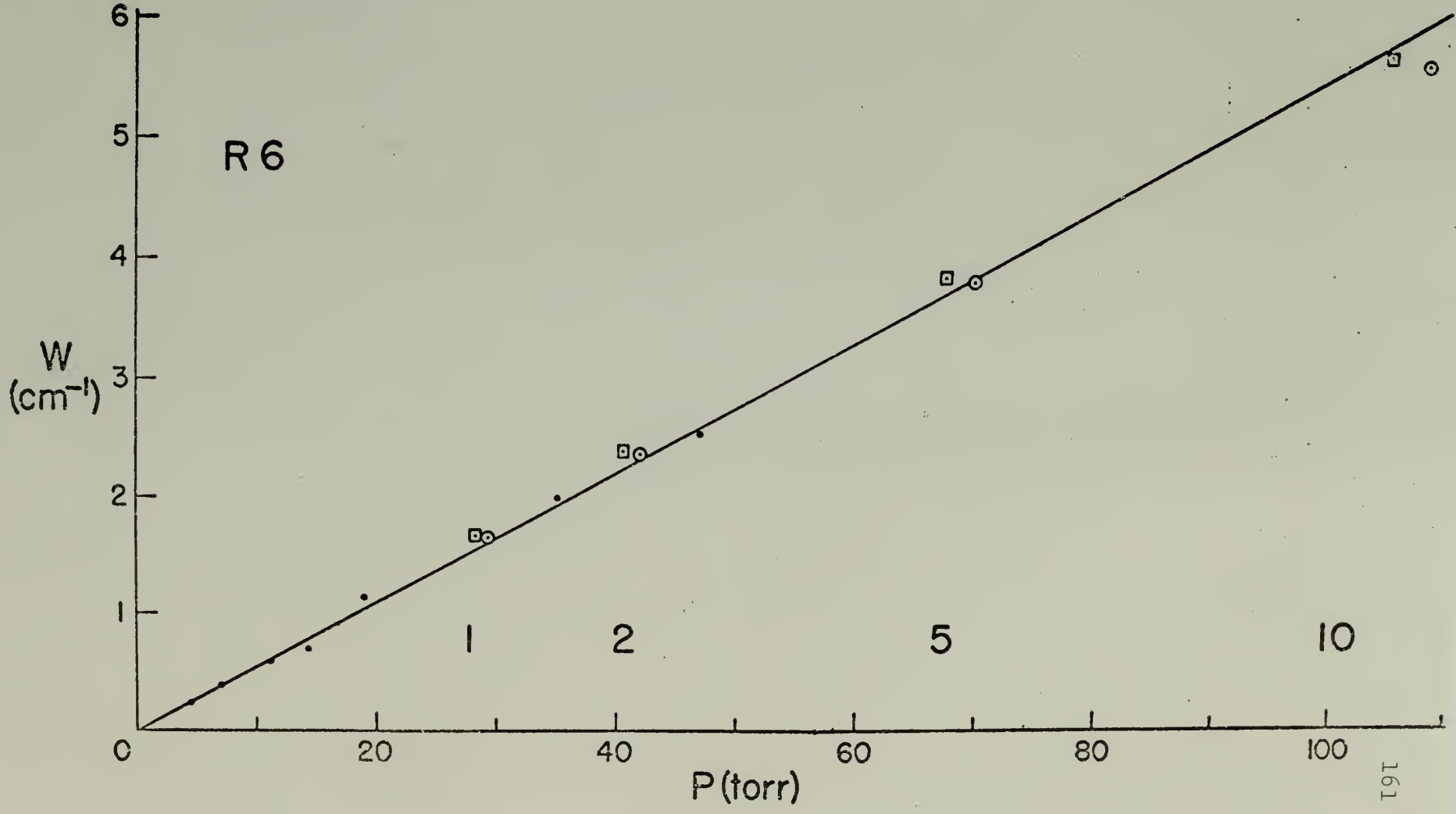
R 6
W
(cm⁻¹)
6
5
4
3
2
1
0
20
40
60
80
100
P (torr)
1
2
5
10

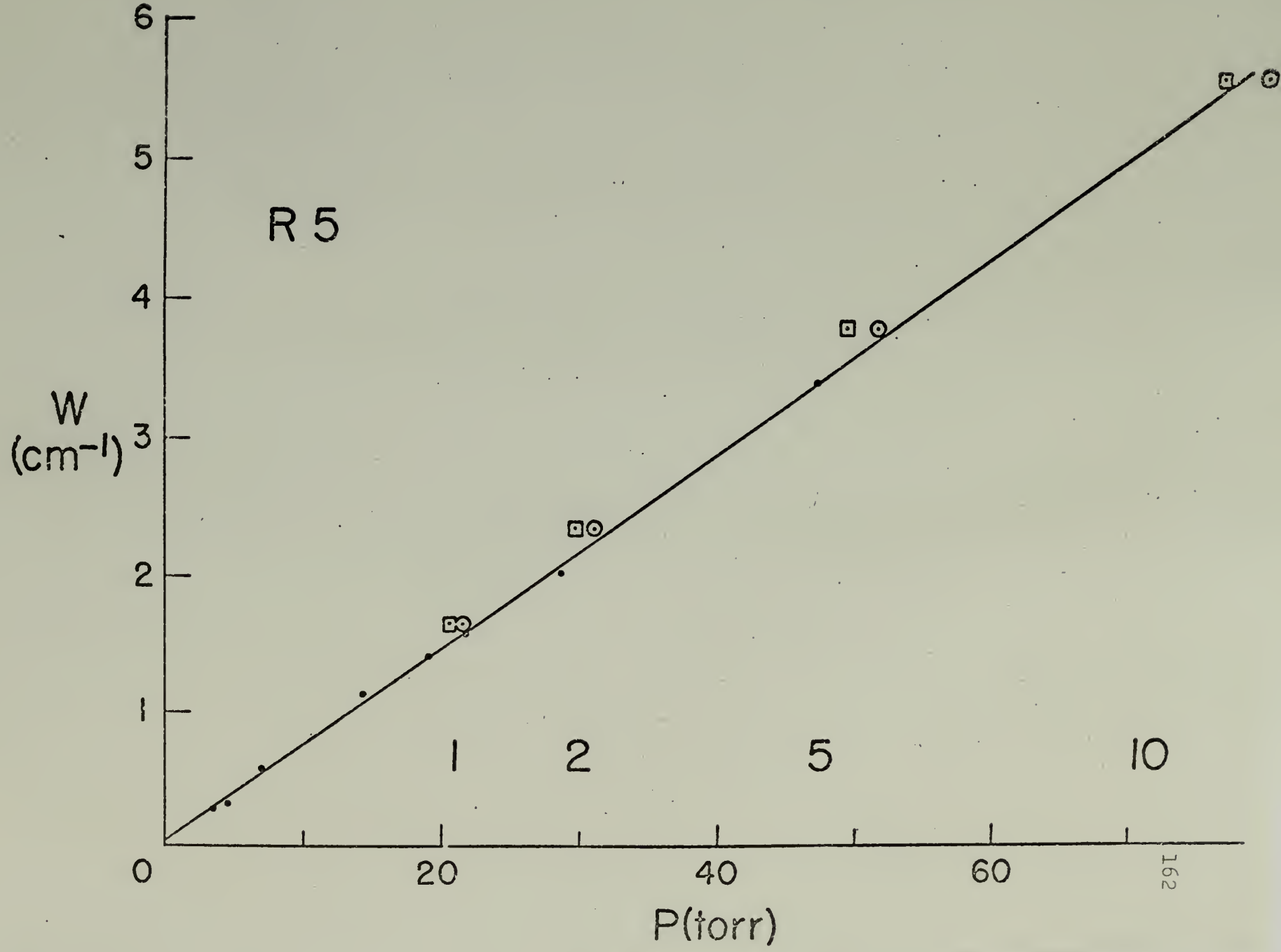
R 5
W
(cm⁻¹)
6
5
4
3
2
1
0
20
40
60
1
2
5
10
P(torr)

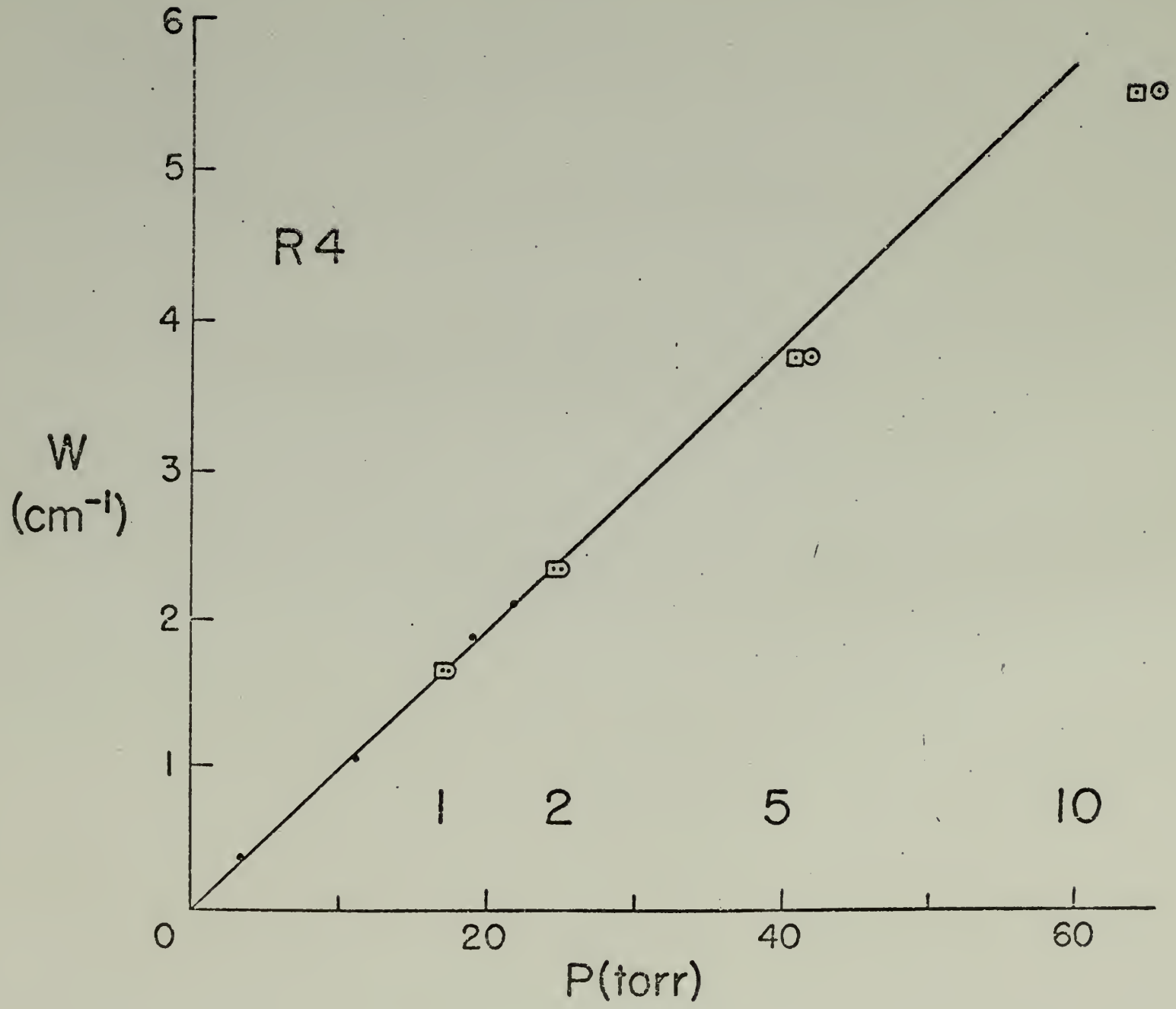
6
5
4
3
2
1
0
W
(cm⁻¹)
R4
1
2
5
10
20
40
60
P(torr)

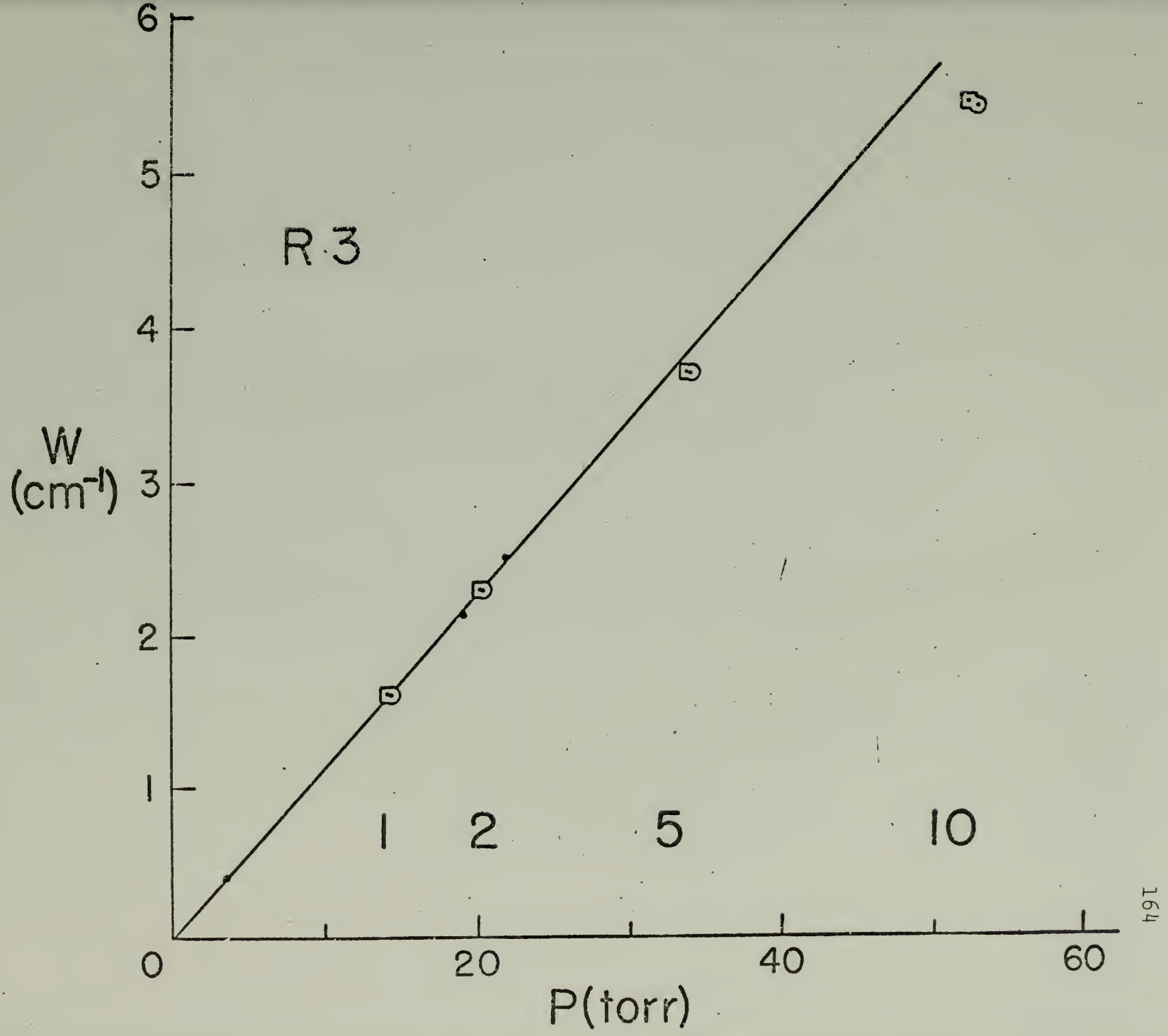
R 3
W
(cm⁻¹)
6
5
4
3
2
1
0
1
2
5
10
20
40
60
P(torr)

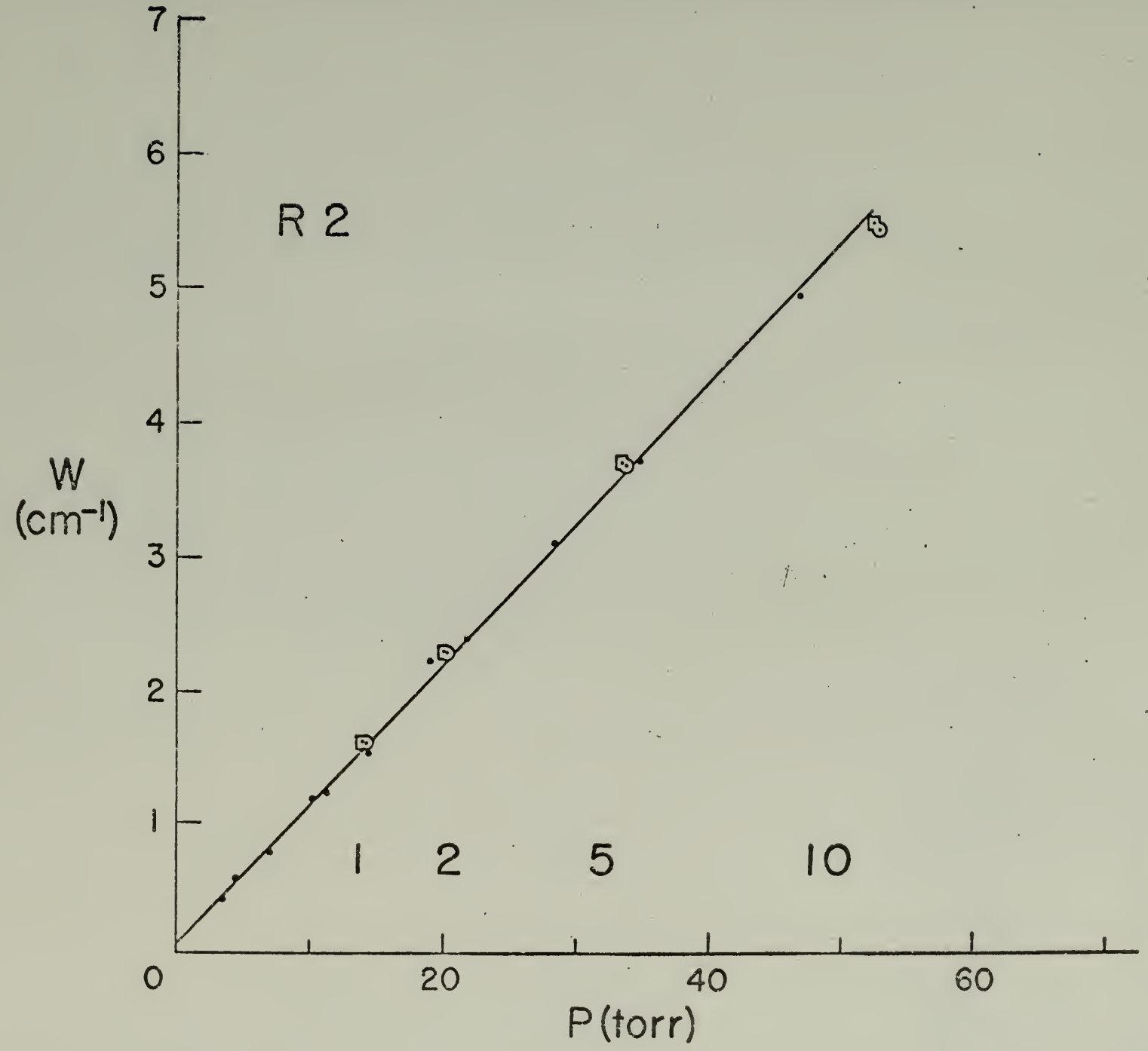
R 2
W
(cm⁻¹)
7
6
5
4
3
2
1
0
20
40
60
P(torr)
1
2
5
10

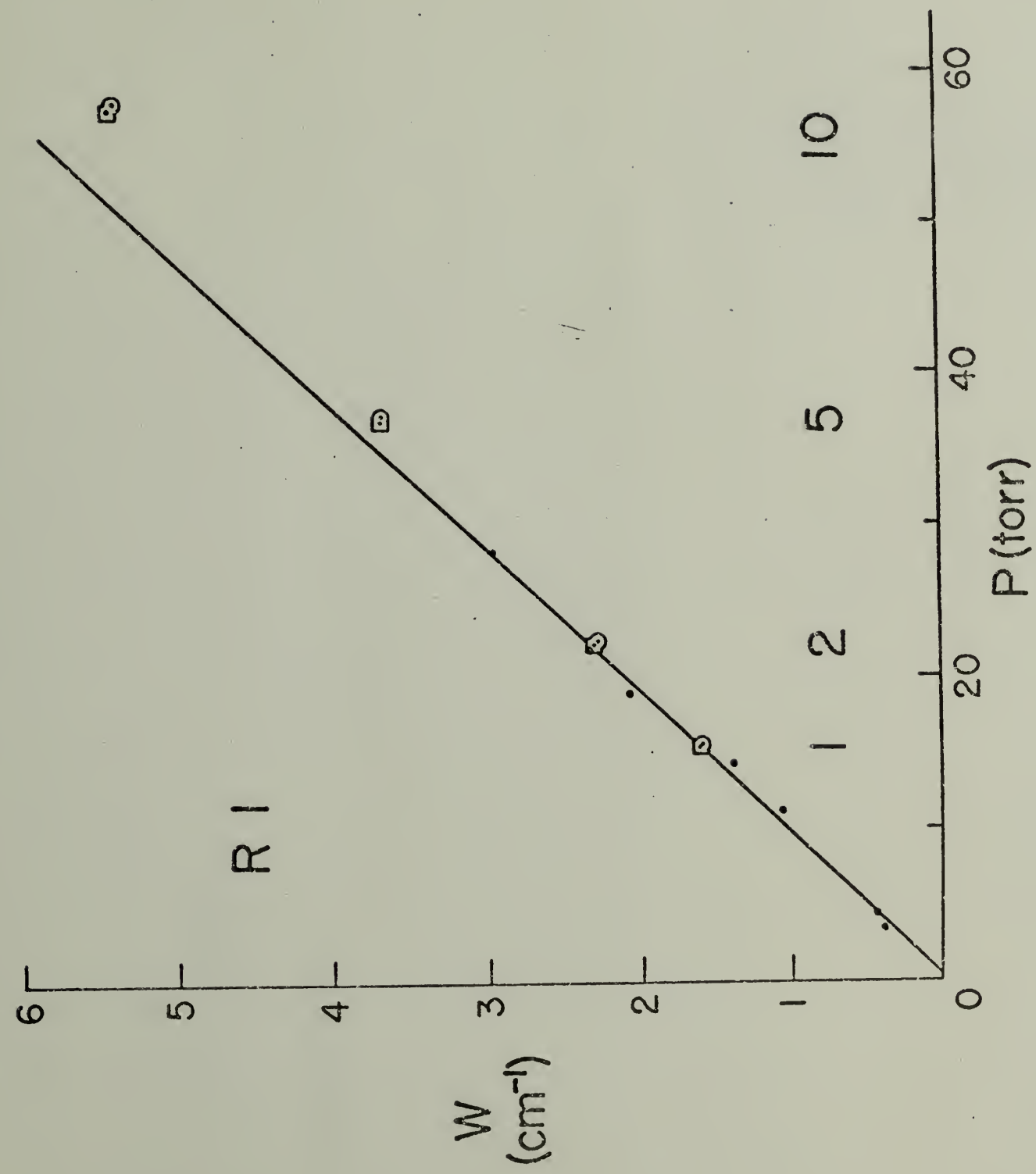
R I
W (cm⁻¹)
P (torr)
0
1
2
3
4
5
6
20
40
60
1
2
5
10

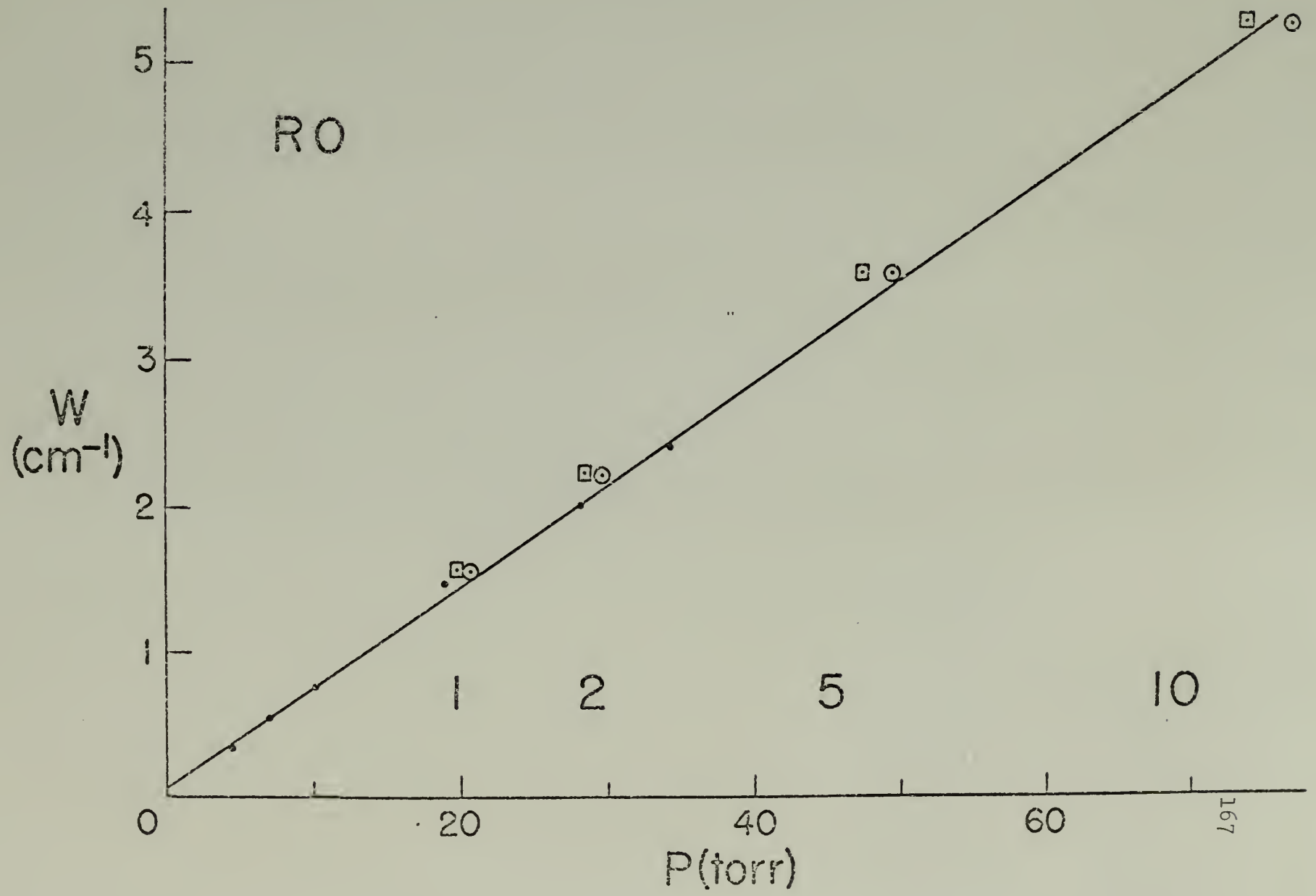
RO
W
(cm⁻¹)
5
4
3
2
1
0
20
40
60
P(torr)
1
2
5
10
167

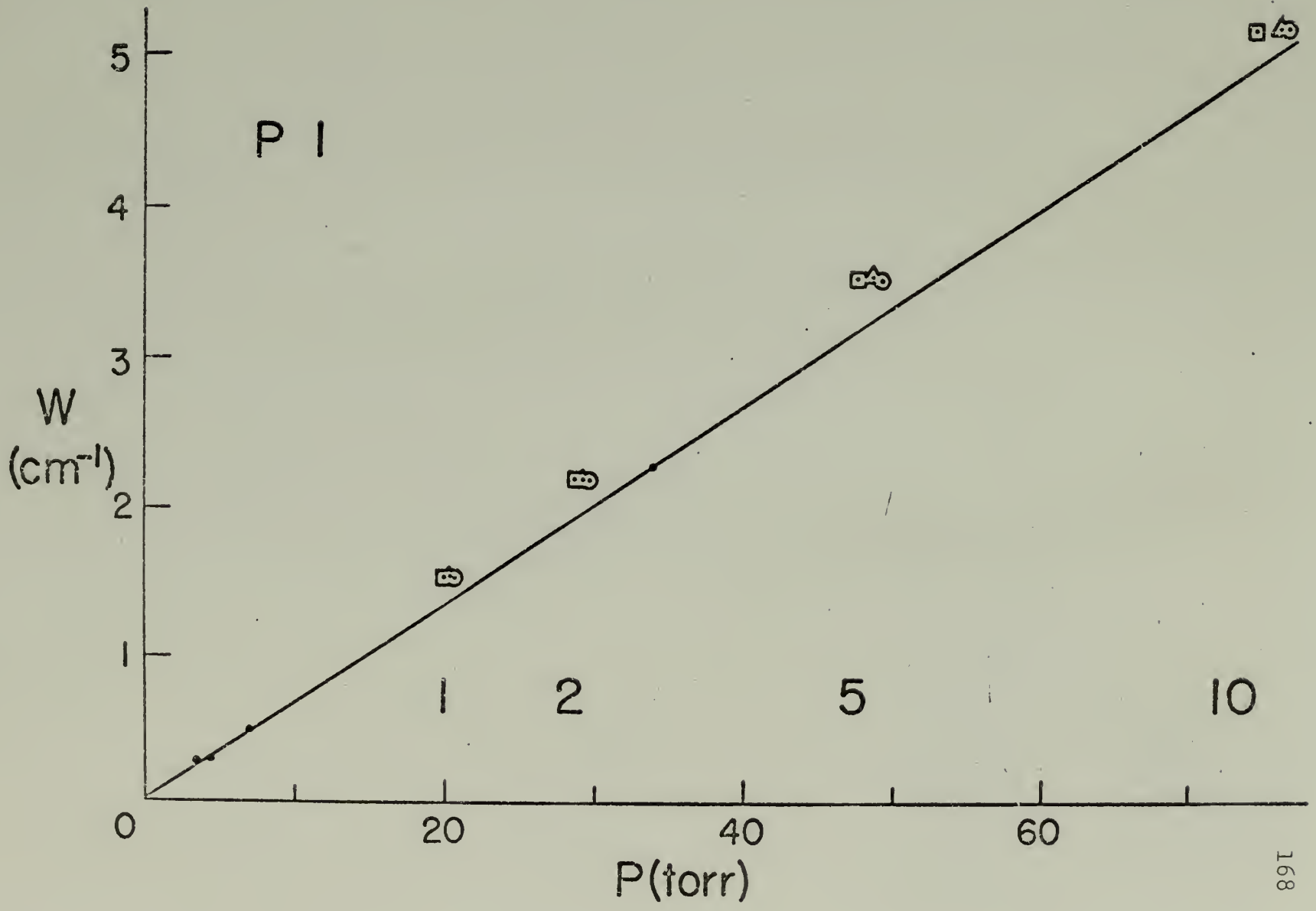
P 1
W
(cm⁻¹)
5
4
3
2
1
0
20
40
60
P(torr)
1
2
5
10

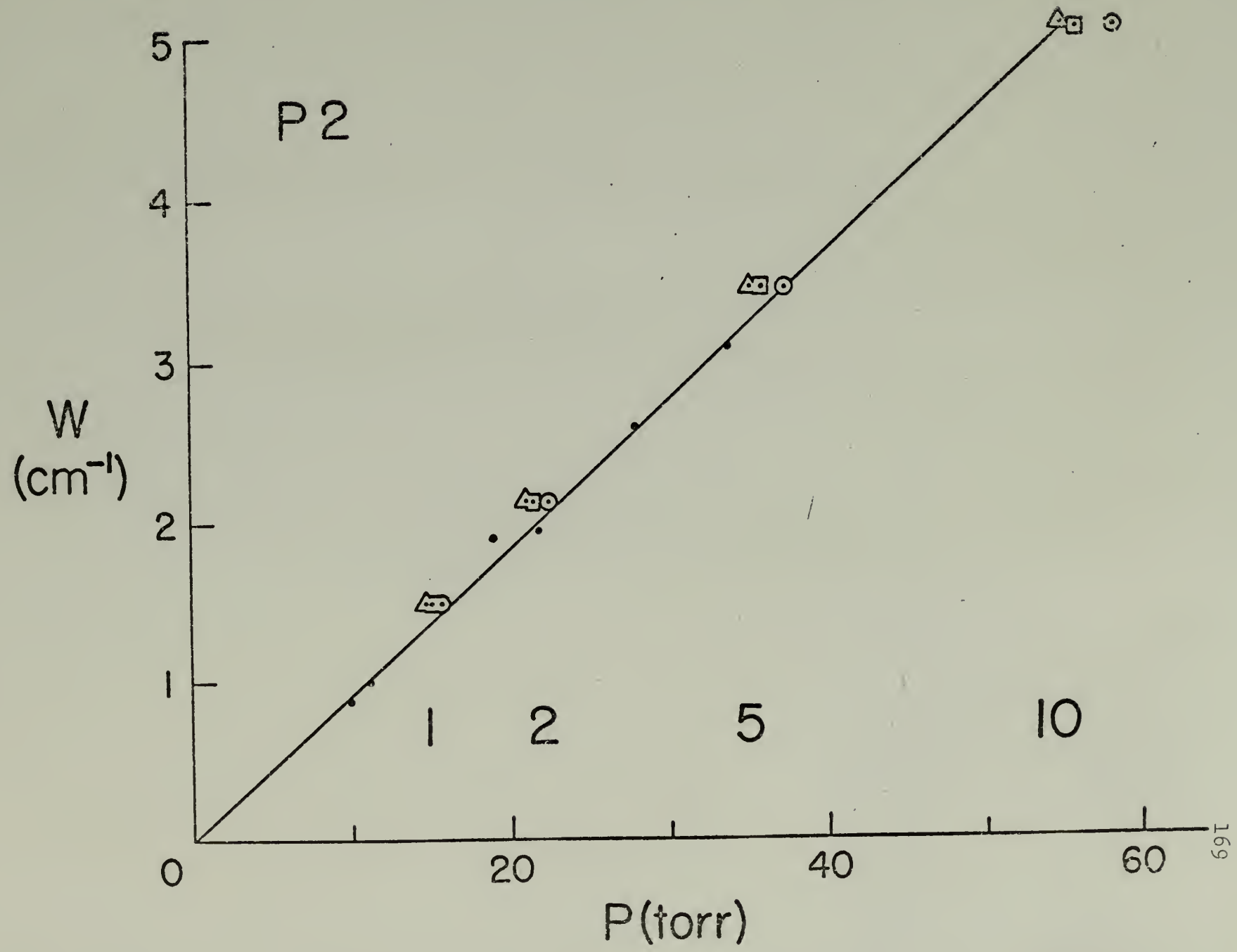
P 2
W
(cm⁻¹)
5
4
3
2
1
0
20
40
60
P(torr)
1
2
5
10
169

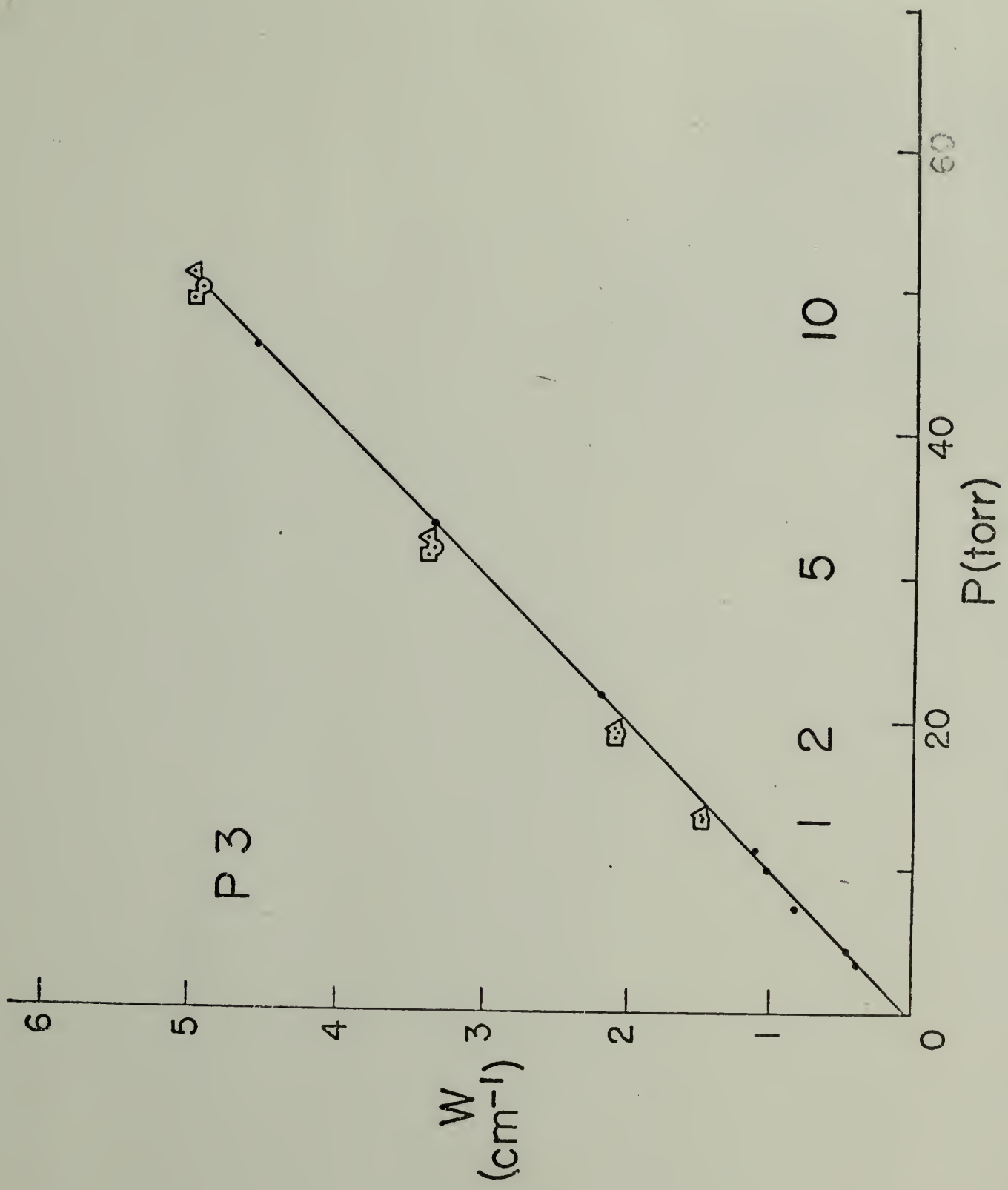
P 3
W (cm⁻¹)
P(torr)
0
1
2
3
4
5
6
20
40
60
1
2
5
10

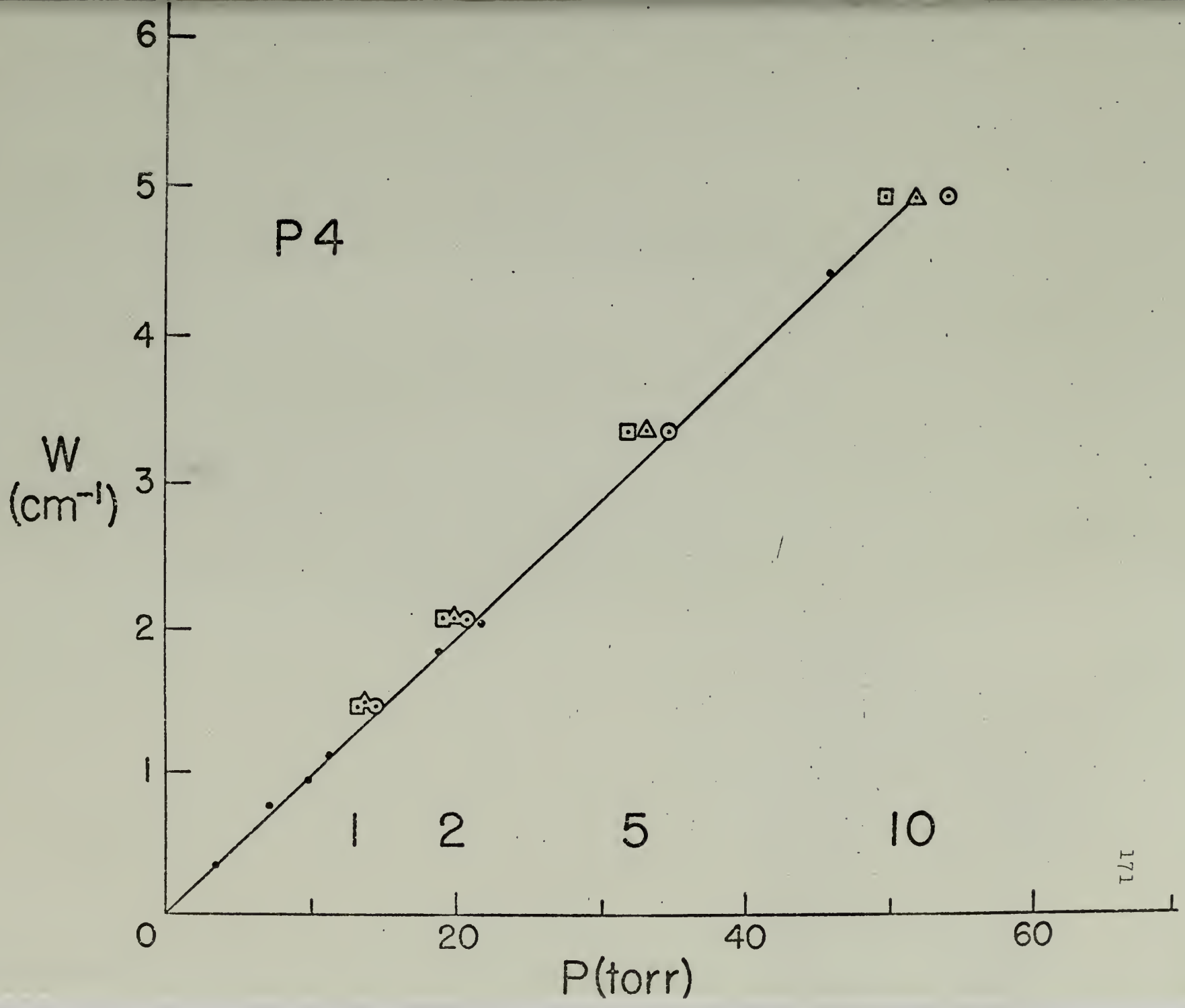
P4
W
(cm⁻¹)
0
1
2
3
4
5
6
20
40
60
P(torr)
1
2
5
10
171

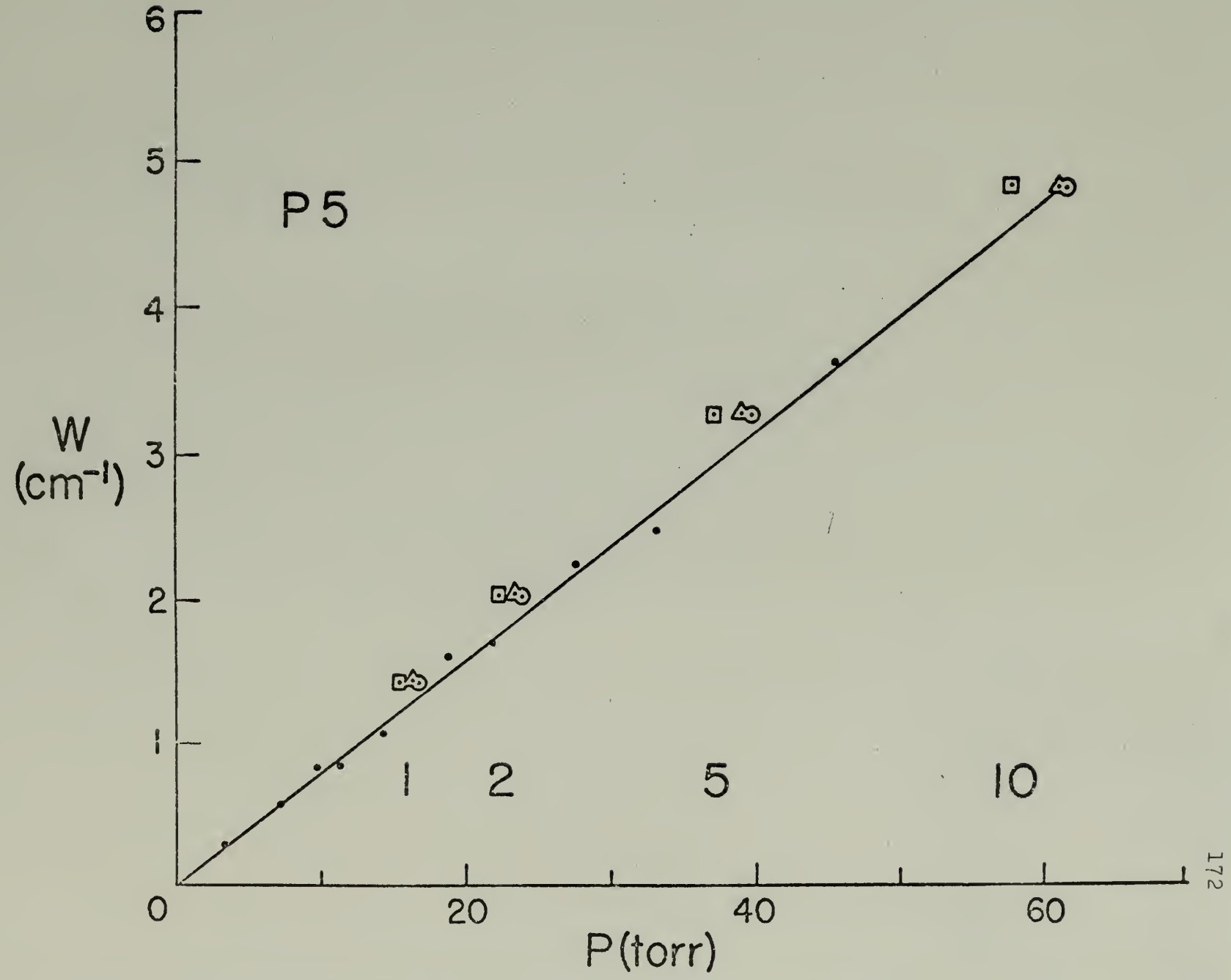
P5
W
(cm⁻¹)
6
5
4
3
2
1
0
20
40
60
P(torr)
1
2
5
10
172

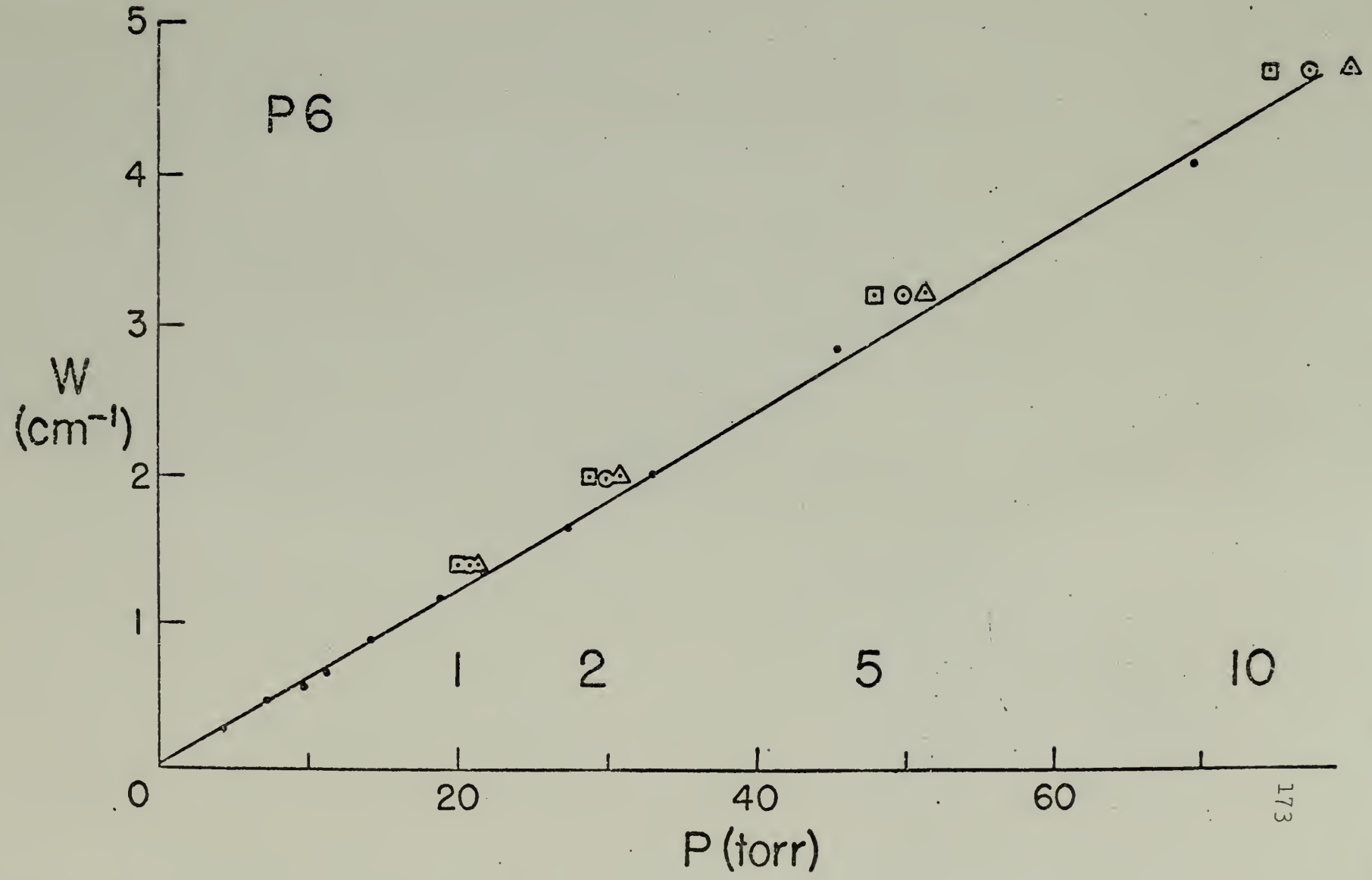
P6
W
(cm⁻¹)
5
4
3
2
1
0
1
2
5
10
20
40
60
P (torr)

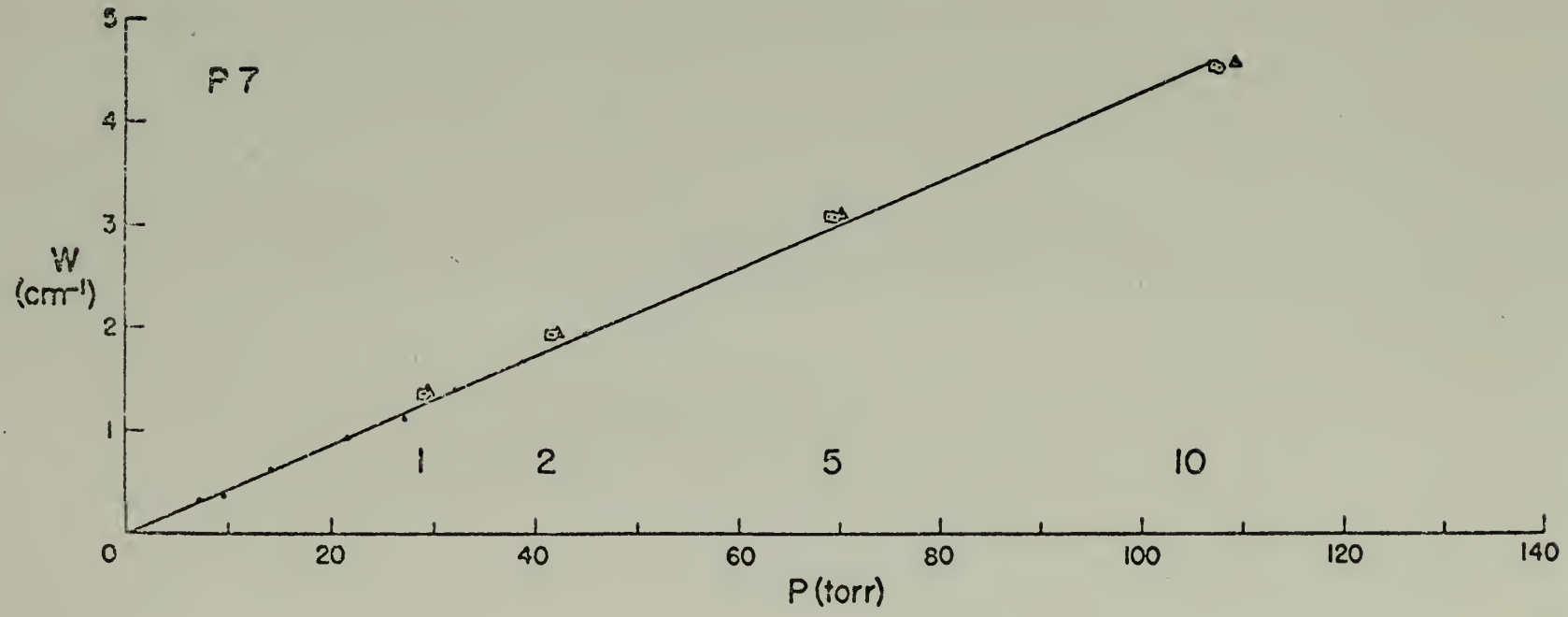
P7
W
(cm⁻¹)
1
2
5
10
0
20
40
60
80
100
120
140
P (torr)

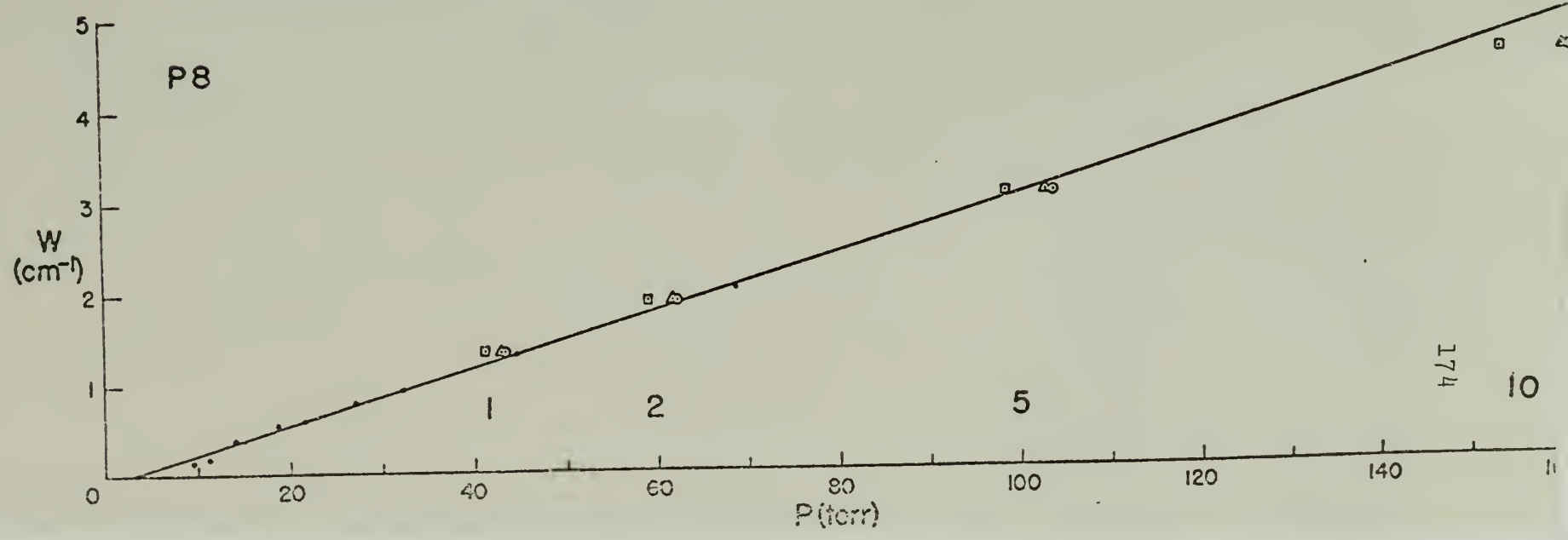
P8
W
(cm⁻¹)
1
2
5
10
0
20
40
60
80
100
120
140
P (torr)

Fig. 43

The Ladenburg-Reiche function plotted as a function of the Ladenburg-Reiche parameter, ζ and Strong's parameter, z. The conversion is indicated. Beyond $z = \pi$, the line absorbs in the square root region.

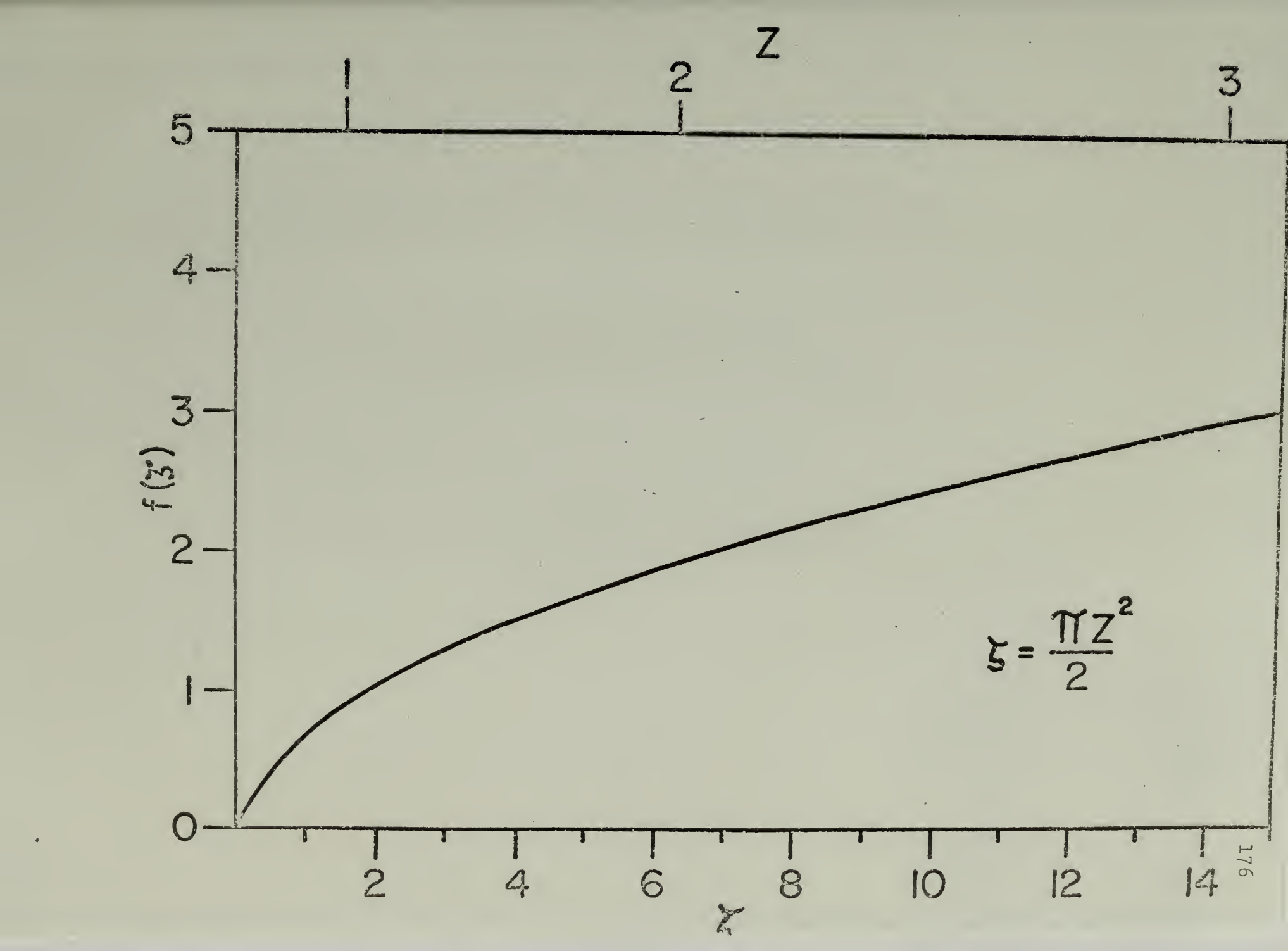
Z
1
2
3
5
4
3
2
1
0
f(ζ)
$\zeta = \frac{\pi Z^2}{2}$
2
4
6
8
10
12
14
ζ

LITERATURE CITED

1. C. Flammarion, The Flammarion Book of Astronomy (rev., G. C. Flammarion and A. Danjon), p. 331-2, Simon and Schuster, New York (1964).

2. N. Bohr, Phil. Mag., 26, 1 (1913).

3. R. T. Weidner and R. L. Sells, Elementary Modern Physics, p. 196, Allyn and Bacon, Boston (1964).

4. U. Fano and L. Fano, Physics of Atoms and Molecules, Chs. 2 and 20, The University of Chicago Press, Chicago (1972).

5. J. A. Chalmers, Atmospheric Electricity, p. 150, Pergamon Press, London (1957). See also J. E. MacDonald, UFOs-An International Scientific Problem, p. 20, Canadian Aeronautics and Space Institute Astronautics Symposium, Montreal (1968).

6. G. Herzberg, Spectra of Diatomic Molecules, 2nd ed., Chs. 5 and 6, Van Nostrand Reinhold, New York (1950). See also P. R. Bunker, J. Mol. Spectrosc., 39, 90 (1971).

7. D. Q. Wark, J. H. Lienesch and M. P. Weinreb, Appl. Opt., 13, 507 (1974).

8. D. Buhl and C. Ponnamperuma, Space Life Sci., 3, 157 (1971).

9. S. Y. Ho, Infrared Phys., 13, 83 (1973).

10. I. Fild and D. J. Lovell, J. Opt. Soc. Am., 60, 1315 (1970).

11. B. Fridovich, Dissertation, Technical Report #979, The University of Maryland (1969).

12. W. S. Benedict, R. Herman, G. E. Moore and S. Silverman, Can. J. Phys., 34, 850 (1956).

13. H. Babrov, G. Ameer and W. Benesch, J. Chem. Phys., 145 (1960).

14. D. Mihalis, Stellar Atmospheres, Ch. 9, W. H. Freeman, San Francisco (1970).

15. H. Margenau and W. W. Watson, Rev. Mod. Phys., 8, 22 (1936).

16. W. S. Benedict, R. Herman, G. E. Moore and S. Silverman, Can. J. Phys., 34, 830 (1956).

17. L. Spitzer, Phys. Rev., 58, 348 (1940).

18. H. R. Griem, Plasma Spectroscopy, McGraw Hill, New York (1964).

19. J. Cooper, Reports Prog. Phys. (GB), 29, 35 (1966).

20. H. A. Lorentz, Proc. Amst. Akad. Sci., 8, 591 (1906).

21. J. Strong, Appl. Opt., 11, 2657 (1972).

22. B. A. Lengyel, Lasers, 2nd Ed., p. 19, Wiley Interscience, New York (1971).

23. S. C. Burnett and R. J. Lovell, J. Opt. Soc. Am., 60, 1319 (1970).

24. P. E. Rouse and R. Engleman, JQSRT, 13, 1503 (1973).

25. F. Saiedy, Quart. J. Roy. Meteor. Soc., 87, 578 (1961).

26. W. S. Benedict and L. D. Kaplan, J. Chem. Phys., 30, 388 (1959).

27. G. N. Plass and H. Yates, Handbook of Military Infrared Technology, (ed., W. L. Wolfe), p. 189, Office of Naval Research, Washington, D. C. (1965).

28. C. D. Rogers and A. P. Williams, JQSRT, 14, 319 (1974).

29. D. Williams, D. C. Wenstrand, R. J. Brockman and B. Curnutte, Mol. Phys. (GB), 20, 769 (1971).

30. W. F. Herget, W. E. Deeds, N. M. Gailar, R. J. Lovell and A. H. Neilsen, J. Opt. Soc. Am., 52, 1113 (1962).

31. P. Varanasi, S. K. Sarangi and G. D. T. Tejwani, JQSRT, 12, 857 (1972).

32. P. Varanasi, JQSRT, 12, 1283 (1972).

33. L. L. Abels and L. M. De Ball, JQSRT, 13, 663 (1973).

34. W. S. Benedict, R. Herman, G. E. Moore and S. Silverman, Ap. J., 135, 277 (1962).

35. B. H. Winters, S. Silverman and W. S. Benedict, JQSRT, 4, 527 (1964).

36. D. E. Burch, R. R. Patty, D. A. Gryvnak and C. E. Bartky, J. Opt. Soc. Am., 59, 267 (1969).

37. D. E. Burch, R. R. Patty and D. A. Gryvnak, J. Opt. Soc. Am., 55, 606 (1965).

38. G. N. Plass and D. I. Fivel, Ap. J., 117, 225 (1953).

39. J. Strong and G. N. Plass, Ap. J., 112, 365 (1950).

40. R. Ladenburg and F. Reiche, Ann. Physik, 42, 181 (1913).

41. F. Reiche, J. Opt. Soc. Am., 46, 590 (1956).

42. H. Sakai and F. R. Stauffer, J. Opt. Soc. Am., 54, 759 (1964).

43. G. N. Plass, J. Opt. Soc. Am., 55, 104 (1965).

44. H. Sakai, J. Opt. Soc. Am., 56, 127 (1966).

45. W. S. Benedict and R. F. Calfee, Line Parameters for the 1.9 and 6.3 Micron Water Vapor Bands, ESSA Professional Paper 2, U. S. Department of Commerce Washington, D. C. (1967).

46. B. Fridovich and J. R. Kinard, J. Opt. Soc. Am., 62, 542 (1972).

47. R. A. Toth, R. H. Hunt and E. K. Plyler, J. Mol. Spectrosc., 35, 110 (1970).

48. Tables of Wavenumbers for the Calibration of Infrared Spectrometers, International Union of Pure and Applied Chemistry, Commission on Molecular Structure and Spectroscopy, Butterworths, Washington, D. C. (1961).

49. R. St. C. Smart and N. Sheppard, Proc. Roy. Soc. Lond., A, 320, 417 (1971).

50. W. M. Elsasser, Phys. Rev., 54, 126 (1938).

51. G. N. Plass, J. Opt. Soc. Am., 48, 690 (1958).

52. P. J. Wyatt, V. R. Stull and G. N. Plass, J. Opt. Soc. Am., 52, 1209 (1962).

53. H. Mayer, Methods of Opacity Calculations, LA-647, Los Alamos, New Mexico (1947).

54. R. M. Goody, Quart. J. Roy. Meteor. Soc., 78, 165 (1952).

55. L. D. Kaplan and D. F. Eggers, J. Chem. Phys., 25, 879 (1956).

56. P. Connes, J. Connes, W. S. Benedict and L. D. Kaplan, Ap. J. Letters, 147, L1230 (1965).

57. R. F. Mueller, Nature, 220, 55 (1968).

58. B. C. Murray, Scient. Amer., 228, 48 (1973).

59. Y. Ben Aryeh, JQSRT, 7, 211 (1967).

60. H. W. Yates, J. Opt. Soc. Am., 64, 408 (1974).

VITA

Harold Irving Heaton was born in Fitchburg, Massachusetts in 1946 and received his secondary education in the public schools of Lunenburg. He entered the University of Massachusetts on scholarships in 1964 where he majored in astronomy and art. He received the B.A. degree in astronomy in October, 1968.

In the fall of 1968, he enrolled as a graduate student in the Five College Astronomy Department at the University of Massachusetts simultaneously tutoring mathematics for the Committee for the Collegiate Education of Black Students (CCEBS). Since receiving the M.S. degree in astronomy and astrophysics in 1970, he has held concurrent research and teaching assistantships, researching scattering in Saturn's atmosphere with Dr. William Irvine and infrared molecular spectroscopy at the Astronomy Research Facility with Dr. John Strong. Teaching appointments were held in the Department of Physics and Astronomy, the Division of Continuing Education and in Project 10 Experimental College.

In the spring of 1973, he won national recognition for conveyance of space science to the general public from a paper written for the Griffith Observatory in Los Angeles. In the fall of that year, he founded and edited the Five College Astronomy Calendar after having continued his studies

in art as a summer student at McGill University in Montreal.

Since June, 1974, he has been a Lecturer in the Department of Physics and Astronomy at the University of Massachusetts and a regional investigator for the Center for UFO Studies, directed by Dr. J. Allen Hynek, in Illinois.

Heaton is the author of numerous scientific papers and is a member of the American Astronomical Society, the Society of the Sigma Xi, the Optical Society of America and the American Association for the Advancement of Science.

He is currently a candidate for a National Research Council NASA Post-Doctoral Research Associateship at the Goddard Spaceflight Center in Maryland.